Investigation of Laser Deposited Wear Resistant Coatings on Railway Axle Steels

A Thesis Submitted in Fulfilment of the Requirements for the Degree of Master of Engineering

Mona Soodi

School of Aerospace, Mechanical and Manufacturing Engineering
RMIT University

July 2013

To my PARENTS, my BROTHER and my HUSBAND with deepest love

Table of Contents

List of Figures

List of Tables

List of Abbreviations

SEM: Scanning Electron Microscope

AAR: The Association of American Railroads

HAZ: Heat Affected Zone

NDT: Non-Destructive Testing

SCRS: Surface Compressive Residual Stress

LME: Liquid Metal Embrittlement

VHCF: Very High Cycle Fatigue

MPI: Magnetic Particle Inspection

SE: Surface Engineering

HV: Hardness Vickers

PVD: Physical Vapour Deposition

TIG: Tungsten Inert Gas

CNC: Computer Numerical Control

RPM: Revolutions per Minute

OD: Outer Diameter

Investigation of Laser Deposited Wear Resistant Coatings on Railway Axle Steels

Abstract

Railway axles are one of the most critical components in rail industry since their failure can lead to the derailment of railway vehicles and loss of lives and properties. These components suffer from a wide range of damage including corrosion, electrical arcing, and fatigue and most importantly wear due to excessive loading.

Every year rail operators around the world scrap thousands of railway axles due to the size of their two bearing journals being under tolerances and sizes defined for them. The current standards for manufacturing and maintenance of rail axles only allow for non-thermal processes such as brush plating to be used to repair the worn rail axles as thermal processes as they may create heat affected zones with degraded properties in these components. In this study the possibility of using laser cladding which is a thermal process as a repair technology for refurbishment of railway axles is investigated which was proposed for the first time in 2010 by Hardchrome Engineering Pty Ltd, Melbourne, Australia. The economic rationale behind this idea was that replacing each worn axle would cost 2500 Australian dollars whereas repairing them with laser cladding would cost only 1000 Australian dollars per axle, provided that the feasibility of this technology and suitability for railway axle applications is proven.

Mild steel which is one of the most widely used materials in the manufacturing of rail axles was used to prepare hour glass fatigue samples to be tested under rotary bending fatigue condition using a dedicated testing machine which was designed and used at Hardchrome Engineering. These samples were tested without any laser deposition to demonstrate the fatigue data of axles which were not worn. To simulate worn railway axles, a groove was machined in each fatigue sample which was later filled by laser cladding as a simulation of a refurbished rail axle. Two different cladding materials were used to build up undersize

machined samples which were 420 stainless steel and CrMoV. The laser clad samples were then heat treated at a wide range of temperatures to investigate the effect of post-clad heat treatment conditions on the fatigue properties of laser clad samples. The fatigue results of the clad samples were compared to those of the non-clad samples to investigate the effect of laser cladding on the fatigue properties of the samples.

The results indicate that it is possible to refurbish worn railway axles using laser cladding technology without affecting their fatigue properties provided that the right choice of material, processing parameters, pre-clad and post-clad heat treatment conditions are made. 420 stainless steel clad samples had an average fatigue strength which was 8.4% less than that of the non-clad samples, showing that 420 stainless steel was not a suitable choice of material for refurbishment of railway axles. The CrMoV clad samples lasted an average number of cycles to failure which was 16.9% more than that of the non-clad samples, suggesting that CrMoV was a suitable choice of material for repairing worn railway axles. It was also shown that post-clad heat treatment had a positive effect on the fatigue properties of the laser clad samples since it released some of the residual stresses formed in the samples during laser cladding and also softened the clad layer.

The fractured samples were investigated by scanning electron microscope (SEM) and optical microscopes and it was shown that the presence of metallurgical defects such as pores had a strong negative effect on the fatigue properties of the laser clad samples since these pores acted as stress concentrators and cracks initiated from those areas and propagated into the clad layer and substrate and led to the premature failure of the defected samples.

Investigation of Laser Deposited Wear Resistant Coatings on Railway Axle Steels

Declaration

I certify that except where due acknowledgement has been made, the work is that of the author alone; the work has not been submitted previously, in whole or in part, to qualify for any other academic award; the content of the thesis is the result of work which has been carried out since the official commencement date of the approved research program; any editorial work, paid or unpaid, carried out by a third party is acknowledged; and, ethics procedures and guidelines have been followed.

_____

Mona Soodi

May 10, 2013

Acknowledgements

There are many people whom I would like to thank. The completion of my Master of Engineering degree would not have been possible without their assistance.

Firstly and foremost, I would like to express my heartfelt gratitude to my senior supervisor, Professor Milan Brandt for his never-ceasing enthusiasm, encouraging attitude, persistent support and guidance in all aspects. His valuable guidance, patience and ongoing support over the past two years are greatly appreciated. It has been a privilege to work with him, and his knowledge and insight about the subject ensured the successful completion of this work.

I also wish to thank my second supervisor, Dr. Nazmul Alam. His suggestions, comments and additional guidance were invaluable to the completion of this work. His great knowledge in laser cladding has greatly supported this project. I feel very fortunate and glad to have the opportunity to use his guidance.

Many thanks to Mr Andrew Dugan, General Manager of Hardchrome Engineering Pty Ltd, and Mr Mehdi Soodi, Laser Department Manager of Hardchrome Engineering Pty Ltd, for their unparalleled practical engineering knowledge and for providing me with access to laser cladding equipment.

I would like to acknowledge the financial support for my scholarship from Hardchrome Engineering and CSIRO, Victoria, Australia.

Lastly, I would like to thank my husband for his support and encouragement and for putting up with me in the past two years. It was good to know that there was always someone to count on when times were rough.

List of Publications and Presentations

- **Mona Soodi**, Milan Brandt, Nazmul Alam, "Investigation of Laser Deposited Wear Resistant Coatings on Railway Axle Steels", to be submitted to the Journal of Laser Applications, 2013.
- Mehdi Soodi, **Mona Soodi**, Milan Brandt, Nazmul Alam, "Fatigue Strength Properties in Rail Axles Refurbished by Laser Cladding", Conference on Railway Engineering CORE 2012 proceedings, Brisbane, QLD, Australia, September 2012.
- **Mona Soodi**, Milan Brandt, "Laser Cladding and Fatigue Results of Railway Axles", Manufacturing Innovations in Laser Additive Manufacture Workshop, Melbourne, Australia, June 2012.

Chapter 1

Introduction

1.1 Background

Railway axles are one of the most critical components in railway vehicles, both wagons and locomotives, with regards to safety since their failure can lead to their derailment and potentially major loss of property and human lives. The first reported accident caused by a broken axle occurred on 8th May 1842. The broken axle of a locomotive on the line between Paris and Versailles led to the death of 60 people. This accident initiated the research and study on the failure mechanisms of railway axles including their wear and fatigue [1].

Braithwaite was the first person who studied the fatigue properties of axles but his work was completed by August Wöhler in 1871 when he introduced the S-N curves (stress versus number of cycles to failure) for the first time [2, 3]. Since Wöhler's early work technological and analytical tools have been developed, which ensure that the number of broken railway axles is very low today.

There are several metal parts and components in the rail industry that require regular refurbishment or replacement due to strict size limitations and operational regulations to ensure the safety of the train and its cargo or passengers. One major category of such parts or components is the axle, for both wagon and locomotive.

Every year, the rail operators across the world scrap thousands of rail axles due to the size of the two bearing journals being under tolerances and size defined for them or deep scratches on the journals which occur while changing the wheels (Figure 1.1).

Figure 1.1: Scrapped railway axles with worn journals

According to the manual of standards and recommended practices section A, part III of Association of American Railroads -Operations and Maintenance department, mechanical division [9], any axle that has the following conditions should be replaced:

1. Broken,
2. Damaged due to overheating,
3. Damage between wheel seats of a depth of 1/8 inch or deeper,
4. Journal found rusted or pitted,
5. Axle bent when determined at wheel shop,
6. Axle damaged as a result of being in fire.

It adds that axles when reclaimed must be in accordance with the AAR Wheel and Axle Manual Section G, Part II of the Manual of Standards and Recommended Practices.
The current standards for rail axle maintenance and also the above mentioned American standard recommends: “Axles removed from service due to overheating must not be reconditioned and must be immediately stencilled in 1 inch letters overheated scrap and journal mutilated to prevent reuse.”; hence only allowing for non-thermal processes such as brush plating to be used to repair them.

These non-thermal methods are extremely slow and very expensive therefore they are not used by the industry or the rail operators to repair and refurbish axles. Today axles are only reclaimed by machining them from their worn size to sizes suitable for other types and sizes of axles and then are used as second hand axles [4].

In 2010, Hardchrome Engineering Pty Ltd in Melbourne, Australia carried out trial refurbishment of rail axles with undersize bearing journals using laser cladding technology. The technology is used to deposit metallic alloys – usually in powder or wire form - onto metal parts and components by melting them using the heat from a laser beam which is fed through a processing head onto the surface of the part.

Figure 1.2 shows the schematics of laser cladding process where the substrate in the case of this research is the rail axle journal. The laser cladding process is discusses in detail in Chapter 2.

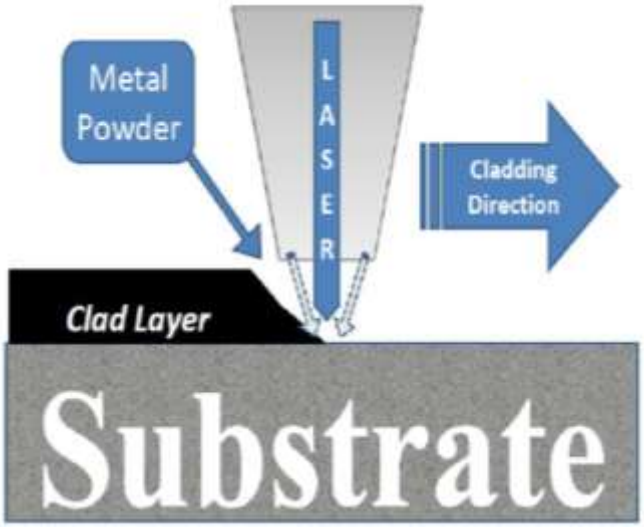

Figure1.2: Schematic of Laser Cladding

Figure 1.3 shows the trial laser cladding of a railway axle in Hardchrome Engineering Pty Ltd in Melbourne Australia.

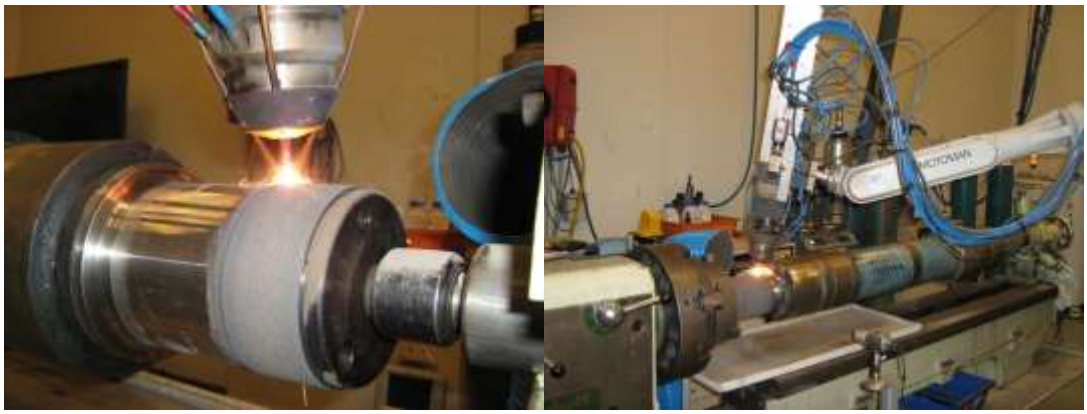

Figure 1.3: Laser Cladding of a worn railway axle in Hardchrome Engineering Pty Ltd

The justification behind using this technology despite the recommendation of the relevant standards of not using thermal processes or more specifically over-heating the axles was that laser cladding process is a unique technology among the thermal processes used to deposit metal on metal in which it introduces the least amount of heat into the part and results in the smallest heat affected zones in the substrate. The heat generated from the laser beam is only used to melt the surface of the part and the metal powder which is injected to the same spot where the laser beam meets the surface of the part. This spot is usually about 2-5 mm in diameter and travels at speeds of up to 4 meters per minute. Therefore, the heat which is introduced inside the axle is minimal and it also dissipates very rapidly especially considering the size of the axle compared to the size of the melt pool being only 2- 5 mm in diameter.

Other researchers have shown interest in the railway axles and their fracture and failure mechanisms as well. U. Zerbst [2] reports on the parameters affecting the damage tolerance behaviour of railway axles and factors influencing their residual life time. In their research two of the main factors studied were the fatigue crack propagation threshold and rotating bending effect in the axles. This research emphasizes the importance and vitality of maintaining high fatigue resistance properties in rail axles.

A study by M. Novosad [5] on the fatigue of railway axles compares the result of testing full scale axles and wheels versus fatigue test results obtained from small specimens. The paper concluded that testing real size full scale axles is a costly practice but verified the design models used in their fabrication and that only very small uncertainty exists in the results they obtain from full scale axle fatigue tests. The paper recommends an ongoing effort should be made by axle manufacturers to increase the fatigue resistance of their products.

L.P. Borrego et al [5] worked on the fatigue behaviour of laser repairing welded joints and reported that in the presence of defects as a result of laser melting, the material demonstrates weaker fatigue behaviour in comparison to the parent metal. However, flawless and defect free laser cladding results can be achieved and therefore the fatigue behaviour of the parent metal or the clad will not be adversely affected.

Another research done by Jianqiao Chen et al [7] on the effect of laser cladding on fatigue strength of an alloy steel concludes that the laser cladding of the specimens improved the fatigue life of the parent metal by 2-5 times as compared with the un-clad specimens.

However this research also demonstrates that in the presence of defects such as voids in the cladding layer they will control the fatigue strength and cause a larger scatter in fatigue life of the parts. They had observed that the specimens without voids were strengthened more notably.

The present work investigates the soundness and practicality of using laser cladding technology as a repair process for rail axles. This research mainly involves evaluating the effect of laser cladding refurbishment of rail axles on the fatigue strength of these parts. While there have been several research projects focusing on the fatigue strength of laser clad parts in the past, this research focuses on this aspect of the process on railway axles to better satisfy the needs of this industry and the relevant standard committees.

1.2 Research Objectives

This section will present some important questions related to the laser deposited wear resistant coatings on railway axle steels. The three main research questions of this project are:

1. *Is laser cladding a suitable process for refurbishment of worn railway axles?*

As mentioned in the background section, the relevant standards for railway axles do not allow the use of thermal processes to avoid any potential risks to the fatigue properties of these components. The rationale behind this idea is the fact that thermal processes can change the properties of the base material and can create a heat affected zone in the substrate with degraded properties and high susceptibility to cracking. In the present work it is suggested that due to the nature of laser beam it is possible to focus the heat only on the surface and minimize the formation of heat affected zone in the substrate. Also it is shown that it is possible to increase the fatigue strength of the clad samples by tailoring processing parameters and by adopting post clad heat treatments.

2. *How does the fatigue performance of laser clad axles compare to non-clad axles? Dose laser cladding have a negative effect on the fatigue properties of the railway axles?*

Since fatigue is the most common failure mechanism for railway axles, the focus of this research is concentrated on the fatigue properties of the laser clad parts and a comparison is made between the clad and non-clad parts.

3. *What are the factors that influence crack initiation and propagation in laser clad axles?*

The cross section of the fractured samples was investigated to analyse the causes of the failure. In most cases the metallurgical defects in the clad layers were responsible for the premature failures of the laser clad specimens. These defects such as pores and cracks can be avoided by adapting preheat and post clad heat treatments and by optimising the processing parameters.

The objectives of the present study are:

- Justifying the possibility of using laser cladding technology as a repair method for refurbishment of worn railway axles without jeopardizing their fatigue properties.
- Analysis of crack initiation and propagation in laser clad samples. Investigating the root causes that lead to cracking in the clad layer or the HAZ of the base material.
- Suggesting some preventive methods to avoid the formation of the defects that are responsible for the formation of cracks including processing parameters optimization and finished surface quality.
- Studying the effect of post clad heat treatment on the hardness and fatigue properties of laser clad samples. The experimental outcome of this thesis can provide referable evidence in the means of studying and developing further heat treatment processes to prevent the cracking of laser clad axles.
- Investigating the effect of cladding material on the fatigue life of the clad railway axles.

1.3 Outline of Thesis

This thesis includes 6 chapters. In chapter 1, the importance of railway axles, refurbishment of worn axles using laser cladding, objectives for this thesis and research questions have been outlined. The remainder of this thesis is divided into five additional chapters. Chapter 2 (Literature review) gives a background on railway axles and their fatigue properties, the current technologies that are employed for the improvement of fatigue properties of railway axles, surface engineering, laser cladding technology and the major concern with laser cladding technology. In Chapter 3 (Experimental Procedures), the experimental design of the project including the testing equipment, materials and sample preparation, laser cladding,

heat treatment and fatigue testing of the samples are described. Chapter 4 (Results and Discussion) depicts the experimental results of the laser clad samples and un-clad samples including the fatigue results and metallurgical investigations. Also comparison has been made between the fatigue results of the samples clad with two different cladding materials to investigate the effect of cladding material on the fatigue properties of the clad samples. The effect of post-clad heat treatment on the fatigue strength of the clad samples has been also demonstrated by analysis of the statistical data obtained from the samples which were heat treated at different temperatures. Chapter 5 (Conclusion and Future Developments) illustrates the major outcomes of this thesis and suggestions for future research directions. Finally, the list of references is presented in chapter 6 (References).

Chapter 2

Literature Review

2.1 Designs and Methods to Prevent Fatigue Failure of Railway Axles

Railway axles are safety relevant components and their failure can lead to the derailment of vehicles and possible loss of property and human lives. Since the work of Reuleaux in 1861 who published "The Constructer: A Hand Book of Machine Design" different standard axle design guides are being used for axle manufacturing [8]. Fatigue design of axles requires a comprehensive understanding of the input loads, material properties and how the component is managed in service. Little is known about the applied loads to axles and only measured data of full scale axles can give a real understanding of in service loads. Design guides are very conservative and consider the worst case scenario where the axle experiences maximum stresses. The rationale behind the design methods is to choose the axle parameters such as diameter and material so that the applied stresses are lower than the fatigue limit of the component [8].

Figure 2.1 shows a schematic design of a simple railway axle.
The maximum applied stress on the axle is calculated as

$$\sigma = m \sum M \frac{y}{l} = m64 \sum \frac{M}{\pi d^3} \qquad \text{(Eq 2.1)}$$

In the above equation "m" is a safety factor. By equating the maximum applied stress as calculated above to the fatigue limit of the material, "d" can be determined. In order to prevent failure, the diameter of the central portion of the axle must be greater than the value obtained from equation 2.1 [9].

There are other ways to modify axle design that can affect the fatigue strength of railway axles. Hollow and solid axles, axles with different journal length and axles with stress relief groove are examples of different axle designs.

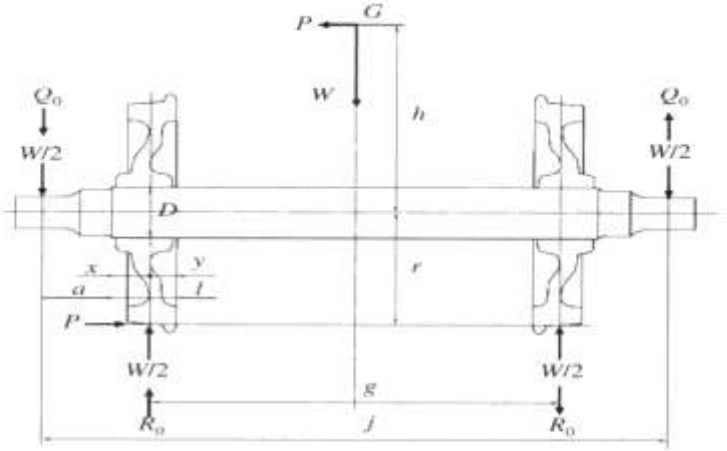

Acting forces of railway axle assembly

W	Wagon dead weight per wheel-set
P	$= W\alpha_1$, Horizontal force
α_1	Horizontal acceleration coefficient
Q_0	$= P\,(h/j)$, Vertical force of journals by P
R_0	$= (h+r)P/g$, Vertical force of treads by P

Dimension of railway axle assembly

d	Axle diameter
r	Wheel radius
j	Distance between journal centers
g	Wheel tread distance
a	Distance between journal center and the end of the wheel seat
h	Height from axle to gravity center
x	Distance from the outside wheel hub to the contact load
y	Distance from the inside wheel hub to the contact load
l	$x + y$

Another symbol

G	Gravity center

Bending stress of the axle at the wheel seat σ_b

$M_1 = (j-g)W/4$

$M_2 = \alpha_v M_1$

$M_3 = rP + Q_0(a+l) - yR_0$

$\sigma_b = m(M_1 + M_2 + M_3)/Z$

α_v	Vertical acceleration coefficient
m	Safety factor
Z	Section modulus of axle at the wheel seat

Figure 2.1: Loads applied on railway axles [8]

2.1.1 Hollow and Solid Axles

In a vehicle where parts are connected to each other by suspension, the parts like wheel axles, bearings and wheel hubs which are not supported by suspension are called unsprung mass. The unsprung mass of a vehicle has an inverse relation with the vibration isolation ability of that vehicle. Therefore, when a vehicle is tracking over a road bump, a lighter unsprung mass absorbs more vibration caused by the bump compared to a heavier unsprung mass and provides a higher ride quality. Therefore, lower unsprung masses are required for high-performance applications [10]**.** One way to reduce the unsprung mass of railway axles is to

use light high strength materials. High strength materials are considered brittle materials and therefore have high notch sensitivity which makes them unsuitable for manufacturing of railway axles. Another solution is the use of hollow axles instead of solid axles. The least stressed part of an axle is its core so boring out the core can increase the strength-mass ratio [11]. The main difference between hollow axles and solid axles is the NDT threshold. Since hollow axles allow the use of high angle scan, the detected cracks are much smaller than those of solid axles. Therefore the propagation life for the micro cracks in hollow axles is assumed to be longer than that of solid axles [4].

2.1.2 Journal length of Railway Axles

The Association of American Railroads (AAR) uses standardized classes of axles for different applications. These classes of axles are defined by their journal sizes. Axles with shorter journals have lower stresses in the journal area due to a lower moment arm. Class K of AAR axles with journal size of 6-1/2 × 9 and Class M of AAR axles with the journal size of 7 × 9 have lower stress in the journal area comparing to class F (6-1/2 × 12) and class G (7 × 12) [12, 13].

2.1.3 Stress Relief Groove

In order to avoid the fretting mechanism under the press fitted parts which can lead to the fatigue failure of railway axles, a design countermeasure has been introduced which is the stress relief groove at the closely fitted part of the axles (Figure 2.2). This groove can increase the endurance limit of the press fitted part of an axle one and a half times. None of the axles with the stress relief grooves have failed in service. A study has been done to compare the fatigue strength of axles with groove and without a groove. Figure 2.2 shows the S-N curves of conventional axles and axles with stress relief groove [14].

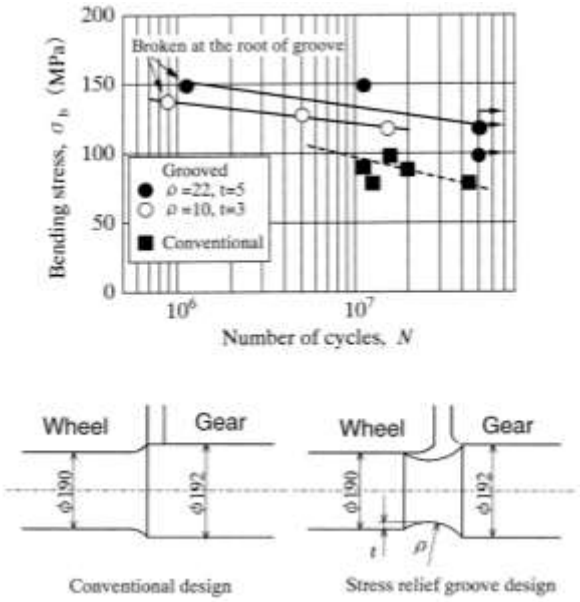

Figure 2.2: Effect of stress relief groove on fatigue strength of axles [14]

2.1.4 Compressive Residual Stresses

Fatigue properties of a particular component are directly controlled by the tensile and compressive stresses, either applied on the material during service loading or already existing in it as residual stresses. This is simply understood by the fact that "Fatigue is a surface effect and fatigue is a tension effect". The surface stresses which lead to the fatigue failure of a component are always tensile [15]. Any tensile residual stress caused by manufacturing processes such as grinding reduces the fatigue life of railway axles dramatically [16]. The best way to obtain better fatigue properties is to reduce the tensile stresses by producing compressive residual stresses in the surface [15] as the endurance or fatigue limit. This limit can be increased up to 50 percent in the presence of surface compressive residual stress (SCRS) [15].

Applying an armor of compressed material on the surface of high value components is a very practical technique to increase the fatigue life of them. There are many different ways of producing a compressive stress field in the surface of materials. All these techniques are based on one fact: to deliberately make a local difference between one region of a part and another. It can be a difference between the microstructures, chemical compositions or temperatures.

SCRS can favor the fatigue properties of a part not only by increasing the endurance limit but also by preventing the initiation and propagation of fatigue cracks. Compressive residual

stresses increase the ductility of a material and therefore provide the possibility of using harder materials which are considered “brittle” when there is no compressive stress. Harder materials are more resistant to fatigue; therefore SCRS has an indirect positive effect on the endurance limit by increasing the ductility [15].

The compressive residual stresses remain in the surface as long as the sum of the in service applied stresses and residual stresses does not exceed the yield strength of the material. If the yield strength is exceeded, the SCRS will be dispersed or relaxed. At higher loads, since the sum of the applied and residual stresses is also bigger, the effect of SCRS on the endurance limit is less or at some loads is near zero. On the other hand, at lower applied loads there is a big difference between the endurance limit of a part with compressive residual stress and that of a part without SCRS.

Different techniques of surface stressing have been applied on railway axles in order to increase their fatigue life. Among them, the most practical techniques are micro shot peening, surface rolling and induction hardening [15].

2.1.4.1 Micro Shot Peening

In shot peening a layer of overlapped dimples are formed by small round shot impinging on the surface with high velocity, which provides a compressive stress field. The peening tool squeezes the surface depth wise and stretches it along the surface producing a plastic deformation. After the tool is removed the elastic core which was compressed under the tool tries to expand and produces a compressive stress along the surface [15].

Usually when the peening tool is spherical the depth of the compressive field is the same as the diameter of the dimple. For some applications such as railway axles it is important to achieve a thick compressed layer so larger shots are used. The highest compressive stress that can be produced by round shots is almost half the yield strength provided the material is homogenous and the peening tool is harder than the peened material [15].

The fatigue endurance of peened axles can reach high figures. A study was conducted on the fatigue properties of alloy railway axle steel (35CrMo) and a medium carbon railway axle steel (LZ50) which were micro shot peened. The results indicated a 10 % increase of the

endurance limit of 35CrMo steel and 35 % increase for that of LZ50. Also the effect of surface roughness produced during micro shot peening on fatigue properties was studied and the results showed that the use of spherical particles in micro shot peening eliminates the negative effect of the surface roughness on fatigue limit. This means that a micro shot peened part does not need any finishing process and the fatigue life of a poor surface after shot peening is longer than that of an expensive high grade finished surface without shot peening [17].

2.1.4.2 Surface Rolling

Surface rolling is a cold-rolling process used to increase the hardness of materials through growth of dislocation numbers. This process can produce a deep compressive field and is used widely for improving fatigue properties of railway axles. During the surface rolling of railway axles, two cylindrical bodies are pushed on the surface of axle with a certain load in a certain amount of time causing a small plastic deformation in the surface. The elastic subsurface layer tends to expand and return to the original size but it is resisted by the surface layer therefore a compressive residual stress field is produced along the surface [18].
A study was conducted on two groups of railway axle steel LZ50 samples with and without surface rolling. The results showed that the samples which were surface rolled had lower crack density than the samples without surface rolling [19].

2.1.4.3 Induction Hardening

Induction hardening of railway axles involves induction heating and then quenching of the axles which results in a martensitic microstructure with a higher hardness. This phase transformation is associated with a linear expansion which produces compressive residual stress in the surface. Induction hardening of axles is followed by tempering. The tempering temperature of axles after induction hardening has an inverse relation with the compressive residual stress produced in axles. By decreasing the tempering temperature higher compressive residual stresses can be achieved. Also by decreasing the frequency used for induction hardening the martensitic heat affected zone which causes the compressive residual stress becomes deeper [14]. Japanese axles are induction hardened to increase the fretting fatigue strength of the press fitted parts, which are the fatigue critical parts in Shikansen axles. Figure 2.3 shows the induction hardening process of a railway axle [20].

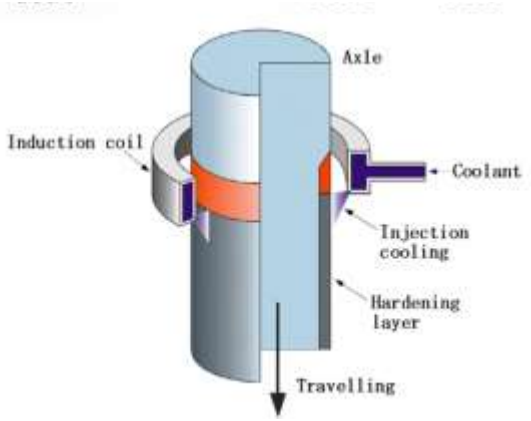

Figure 2.3: Induction hardening process for Shinkansen axles [20]

2.2 Materials Used in the manufacturing of Railway Axles

Different steels are used in manufacturing of railway axles according to different standards. The high strength alloy steels are usually used for high speed trains. These kinds of steels have high allowable stresses which can lead to the reduction of the unsprung axle mass. The axles made of high strength materials for high speed vehicles are usually hollow [4].

Although the high strength materials are suitable for high-speed trains, they do not affect the fatigue resistance under press fits. The main mechanism that causes the initiation of short cracks under press fits is fretting corrosion which also degrades the mechanical properties of the surface layer of the axles. Therefore the high strength of the material will no longer have any positive effects on the fatigue resistance of a mechanically degraded axle [21].

Below, the different steel grades used in railway axle manufacturing are presented with their different mechanical properties.

The Approved Australian grades:

According to Australian standards axles can be made from three different steel grades. Forged axle bars are made from AS 1448/K5 steel grade. Rolled axle bars are made from AS 1442/5FG. Another approved grade for Australian axles is AS 1444/4340. The mechanical properties and chemical compositions of these steel grades are given in Tables 2.1 and 2.2.

Table 2.1: Chemical composition of AS1444/4340

C	Cr	Mn	Mo	Ni	P	Si	S
0.38-0.43	0.7-0.9	0.6-0.8	0.2-0.3	1.65-2	0.035	0.15-0.3	0.04

Table 2.2: Mechanical properties of AS1440/4340

Yield Strength (MPa)	Tensile Strength (MPa)	Elongation at Fracture (%)	Reduction in Area (%)
Min 770	Min 980	14	40

LZ50 Railway axle steel:

LZ50 is a medium carbon steel used for manufacturing of railway axles according to Chinese standards. The chemical composition of this steel grade is given in Table 2.3.

Table 2.3: Chemical composition of LZ50 (Mass %)

C	S	P	Cr	Ni	Mn	Si	Cu	Mo
0.47	0.007	0.014	0.02	0.028	0.78	0.26	0.15	-

The microstructure of LZ50 is ferritic pearlitic. The mechanical properties of the LZ50 steel are given in Table 2.4.

Table 2.4: Mechanical properties of LZ50

Young's Modulus (GPa)	Yield Strength (MPa)	Cyclic Yield (MPa)	Tensile Strength (MPa)	Elongation (%)	Yield-Tensile ratio	Hardness (HV)
210	330	313	629	24.4	0.52	245-262

The axles made of this steel grade are usually normalized for 9000 seconds at 1133 K, and then tempered for 5400 seconds at 843 K [22].

35CrMo:

35CrMo is an alloy railway axle steel according to Chinese standard. The axles made from this steel grade are austenitised at 850 C for 1800 seconds, quenched in oil, then tempered at 580 C for 1800 seconds and air-cooled. This steel grade has a troostitic microstructure. The

chemical composition and mechanical properties of this material are given in Tables 2.5 and 2.6.

Table 2.5: Chemical composition of 35CrMo

C	S	P	Cr	Ni	Mn	Si	Cu	Mo
0.35	0.015	0.016	0.90	0.06	0.55	0.27	0.08	0.20

Table 2.6: Mechanical properties of 35CrMo

Young's modulus (GPa)	Yield strength (MPa)	Cyclic Yield (MPa)	Tensile Strength (MPa)	Elongation (%)	Yield-tensile ratio
215	863	705	982	22.1	0.88

EA1N, EA4T & 34 CrNiMo6:

European railway axles are mainly manufactured from two grades of steels defined by European Standards (EN 13261): EA1N and EA4T. EA1N is a normalized low strength carbon steel with 0.35% Carbon and EA4T (25CrMo4) is a low alloyed steel of fairly high strength. Railway axles for high speed train applications are made from 34CrNiMo6 according to DIN 10083 [21]. The chemical compositions and mechanical properties of these steel grades are given in Tables 2.7 and 2.8.

Table 2.7: Chemical compositions of steels (Mass %)

Steel	C	Si	Mn	Cr	Ni	Mo	P	S
EA1N	0.40	0.24	0.95	-	-	-	0.0027	0.017
EA4T	0.26	0.29	0.70	1.0	-	0.20	0.020	0.007
34CrNiMo6	0.352	0.228	0.61	1.37	1.32	0.19	0.015	0.026

Table 2.8: Mechanical properties at room temperature

Steel	Yield Strength (MPa)	Ultimate Strength (MPa)	Elongation at Fracture (%)
EA1N	Min 320	550-650	Min 22
EA4T	Min 420	650-800	Min 18
34CrNiMo6	Min 600	800-950	Min 13

The matrix of EA1N consists of a ferritic-pearlitic microstructure with a 20-40 µm ferrite grain size [23].

30NiCrMoV12:

30NiCrMoV12 is a high strength quenched and tempered alloy steel used for high-speed train applications according to UNI 6787 Standard. Axles made from this grade of steel are usually hollow.

Mechanical properties and chemical compositions of this material are given in Tables 2.9 and 2.10 [4].

Table 2.9: Chemical composition of 30NiCrMoV12

C	Si	Mn	P	S	Cr	Mo	Ni
0.28-0.34	0.4	0.5-0.8	0.025	0.020	0.6-0.9	0.4-0.6	2.7-3.2

Table 2.10: Mechanical properties of 30NiCrMoV12

Yield Strength (MPa)	Ultimate Tensile Strength (MPa)	Elongation at Fracture (%)	Small-Scale rotating bending fatigue limit (R=-1) (MPa)	Full-Scale fatigue limit for axle body (R=-1) (MPa)	Allowable stresses in axle body (EN 13104) (MPa)
860	975	20	510	315	210

The approved AAR grades:

The North American axles are manufactured from a steel grade specified by the Association of American Railroads (AAR) standard M-101. The axles made from this steel grade are heat treated by double normalizing and tempering. The chemical composition and mechanical properties of this material are given in Tables 2.11 and 2.12 [24].

Table 2.11: Chemical composition of AAR axles

C	Mn	P	S	Si
0.45-0.59	0.60-0.90	0-0.045	0-0.050	0.15

Table 2.12: Mechanical properties of AAR axles

Yield Strength (MPa)	Tensile Strength (MPa)	Elongation at Fracture (%)	Reduction of Area (%)
Min 345	Min 607	22	37

2.3 Failure Mechanisms of Railway Axles

There are mainly two reasons for the failure of the railway axles:

- Failure due to the overheating of the roller bearings
- Failure due to the fatigue effect

In order to identify the failure mechanism mode of railway axles, the fracture surface should be investigated. The aspect of an axle broken due to fatigue failure is cylindrical with a smooth fracture surface with horizontal marks known as “the beach marks” (Figure 2.4). The typical aspect of a burnt-off journal is conical (Figure 2.5) [16].

Figure 2.4: The fracture surface of an axle broken due to the fatigue failure [16]

Figure 2.5: An overheated railway axle [16]

2.3.1 Failure due to overheating of the roller bearings

The overheating of roller bearings usually occurs as a result of the excessive friction caused by mechanical flaws or insufficient lubricant between the in contact surfaces. This situation is known as “The hot box” and the broken journal is referred to as “the burnt off journal” [16]. The roller bearings of railway axles are composed of Babbitt material (any of the several alloys used for bearing surface) on Bronze backings. As a result of high temperatures, the Copper-based material of the bearings melt and cause the liquid metal embrittlement (LME) of the axles which lead to the formation of many short cracks on the axle surface. The overheated axles then break from the centre of the overheated bearing assembly [25].

An example of axle failure due to overheating of roller bearings occurred in 2003. In this case, overheating of the bearings was caused as a result of sliding of the axles in them, which caused friction and warming up of the bearings. The brass cage of the bearings melted as a result of the temperature increase and flowed on the axle surface, which was heated up to austenitic region, leading to the formation of many small cracks on the surface of the axle as a result of liquid metal embrittlement. The cracks then propagated and led to the premature failure of the axle [26].

2.3.2 Failure due to the fatigue effect

Fatigue failure is believed to be the main failure mechanism for railway axles. Railway axles were among the first components which suffered from the fatigue damage and initiated the study on this surface effect.

Fatigue is a structural damage that occurs when a material is subjected to cyclic loading. If the applied loads are above a certain threshold, microscopic cracks will begin to form from the surface. When a crack propagates and reaches a critical size, the fracture happens. Fatigue life, $N_{f,}$ is defined by the number of load cycles a component can sustain before its fatigue failure.

The fatigue behaviours of materials are described by their S-N curves also known as Wöhler curves. S-N curves show the magnitude of the cyclic stress (S) versus the logarithmic scale of number of cycles to failure at that stress (N). The S-N curves of some materials such as some steels and titanium alloys become horizontal at a particular stress limit which is called

"the fatigue limit" or "the endurance limit" of that material. The fatigue limit is a stress level under which there is no number of cycles that will cause failure. By keeping the applied loads on a component below its endurance limit an infinite life of that component can be maintained [27]. It is frequently assumed that the fatigue limit of a material is the same as its elastic limit. Experiments have proven that there is no relation between the elastic limit of a material and its endurance limit, since the elastic limit of a material is the initiation point of its plastic deformation which can occur without the formation of any fatigue cracks, but the experiments have shown that there is a relation between the fatigue limit of a material and its ultimate tensile strength. The results indicate that the fatigue limit is typically between 45 to 55 per cent of the ultimate tensile strength. However, it is shown that the practical fatigue limit of railway axles is below the calculated values due to the occurrence of unexpected events such as formation of stress concentrators or defects during service which are not included in the calculations [27].

Railway axles are subjected to repeated loading cycles. The rotary bending stresses applied on axles cause an element of the material on the surface of the axles go from a compressive state to a tensile state which leads to fatigue of these components [28]. The classical approach for the design of axles is based on the "safe life" methodology [29]. The applied stresses on railway axles during service must be kept below the fatigue limit of axle material so that the fatigue cracks do not form [29, 30]. The axle dimensions and materials are chosen based on this methodology. It can be concluded that a simple way to keep the applied loads below the endurance limit of the axle material is to increase the diameter of the axles, but this is not practical since axles are considered as what is called "the unsprung mass" of the vehicle which must be minimised for better ride qualities and lower dynamic stresses [31].

One of the difficulties of the safe life design of axles is their fatigue limits. The fatigue limits of materials are defined at stress cycles in the range of 10^7, whereas the typical life of railway axles is about 30 years which is equal to about 10^9 cycles [32]. At this number of cycles which corresponds to very high cycle fatigue (VHCF) the failure takes place at stress levels well below the defined fatigue limit of the material. Other uncertainties about the applied loads on the axles, the effects of corrosion, flying ballast and wear are also some of the issues which make the safe life design of axles difficult [29].

As traditional trains are being replaced by higher speed trains, more detailed designs should be employed in the manufacturing of axles. Axles carry more loads in high speed trains and therefore the same standards for the manufacturing of axles in conventional low speed trains cannot be used for these axles. But despite the perfect designing of railway axles, axles still break at stress levels even below their endurance limits. That is explained by the occurrence of in service defects caused by corrosive environments, ballast impact or metallurgical defects that can decrease the fatigue life of these components and are not considered in the designs [30, 33, and 34]. Fatigue is a surface effect and surface defects, subsurface inclusions, surface treatment and manufacturing process can alter the fatigue properties of components [35]. Another cause that can lead to the premature fracture of the axles is the wearing of the axles which reduces the diameters which were chosen based on the required endurance limit for the axles. That is why there are strict size limitations for railway axles and axles which are worn and under sized are replaced with new axles. The axles are regularly inspected by in service NDT methods to find the defects which can act as stress concentrators and be the initiation sites for microscopic cracks on the surface of railway axles. The non-destructive testing schedules are set so that any crack too small to be detected by the NDT methods do not grow to reach the critical size before the next NDT examination [36].

Figure 2.6 shows the different parts of a railway axle. An axle consists of a plain part which is called "journal" and press fitted parts which include wheel seats, gear seats and brake seats. The critical parts of railway axles with regards to fatigue failure are either the press fitted parts which are the brake disk seats, gear seats and wheel seats, or the axle body close to notches and transitions (plain part) [24, 37]. The diameter ratio between the press fitted part and the journals affects the fatigue fracture site in axles [24].

A study was conducted by Hirakawa [14] in 1998 to study the effect of the diameter ratio between the press fitted parts and the journals on the fatigue strength of the press fitted parts of the railway axles. The results showed that in axles with small diameter ratios between the press-fitted parts and the plain sections, the press fitted parts are the fatigue critical parts. As the diameter ratio increases, the fatigue failure happens in the mid-span section of the axles (Figure 2.7). In Japanese axles, the diameter ratio (D/d), where D is the diameter of the wheel seat and d is the diameter of the plain part, is 1.10 and the critical parts are the press-fitted

parts whereas in European axles, the diameter ratio (D/d) is 1.12 which makes the journals the fatigue critical parts [9, 20].

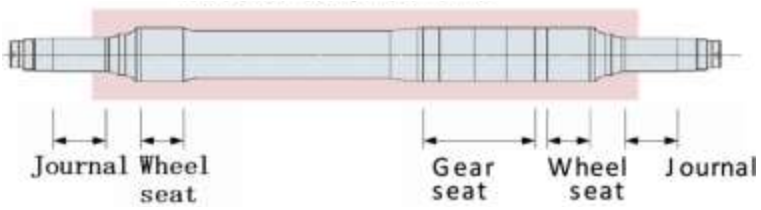

Figure 2.6: Different sections of a railway axle [20]

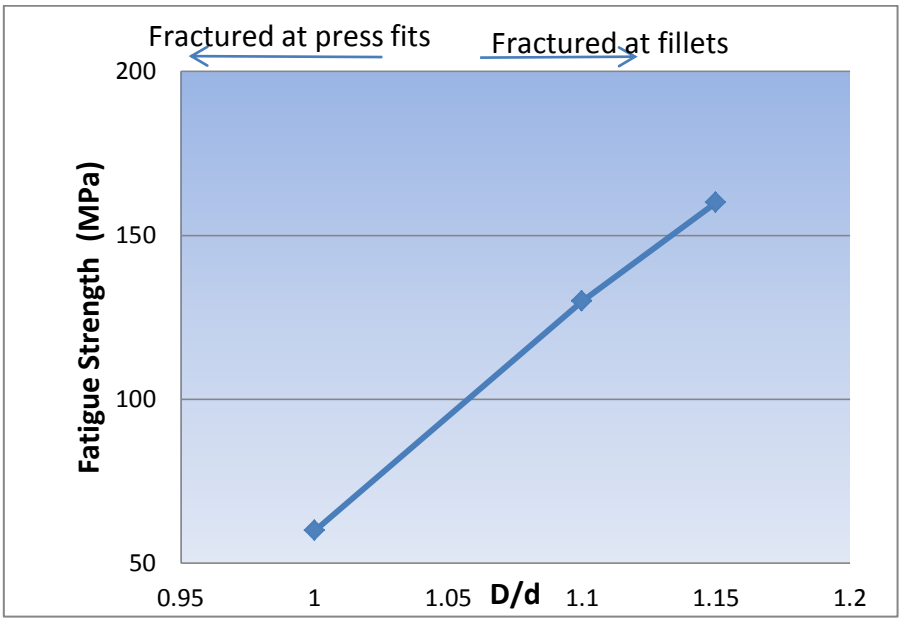

Figure 2.7: Diameter ratio between the press fitted parts and the plain section versus the fatigue strength [14]

Axles are subjected to four point bending and each time the axle rotates the top element of the axle goes from a compressive state to a tensile state. The high number of cycles an axle experiences in service can lead to rotary bending fatigue failure. Fatigue is a surface effect and starts from the surface. Any defects or stress concentrators on the surface of the axles can act as the crack initiation sites. It is known that the cracks on cylindrical components such as axle are in the form of semi-elliptical surface cracks [38]. The crack initiation step is then followed by the crack propagation as the result of the loading of the axles. When a crack grows and reaches its critical size, the final fracture happens. The crack initiation and propagation can occur by different mechanisms which are described in the following section.

2.3.2. 1 Stress Corrosion Fatigue

Stress corrosion fatigue is the combination of the mechanical loading and the presence of a corrosive environment. The damage resulted from this situation can be more severe than the damage caused by mechanical loading or corrosion acting individually. Ferrous alloys, which are used in manufacturing of railway axles, work in humid environments and in the presence of acids. Figure 2.8 shows two retired railway axles with corroded surfaces. As a result of these conditions, pits are formed and their dimensions increase due to the cyclic mechanical loading. These pits can either be semi-circular or sharp pits which are both potential crack initiation sites (Figure 2.9). The pit-to-crack transition and the crack propagation take place a lot faster in the presence of an aggressive environment than in air [39].

Figure 2.8: Two retired axles with corroded surface

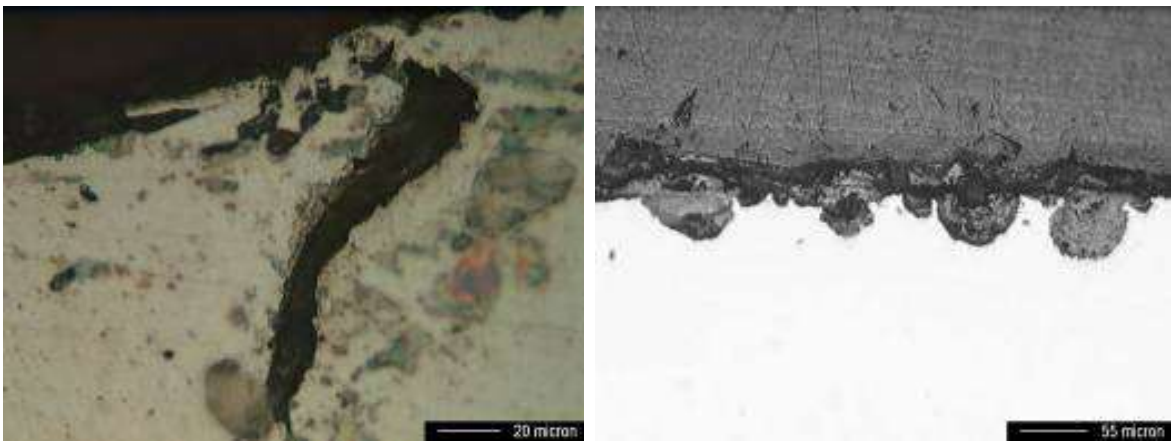

Figure 2.9: Semi-circular and sharp pits [39]

The crack formation and propagation in the presence of an aggressive environment can be classified into 4 stages (Figure 2.10) [40]:

- Stage 1: Pitting, similar to the pitting without fatigue. The pits act as crack initiation sites.
- Stage 2: Formation of micro cracks.
- Stage 3: Coalescence of micro cracks.
- Stage 4: Crack propagation.

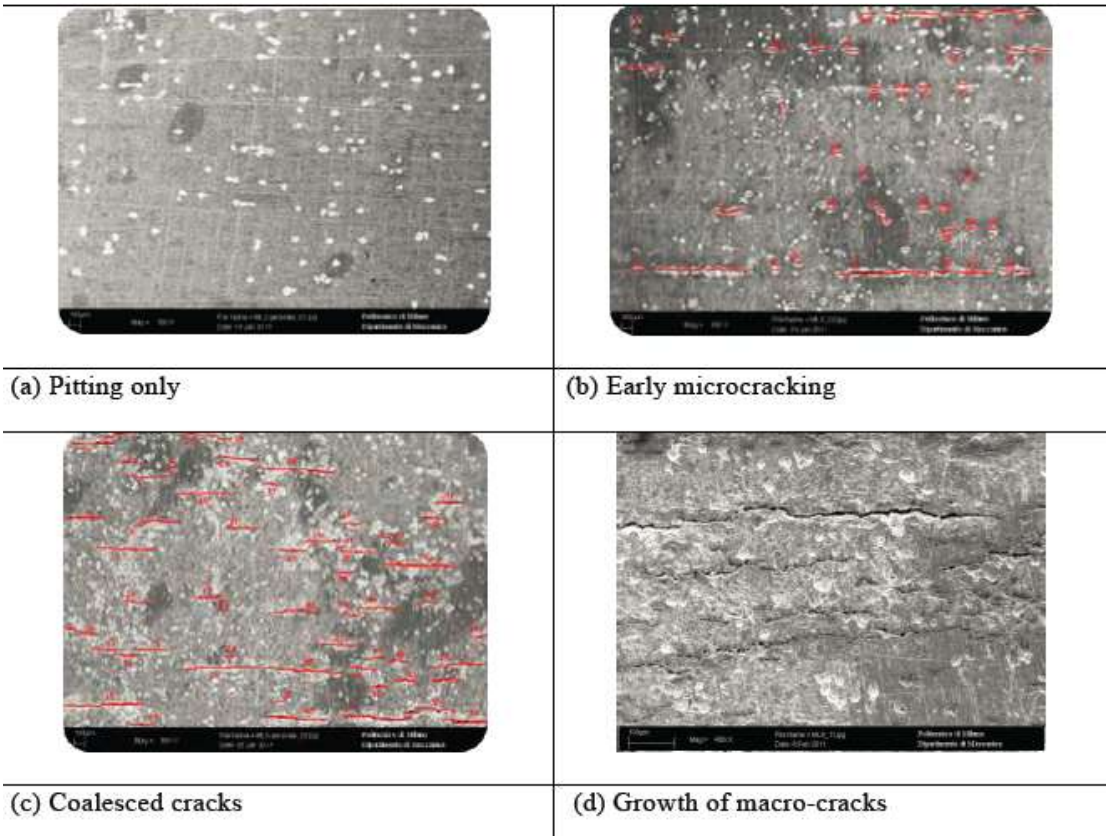

Figure 2.10: The four stages in the "pit-to-crack" transition [40]

M. Sangrirardi and M. Carboni [23] investigated the effects of the presence of a corrosive environment on the fatigue strength of railway axles. EA1N which is a normalized carbon steel widely used in the manufacturing of the European railway axles was used to make hourglass shaped specimens. Table 2.13 shows the chemical composition of EA1N alloy.

Table 2.13: Chemical composition of EA1N alloy

Steel	C	Si	Mn	Cr	Ni	Mo	P	S
EA1N	0.40	0.24	0.95	-	-	-	0.0027	0.017

The specimens were tested with a rotary bending fatigue machine shown in figure 2.11. To stimulate a corrosive environment for the test pieces, a dropping system was used to apply artificial rainwater solution on the specimens. To study the effect of an aggressive environment on the fatigue properties of the samples, similar rotary bending fatigue tests were also carried out in air. The S-N curves for both samples tested in the presence of a corrosive environment and in air were obtained.

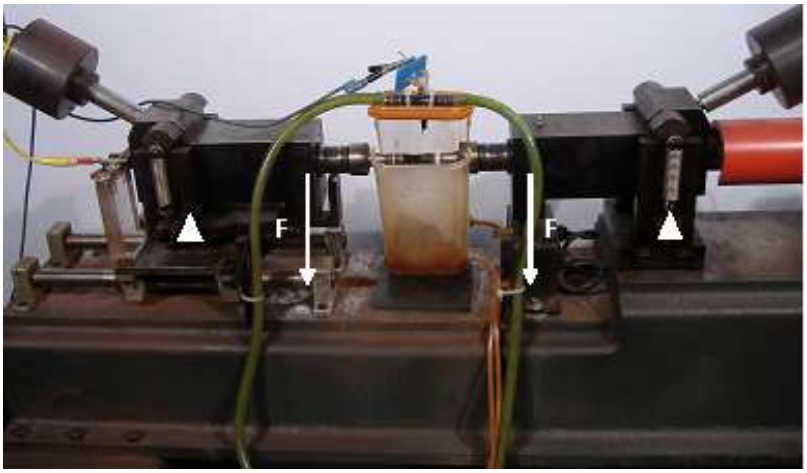

Figure 2.11: Rotary bending fatigue machine and the dedicated dropping system to apply the artificial rainwater [23]

The results indicated that at stress levels higher than the fatigue limit of the testing material in air, there was no significant difference between the fatigue strength of the samples tested in air and under artificial rainwater. But at stress levels below the endurance limit of the EA1N alloy in air, where cracks would not nucleate and propagate, the presence of a corrosive environment can assist the initiation and propagation of the cracks and lead to the premature fatigue failure of the samples. Figure 2.12 compares two S-N curves obtained from the samples tested in the presence of the corrosive environment and in air. The results show that the S-N curve for the sample in corrosive environment had a continuous decreasing trend and the endurance limit was eliminated for such specimens as a result of the corrosive environment [23, 40].

S. Beretta, et.al [41] investigated the corrosion fatigue behaviour of two full scale railway axles to compare the experimental and calculated data. The corrosive environment in this research was artificial water applied to the axles. The railway axle material in their study was A1T mild steel and the axles were tested under three points rotary bending loading condition. The results showed a reasonable relation with the theoretical and experimental life time of railway axles.

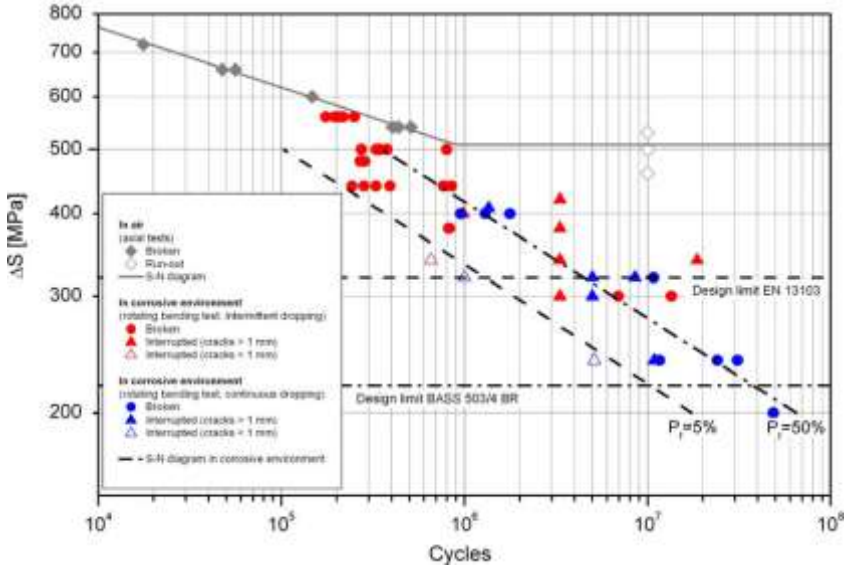

Figure 2.12: The S-N curves in air and in corrosive environment of EA1N alloy [23]

It is also important to note the role of the corrosion debris on the decreasing of fatigue life of railway axles. The cracks on the surface of an axle in the presence of a corrosive environment have a higher propagation rate compared to those of an axle in air since the corrosion debris can act as lubricant on the edge of the growing crack, therefore accelerating its propagation [8].

The following three accidents are examples of railway axle failures for which corrosion fatigue failure was the main mechanism.

Accident 1: The derailment of a freight train at Rickerscote, March 1996

One person was killed in this accident which was caused by a broken axle. When the broken axle was examined, the possible crack initiation sites were detected. At the mid-span section of the axle, where the paint had flaked off the surface, there were corrosion pits mostly about 0.03 mm deep and one about 0.05 mm deep. It is likely that the crack which grew and led the failure of the axle initiated from one of these pits [36].

Accident 2: Fracture of an axle at Shield Junction, Scotland January 1998

The fracture surface of the broken axle was studied and the results showed that the propagation of two cracks had caused the fracture. The damaged bitumen had allowed the salt solution to come into contact with the surface of the axle and remain trapped there and produce a corrosive environment which increased the local stress. This corrosive environment combined with the in service mechanical stresses had caused the failure of the axle. The damage caused by the stress corrosion fatigue is more severe than that of corrosion or fatigue loading acting alone [36].

Accident 3: Fracture of an axle and derailment of the train at Brenerely Junction, June 2002

The broken axle had been tested with magnetic particle inspection method to detect any cracks on its surface when it was fitted with a new set of wheels in 1988. It is possible that a small crack was present at the time of the inspection but was not detected. The reason that the crack could have been missed by the MPI technique is that the axles are grit blasted before they are inspected by magnetic particles to remove all the rust patches on the surface. It is likely that small patches of rust were not removed by grit blasting and the cracks underneath them could not be identified by MPI [36].

2.3.2.2 Electrical arcing

In the trains or locomotives, earth return brushes are used to form an electrical circuit between the earth return brush seats which are on the axles and the running rails to divert the traction motor circuit to the earth. The brushes used for axles are usually bronze/graphite brushes which contain copper, carbon as graphite, tin and lead. Any defects in the railway tracks can lead to electrical arcing between the axle and the rail track. The electrical arcing is associated with high temperatures which can affect the micro structure of the railway axles and reduce their fatigue lives. Two accidents which were caused by fracture of railway axles due to electrical arcing are described below to further explain this failure mechanism.

Accident 1: Failure of an axle due to electrical arcing, July 2002

The presence of some flaws in the railway track and the earth return brush caused an electrical arcing between the return brush and return brush seat of the broken axle. During the

electrical arcing, the return brush seat had been subjected to high temperatures (about 950° C) which caused the formation of a heat affected zone with martensitic microstructure. Since Martensite is a brittle phase, the HAZ is very susceptible to cracking. When the broken axle was investigated (Figure 2.13) it was shown that the initiation and propagation of micro cracks from the brittle HAZ had caused the premature failure. The results also showed the formation of a thin layer of copper on the surface of the axle which was originally in the earth return brush and was melted as the result of high temperatures and was deposited on the axle [36].

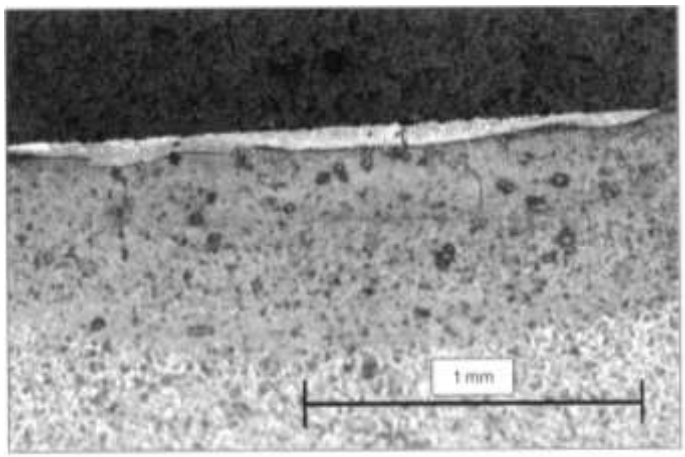

Figure 2.13: A cross section of the broken axle due to electrical arcing showing the 0.05 mm thick copper layer and a martensitic heat affected zone [36]

Accident 2: Damage to the earth return brush track on the axle of a class 442 EMU. December 2002

The axle involved in this accident was also broken due to the electrical arcing between the bronze/ graphite brush and the axle earth return brush seat. Figure 2.14 shows the copper and bronze layer deposited on the surface of the axle with copper penetrated into the cracks of the heat affected zone. The removal of cracks when copper is present is insufficient to guarantee that the axle is safe to be used again and should be replaced by a new axle [36].

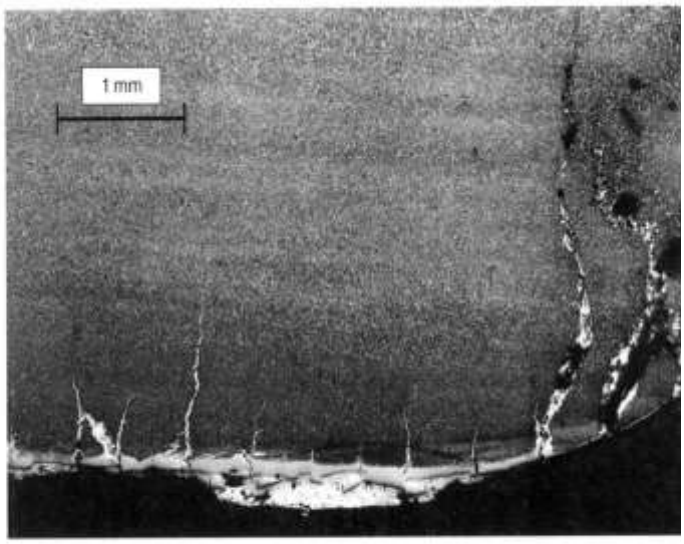

Figure 2.14: The bronze and copper layer in an axle broken due to electrical arcing [36]

2.3.2.3 Fretting Corrosion

Press fit or interference fit is a technology used for fastening two parts using friction between the parts after they have been pushed together. This technology is used for the attachment of railway wheel sets [21]. Brake disk seats, wheel seats and gear seats are the press fitted parts of an axle. The fatigue mechanism under press fitted parts is fretting corrosion [22]. Fretting is a wear or corrosion damage which happens between the asperities of two contact surfaces. Fretting happens under load and in the presence of a small amplitude oscillatory movement like vibration [22]. The movement causes material removal and production of debris which usually follows by the oxidation of the debris and the fresh surface. Fretting can lead to mechanical wear of the material and loss of fit between the surfaces or the growth of the existing small cracks in the part and reduction in the fatigue life of the material [21, 22].

Fretting is one of the most important reasons for railway axle failure of press fitted parts. A recent study investigated the possibility of increasing the fretting fatigue resistance of railway axles by applying thermally sprayed Fe/Ni coatings on them [41]. The results indicated a significant growth in the fatigue life of the Fe/Ni coated axles compared to that of the uncoated axles. The fretting fatigue strengths of coated and uncoated axles were 156 MPa and 103 MPa respectively [41].

2.3.2.4 Stress Concentrators- the Notch Effect

Railway axles are subjected to cyclic rotary bending stresses. The presence of stress concentrators can increase the mean stress that an axle experiences and cause its failure at stress levels well below its endurance limit and decrease its fatigue life. This phenomenon is known as "the notch effect" [35]. Any surface roughness or subsurface inclusions can act as stress concentrators. The fatigue cracks usually initiate from the weakest part of the surface unless the subsurface inclusions are weaker than the weakest part of the surface, which leads to the crack nucleation in the subsurface layer [42]. An example for non-metallic inclusions acting as stress concentrators and crack initiation sites is the accident which was caused by a broken axle in July 2008, Germany [43]. Due to the low speed of the train at the time of accident, no serious injuries were caused to the passengers. The investigations on the broken axle revealed that the level of impurities was higher than the acceptable limit. The non-metallic inclusions detected by the NDT inspections were assumed to be responsible for the formation of the fatigue cracks which then grew and led to the failure of the part [43, 44].

The surface quality is a very important issue in evaluation of fatigue properties of railway axles since the fatigue cracks mostly initiate from the surface of these components. The manufacturing of railway axles includes forging of these components at high temperatures to avoid cracking of carbides and making the formation of the hard steel used in manufacturing easier. Since it is difficult to achieve the precise dimensions and shapes while forging, a large machining allowance is needed which leads to a rough surface with. The scratches are then gouged out which produce notches with the depth of 2-3μm. These notches can form cracks which then propagate under cyclic loading and result in the fracture of the axle. The surface of an in service railway axle is also affected when crushed ballasts impact the surface and reduce the fatigue strength of the axle. It is worth mentioning that although a rough surface can reduce the fatigue life of a component, but it can also have a positive effect on the fatigue strength by producing a compressive residual stress in the surface which will be described later [35].

2.4 Repair and Refurbishment of Railway Axles

One of the major damages to railway axles is wear of their bearing journals due to excessive loading. Every year thousands of railway axles are scrapped due to the size of their bearing journals being under the sizes defined for them. There are several surfacing processes that

can be used to repair the worn axles but the current standards for rail axle maintenance only allow the use of non-thermal processes for the refurbishment of worn railway axles. One of these non-thermal processes is “brush plating”. Brush plating is an electro deposition process where metal is selectively deposited on the areas that need dimensional repair. According to the American Associations of Railroads (AAR) a hard nickel coating with a minimum hardness of 50 RC should be deposited on the worn railway axles and the coating must be capable of withstanding of a burnishing operation following the plating. The thickness of the nickel deposit must be sufficient to build up the worn rail axle to the original size. The brush plating of a worn axle includes 5 steps (Table 2.14) which can be time consuming and expensive. This process is very labour intensive and the technician can only process one part at a time [45].

Table 2.14: Steps of brush plating process for repair of railway axles

Step	Operation
1	Electro clean
2	Etch
3	Desmut
4	Activate
5	Plate with Nickel

There are several surface engineering processes that can be used to build up the worn axles to their original size, but their suitability for this application must be investigated first.

Surface engineering is a term which includes many technologies which are employed to apply changes to the surface of engineering components to obtain the required properties. Melford (1991) [46] defines surface engineering as

> “...the design of surface and substrate together as a system, to give a cost effective performance enhancement of which neither is capable on its own.”

Bell (1992)‘s [47] definition of surface engineering is

> “... the application of traditional and innovative surface technologies to engineering components and materials in order to produce a composite material with properties unattainable in either the base or surface material. Frequently, the various surface

technologies are applied to existing designs of engineering components but, ideally, surface engineering involves the design of the component with knowledge of the surface treatment to be employed."

SE (Surface Engineering) alters the surface properties of an engineering component in order to reduce the degradation over time cause by wear, corrosion or fatigue. The understanding that many mechanisms responsible for the failure of engineering components started from their surfaces initiated the research on surface engineering in 1980s, and the rapid growth in coating and surface technologies added extra impetus and drive for the development of the SE technology [48, 49].

The origins of surface engineering can be found in the traditional coating techniques and surface processes such as quench hardening, nitriding and carburizing which have led to the development of innovative technologies including ion implantation, laser and electron beam processing and plasma thermo chemical techniques [49]. There are many historical examples for the application of surface engineering that show surface engineering is not new.
In 1800 Brugnatelli, a Professor in Davia University described silver plating after the early work of Volta on the production of electricity by metallic corrosion in 1786. In 1840 the silver electroplating was commercially used for the first time. Nickel electroplating, which is the best known technique to improve the corrosion properties of Mild steel, was first established in 1916 [50].

It was in 1983 that the University of Birmingham established the Wolfson Institute for Surface Engineering and in 1985 that the first international journal of Surface Engineering was officially launched [49].

The ancient pre-Christ art of carburising the tools and weapons, to achieve keen cutting edges, was practiced since the passing of the Bronze Age [48, 50]. The new developments in surface engineering have led to the creation of innovative methods such as plasma carburising which offers higher degrees of flexibility and control to the process.

The application of metallic coatings such as Zinc and Nickel to improve the corrosion resistance of the engineering components started in the early days after the industrial revolution in the UK. Zinc coatings used to be applied to metal components with many

traditional techniques which have led to the development of Zinc-rich alloy electrodeposited coatings for preventing corrosion in metallic parts [50]. Hot-dip galvanising, sherardising and electroplating are also old processes which have improved dramatically since 1980s'.
In the late 1940's, the electro less deposition was invented for the first time which allowed the formation of coating processes which produced thin, dense and pore-free layers containing corrosion resistant materials to prevent the corrosion failure of the metallic components [50].

Surface engineering covers three main areas:

- *Optimisation of surface properties*: improving wear, corrosion and fatigue resistance of the surface
- *Coatings technology*: coating related technologies such as painting, electroplating, weld surfacing, plasma and hyper velocity spraying, different thermal and thermo chemical processes.
- *Characterisation of Coatings*: testing and evaluation of the surfaces and coatings based on the required properties and the condition [48, 50].

Surface engineering techniques can be categorized into two groups:

- The processes which add a layer of material with the required properties which changes the dimensions of the part.
- The processes which do not change the dimensions and only modify the existing surface of the component to achieve the desired change.

Table 2.15 shows the above classification with some examples of the surface engineering processes.

Table 2.15: Classification of surface engineering processes [47]

Layer additions	Substrate treatment
Hard facing	**Diffusion methods**
Fusion hard facing (welded overlays)	Carburising
Thermal spray (non-fusion bonded overlay)	Nitriding
	Carbonitriding
	Nitrocarburising
	Boriding
	Titanium-carbon diffusion
	Toyota diffusion process
Coatings	**Selective hardening methods**
Electrochemical plating	Flame hardening
Chemical vapour deposition	Induction hardening
(electro less plating)	Laser hardening
Thin films	Electron beam hardening
(physical vapour deposition, sputtering, ion plating)	Selective carburising and nitriding
	Ion implantation
Ion mixing	Use of arc lamps

The thickness of the added layer in the first group and the depth of the applied change in the second group can vary from nanometre to several millimetres dimensions. The thickness or the depth should be chosen based on the required properties of the coating. Figure 2.15 shows a few of the surface engineering processes with their corresponding layer thicknesses or penetrated depths.

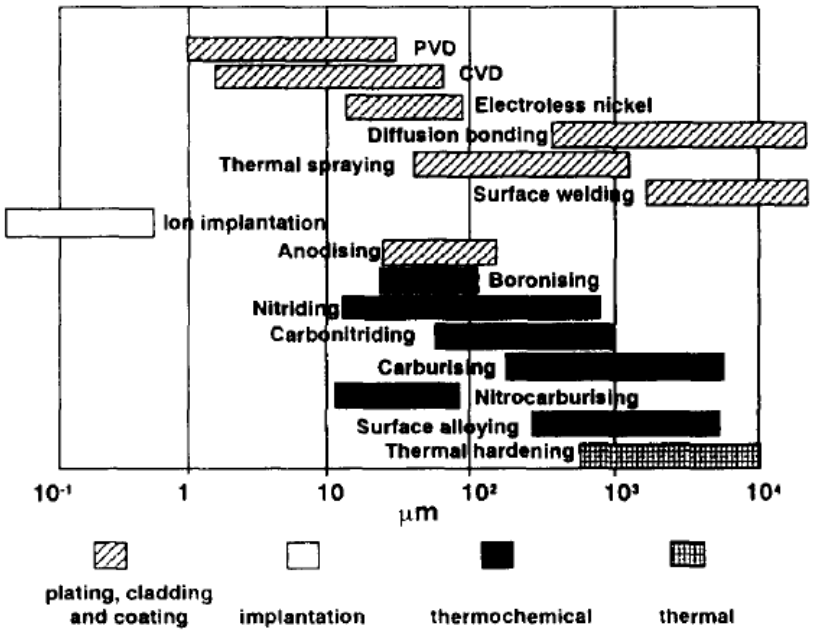

Figure 2.15: Thickness of modified layers for different techniques [46]

The hardness of the engineered layers can be in a wide range from only 250-350 HV for some spray coatings, to 1000 HV for nitride steels. Other surface engineering methods can produce harder layers in the range of 3500 HV (in PVD coatings) [47, 49].

The developments in surface engineering technology have made it possible to deposit almost any kind of material on any substrate. This flexibility, as good as it might be, has caused serious problems for the engineers. The infinite possible combinations that can be applied to a specific condition make the choice of right coating material and surface engineering technique difficult. The "fitness-to-purpose" is the correct understanding of the condition, base material and the required properties and then the choice of technique and coating material. A total engineering approach and a more systematic design methodology must be applied to ensure the success of the surface engineering [50].

Table 2.16 shows the sequence of events in the manufacturing of an engineering component that requires surface engineering. Looking at a surface engineered component as a composite of a substrate and an engineered surface, the engineer must decide based on the requirements of the condition and the existing properties of the substrate, since some of those properties can be adequate for some of the required conditions. Then the surface will be engineered to provide the properties that were not obtainable from the base material [49].

Table 2.16: The sequece of events in the manufacuring of a component that requires SE [49]

Step	Event
1	Application
2	Properties required
3	Design
4	Materials selection
5	Engineering substrate
6	Engineering surface
7	Lubrication
8	Performance

The frequent required properties of engineering components are listed in Table 2.17. In most cases only one of these properties is required for the engineering components, but in some cases requirements are needed for a combination of failure mechanisms such as wear/fatigue/friction/corrosion. The selection of the suitable surface treatment is obviously more complex in these situations but by a logical analysis of the failure mechanisms and the available surface engineering techniques, the selection will be easier [49].

Table 2.17: The typical required properties of engineering components [49]

1	Abrasive wear resistance under conditions of low compressive loading
2	Abrasive wear resistance under conditions of high compressive loading
3	Resistance to scuffing or seizure
4	Bending or torsional strength
5	Bending or torsional fatigue strength
6	Resistance to mechanical pitting
7	Resistance to surface crushing (surface collapse)
8	Resistance to corrosion and erosion

2.5 Laser Cladding

One of the surfacing processes that can be used to repair the worn parts and turn them back to their original dimensions is laser cladding. In this research the feasibility of using laser cladding technology to repair the worn railway axles is investigated.

In laser cladding, the laser beam scans the substrate melting the cladding material and a thin layer of the substrate producing a very strong metallurgical bond between the cladding material and the substrate (Figure 2.16) [51, 52]. Due to the unique properties of laser which can provide localized heating of the substrate, a high quality coating can be achieved which is pore free, crack free and has a strong bond with the base material. Laser cladding makes it possible to coat almost any kind of component with a wide range of cladding materials [53].The only process that can deposit a coating with low porosity and strong fusion bond, with minimum dilution is laser cladding. In laser cladding, due to the nature of the laser beam, it is possible to focus the energy only on the surface of the component and therefore avoid the penetration of heat into the substrate [50, 54].

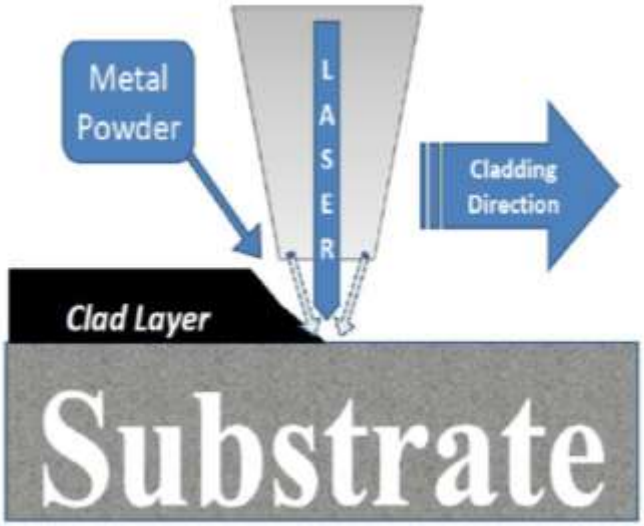

Figure 2.16: Schematic of laser cladding

Laser metal processing attracted a lot of research interest and the work of researchers developed this technology. Among these researchers was W.M. Steen whose work had a big impact on laser cladding. Laser cladding was done for the first time in the late 1970's by Gnanamuthu at Rockwell International Corporation in California. The first reported commercial use of laser cladding was the hard facing of Nimonic turbine blade at Rolls Royce in 1981 [52, 55].

Laser cladding has found a wide application in the remanufacturing and repairing of metal parts in many countries like USA, UK and China. These companies utilize laser cladding to repair turbine blades, automotive and aircraft parts and engine valve seats.

There are different conventional cladding techniques such as plasma arc, spraying, welding techniques like TIG welding and chemical vapour deposition. Some of these techniques are like laser cladding; thermal processes, which means that the coating procedure includes introducing some heat into the component. The main concern with such processes is the effect of the heat input on the properties of the parent metal and the formation of the "heat affected zone".

A well confined and intense source of energy like laser beam has the ability to heat and melt only specific areas without affecting the base material heavily. Hence, the HAZ formed during laser cladding is much smaller than the heat affected zones formed in other thermal processes.

Other advantages of laser cladding are the high input energy, low physical distortion and high surface quality. The process is also very flexible since any kind of material can be deposited on any substrate which makes laser cladding suitable for a wide range of applications [56]. Also rapid heating and cooling rates in laser cladding lead to the formation of non-equilibrium phases which possess useful properties [57].

2.5.1 Different methods of Laser Cladding

Laser cladding can be done in two different ways:

- Two-step laser cladding
- One-step laser cladding

In two-step laser cladding the cladding material is preplaced on the surface of the substrate in the form of powder bed while in the one-step laser cladding the coating material is injected to the melt pool in the form of powder, wire or paste [54].

2.5.1.1 Two-step laser cladding

The first stage in the two-step laser cladding is applying a preplaced layer on the part in the form of a powder bed. This is then followed by scanning the powder bed with the laser beam and an inert gas (Figure 2.17). A melt pool is formed on top of the preplaced powder bed as the result of laser radiation and is then expanded to the surface of the substrate. As the melt pool penetrates the substrate the fusion bond is formed between the clad layer and the base metal [52].

This method is the simplest laser cladding method but there are some concerns about it. The first important issue is the cohesion between the powder particles and also between the powder bed and the substrate. Since the powder bed should be shrouded in the inert gas, if the powder particles do not have enough cohesion with the substrate they cannot stick to it and the clad dose not form [54]. To prevent this, ethanol is used as a binder to mix with the powder. The side effect of using this chemical binder is the formation of pores due to its evaporation which is an important shortcoming of this method [52, 54].

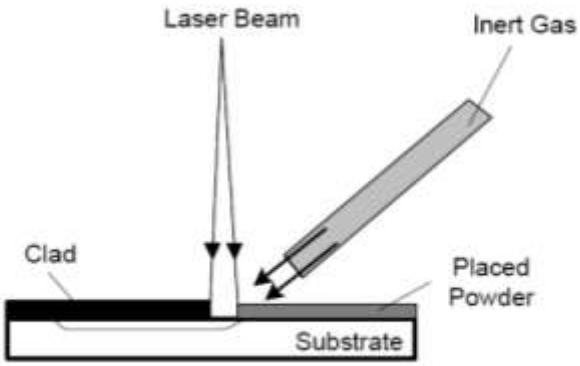

Figure 2.17: Two-step laser cladding [52]

2.5.1.2 One-step Laser Cladding

In single-step laser cladding an additive material is injected into the melt pool in the form of powder, wire or paste. Among all, laser cladding by powder injection has attracted the most interest [57]. A carrier gas, usually Argon or Helium, is used to inject the powder into the melt pool. This process solves the problem with complex geometries and needs minimum surface preparation. Powder can be injected into the melt pool in two ways: side feeding or coaxial feeding. When the powder is fed coaxially it is possible to produce uniform tracks [56]. When the powder is injected from the sides the accurate alignment of the powder stream

and the melt pool can cause difficulty. Figure 2.18 shows a schematic view of laser cladding with powder injection.

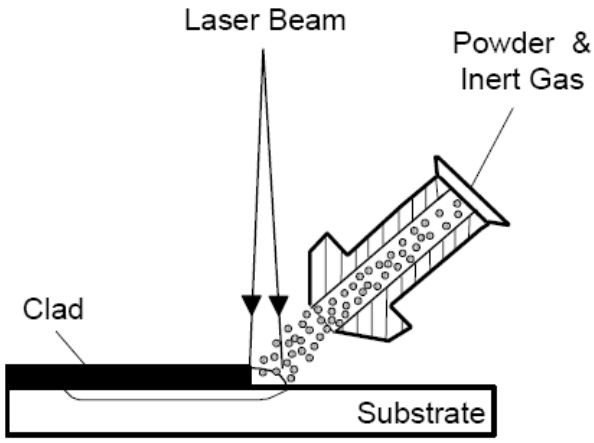

Figure 2.18: One-step laser cladding with powder injection [52]

In one-step laser cladding with wire, instead of metal powders, metal wires are fed to the melt pool. Metal wires are cheaper than metal powders and less material is wasted in laser cladding with wire compared to powder injection method but the result has a lower surface quality compared to that of the laser cladding with powder injection [52]. Figure 2.19 shows laser cladding with wire.

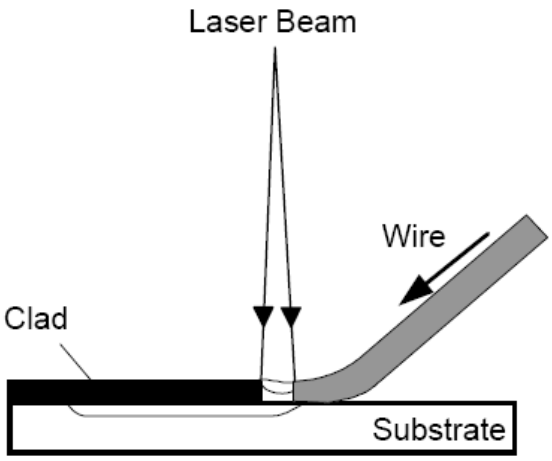

Figure 2.19: One-step laser cladding with wire feeding [52]

In laser cladding with paste injection, the metal powder is mixed with a binder to form the metal paste. This process is very sensitive to the paste feeding system. If insufficient paste is fed to the substrate, the desirable thickness will not be achieved. And if too much paste is injected, the clad will be porous due to the evaporation of the binder [52].

2.5.2 Clad geometry and important dimensional characteristics

In laser cladding with powder injection, when laser heats and melts the powder and the thin layer of the substrate, a single track is formed. Wide areas can be covered by overlapping of the single tracks with typically 50% -60% step-over. The cross sectional view of a single bead includes three different regions:

- The clad
- The melted substrate
- The heat affected zone (HAZ)

The clad is the melted powder which was injected to the melt pool and the melted substrate is the substrate penetrated area (Figure 2.20).

Figure 2.20: The cross sectional view of a single track

Weerasinghe and Steen (1983) found that different combinations of cladding parameters can form three different shapes of clads. Figure 2.21 shows the different cross sectional views that can be obtained from different parameters. The first form (Figure 2.21.a) can be caused by rapid scanning speeds and insufficient laser energy to melt the injected powder which can also lead to the formation of inter-run porosity. Low powder feed rates can lead to a clad with the cross sectional view of shape in Figure 2.21.b, in which only a small portion of laser energy is absorbed by the powder and most of the laser energy penetrates the substrate causing the formation of major dilution. The last shape (Figure 2.21.c) is the optimum result with minimum dilution and reasonable thickness which can suit the needs of many applications [57, 58].

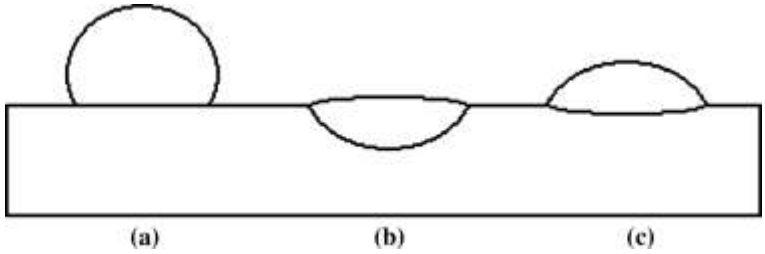

Figure 2.21: The three cross sectional views of a single track [58]

One of the most important requirements of a laser clad part is having low amounts of dilution. The penetrated substrate as shown in figure 2.20, which is also called "the alloying zone", is a mixture of the added material and parent metal [51]. Dilution is calculated from the following equation (Eq.2.2).

$$Dilution\ (\%) = \frac{Melted\ Area}{Clad\ Area + Melted\ Area} \times 100 \qquad \text{(Eq.2.2)}$$

One of the dimensional characteristics of a single bead in laser cladding is wetting angle or contact angle (Figure 2.22). The contact angle shows the adherence between the clad and the substrate. Small contact angles show good adherence whereas obtuse angles show insufficient adherence. When the clad makes an obtuse angle with the substrate, it means that the clad is too high with respect to its width (Figure 2.22). In this case the clad blocks the laser and stops it from reaching and melting the powder between overlapping tracks, causing the formation of inter-run porosity [59, 60]. Aspect ratio which is the ratio of clad width to the clad height is used to define the possibility of the occurrence of inter-run porosity and can be calculated from equation 2.3. W.M. Steen (1987) [54] suggests that in order to avoid the formation of porosity in multiple track claddings, the aspect ratio must be above 5.

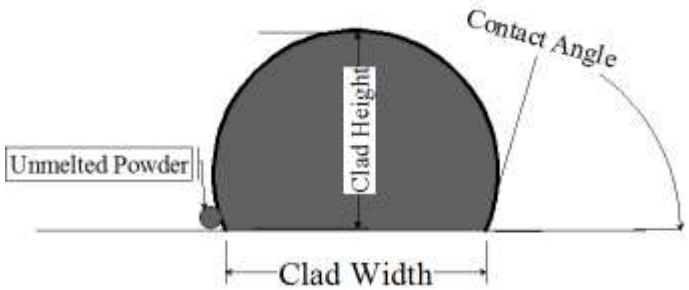

Figure 2.22: Contact angle and inter-run porosity

$$Aspect\ Ratio = \frac{Clad\ Width}{Clad\ Hight} \qquad \text{(Eq. 2.3)}$$

2.5.3 Important Input Parameters in Laser Cladding

The processing parameters of laser cladding must be chosen to obtain a crack-free, pore-free and high quality clad with low dilution. Many factors affect the output of the cladding process but among all, the most important parameters are:

- Laser power
- Powder feed rate
- Laser scanning speed
- Laser beam spot size
- Laser beam energy distribution
- Gas supply

The laser power density should be in the range of 10^2-10^4 W/cm^2 with an interaction time of 10^{-3}-0.5 seconds, which is the required amount of energy to build a strong metallurgical bond between the clad layer and the substrate, yet does not cause high amounts of dilution [56]. The clad characteristics like clad height, width and dilution are governed by the processing parameters. The height of a single track increases by a slower scanning speed or higher powder feed rate. Clad width is usually equal to the laser beam but an increase in the gas supply, scanning speed or the powder feed rate can result in narrower tracks [51]. Minimum dilutions are obtained by high amounts of gas supply, rapid scanning speeds and low amounts of laser energy.

The processing parameter optimization is one of the main steps which should be carried out prior to cladding itself. For each substrate/cladding material and cladding equipment combination, a new set of experiments should be done to achieve the optimum parameters. Many studies have been done on the parameter optimization of different cladding situations and investigation of the effect of the cladding parameters on the geometrical characteristics of the clad [61, 62].

2.5.4 Applications

The main areas for laser cladding can be categorized in three different applications:

1. Coating
2. Repair and Refurbishment
3. Rapid Prototyping and Tooling

Rapid prototyping and tooling is a novel technique to manufacture complex components which were traditionally produced by mold makes, CNC and electrical machining. Laser cladding has offered an easier, cheaper and faster technique to produce these tools and components.

Here the other two applications of laser cladding are discussed due to the relevance of these areas to the current work.

2.5.4.1 Coating

Laser cladding has been widely used to coat the industrial parts and components that require some surface properties that are irreconcilable with the bulk properties. The properties such as high wear resistance, corrosion resistance and high temperature resistance can be achieved by applying a thin layer of the selected material which possesses the required properties while the bulk provides the load carrying capability. Some of the examples of the materials that can be used as the cladding material are: chromium, titanium, nickel and copper based alloys. Molds, engine valve seats and hydraulics pump components are now widely coated by laser cladding technology. Aircraft gas turbines are also another example of the parts coated with laser cladding. Gas turbines operate in high temperature and therefore require some surface properties such as high temperature resistance. Nickel based super alloys which possess this particular property as well as high strength are widely used to coat the gas turbines. The shroud interlock between turbine blades also require high wear resistance as the friction between the sliding surfaces can lead to material loss of the blades [52].

2.5.4.2 Repair and Refurbishment

Laser cladding has found a wide application in the repair and refurbishment of high value components. The industrial parts and components often suffer from over machining in manufacturing, loss of fit due to wear and deep scratches. Replacing the part with a new part can be very expensive and the economic approach is repairing and refurbishing the part using a technology that leaves the original properties of the material untouched. Laser cladding can be used to build up on the under machined, worn or scratched component and bring it back to size. The conventional method for refurbishment and repair of such parts and components were different welding techniques. The concern with those processes was the creation of HAZ and therefore degrading of the mechanical properties of the component. Another

priority of laser cladding to the conventional welding techniques is that laser cladding has made it possible to use any un-weldable material (e.g., Aluminium alloys) as the cladding material [52].

Many parts and components are repaired and refurbished by laser cladding. Gas turbine blades are an example of such parts which operate in very high temperatures and under a lot of pressure which is why the turbine blades suffer from different damages during operation such as erosion caused by the condensation of water droplets from the hot steam and life cycle fatigue [63]. The damaged turbine blades are usually repaired by laser cladding turning them back to size while maintaining the original properties of the base material.

In the following section, refurbishment of railway axles with laser cladding is discussed as a potential future application of laser cladding.

2.5.5 Cracking of laser clad coatings

The most important issue with laser cladding is that the laser clad parts sometimes crack and fail during service. The major reasons for cracking of laser clad parts are:

- The presence of residual stresses which form in the part during and after laser cladding. The main sources of residual stresses are phase transformations that happen as a result of rapid heating and cooling during laser cladding, thermal stresses as a result of high temperature gradients and mismatch of properties between the clad layer and the substrate.
- The presence of metallurgical defects such as pores and voids.
- Mechanical defects such as rough surfaces and inclusions.

The preventive techniques to avoid the formation of clad cracks in wear resistant coatings cover three major steps:

1) The cladding material
2) The cladding parameters
3) The pre-treatment and post treatment processes

The preventive measures for clad cracking which use the features of cladding materials are:

1) Choosing a cladding material with a thermal expansion coefficient close to that of the substrate. This is referred to as "the thermal expansion and heat capacity matching principle" which eliminates some of the thermal residual stresses generated during laser cladding. Also the substrate should have a low heat capacity to absorb minimum heat and avoid the formation of temperature gradients.
2) Increasing the toughness of the cladding material by adding alloying elements to the cladding material. As mentioned earlier, the crack growth is favoured by the presence of low toughness material. An example can be adding Ni and Co to Fe based alloys which stabilize tough phases in steels.
3) Helping the generation of phases with high solubility for impurities and harmful elements by alloying the cladding material to change the tissue morphology. This will prevent the formation of hot cracks as described earlier.
4) Using and intermediate transition layer of a material with high resistance to cracking and similar thermal coefficient with the substrate. An example would be the use of Ni based alloys as the interface cladding layer for Fe based substrates since Ni based alloys have a close thermal coefficient to that of the Fe based alloys [64].

Other preventive measures which uses pre-treatment and post treatment processes are also used to avoid the formation of cracks in the clad layer and HAZ. The substrate preheating before treatment and slow cooling after treatment are effective preventive methods. The essence of preheating and slow cooling is that these processes decrease the temperature gradient which is helpful to decrease the residual stresses [64]. A study was carried out to investigate the influence of base preheating on cracking of the laser clad cobalt-based satellite SF6 coatings in 2003 [65]. The base material was X2OCrMoV12-1 and X1OCr13 chromium steels. The results indicated that the preheating decreased the cooling rates and thermal gradients which resulted in lower levels of residual stresses. The samples which were preheated at 750 K had a reduced number of cracks and there were no cracks in the samples which were preheated at 920 K [65].

Another study was conducted by Wang and Xie in 2002 to investigate the effect of substrate temperature on the cracking behaviour of the transitional zone between an Al-Si substrate and a Fe based coating. Since Aluminium can react with most common elements, the transitional zone between the Al-Si substrate and the Fe based clad layer contained brittle aluminides such as FeAl3, Fe2Al5 and NiAl3 which had very low tensile strengths. The laser clad

samples were examined to see the effect of different substrate temperatures on the cracking behaviour of the transitional zone. The results indicated that the samples at lower temperatures (200-220 C) contained some residual cracks in the transitional zones due to rapid cooling rates and high temperature gradients. These cracks were eliminated in the samples which were preheated to higher temperatures (275 C).It was concluded that preheating the substrate prior to cladding produces a more homogenous transitional zone and also increase the resistance to cracking [66].

Chapter 3

Experimental Procedures

3.1 Sample Preparation

AISI 1018 mild steel was chosen as the railway axle steel for the tests since it is one of the most widely used materials for the manufacturing of railway axles. The chemical composition and mechanical properties of mild steel are presented in Tables 3.1 and 3.2. Round bars with the dimensions of 2000 mm x 25 mm were CNC machined to make hourglass fatigue samples (Figure 3.1). These samples were prepared in order to obtain the fatigue strength of mild steel (without any claddings) as a reference to be used later for comparison with the clad samples.

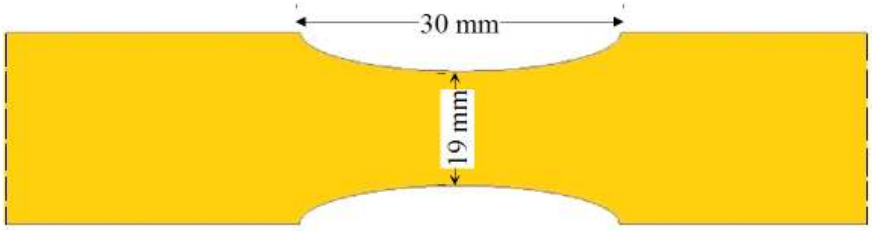

Figure 3.1: Middle section of the hour glass shaped fatigue samples

To prepare samples for laser cladding, an extra groove was machined out in the already existing reduced area of the hourglass shaped fatigue samples, to be later built up by laser cladding. The diameter of the reduced area of the fatigue samples was 19 mm and the extra groove had a diameter of 18 mm to allow a 0.5 mm built up with laser cladding on each side (Figure 3.3). Figure 3.2 shows the schematic of the fatigue samples with the extra groove. To ensure that all the notches are exactly identical all samples were machined using a CNC system and with the same dedicated tool, leaving a smooth surface which eliminated the need of pre-cladding surface preparation.

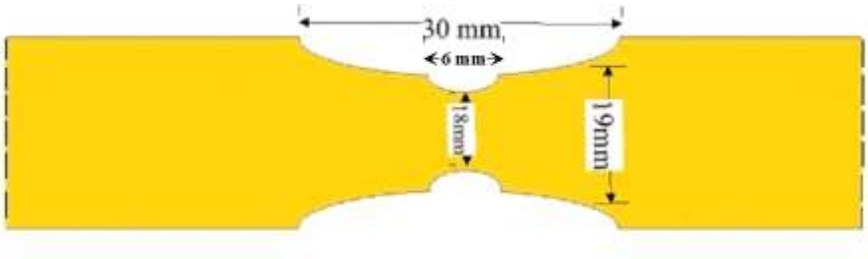

Figure 3.2: Reduced area of the fatigue sample with an extra groove machined in the middle for laser cladding

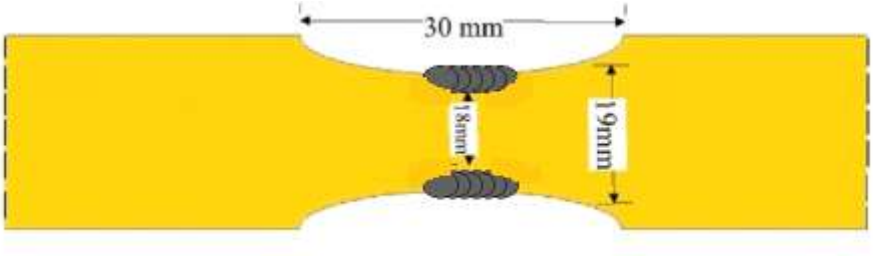

Figure 3.3: Schematic of a laser clad sample

Table 3.1: Chemical composition of AISI 1018 mild steel (Mass %)

Fe	C	Mn	P	S
98.81-99.26	0.14-0.25	0.6-0.9	Max 0.04	Max 0.05

Table 3.2: Mechanical properties of AISI 1018 mild steel

Tensile Strength, Ultimate	Tensile Strength, Yield	Elongation	Reduction of Area	Modulus of Elasticity
440 MPa	370 MPa	15%	40%	205 GPa

The samples with an extra groove in their reduced areas also simulated the undersized worn railway axle; therefore to be able to compare the fatigue strength of the laser clad samples with worn railway axles, some of these samples were not laser clad for future fatigue testing.

3.2 Laser Cladding

A 4 KW IPG fibre laser was used for laser cladding the samples. In fibre lasers, the active medium for producing the laser is an optical fibre doped with rare-earth elements such as Ytterbium.

Figure 3.4: IPG fibre laser

A 6-axis robot (Motoman XRC SK 16 X) was used to control a coaxial laser nozzle to deposit about 2 mm wide single track clads (Figure 3.5).

Figure 3.5: 6-axis robot used to control the laser nozzle

The laser head (Figure 3.6) delivers powder to the melt pool coaxially to the laser beam.

Figure 3.6: Coaxial laser heads

Only the powders that fall directly into the laser spot melt and therefore contribute to the formation of the clad layer. Melting efficiency is described as the part of the powder coming out of the nozzle that falls into the melt pool and forms the clad. In order to have the maximum melting efficiency the standoff distance from the laser head to the surface of the working piece was set so that the focal point of the powder stream was set on the surface where the melt pool was located.

Due to the wearing of the laser head and powder nozzle eventually the laser beam and the powder focus can be misaligned. For optimum operation, the alignment of the laser beam and the powder focus was checked before each cladding to avoid loss of material. If the laser beam is not exactly in the centre of the laser head, only part of the laser power can be used to melt the powder which decreases the melting efficiency. Figure 3.7(a) and 3.7(b) show the two possible positions of the laser beam with respect to the laser head. In this experiment, the alignment of laser beam and the laser head was checked prior to each cladding.

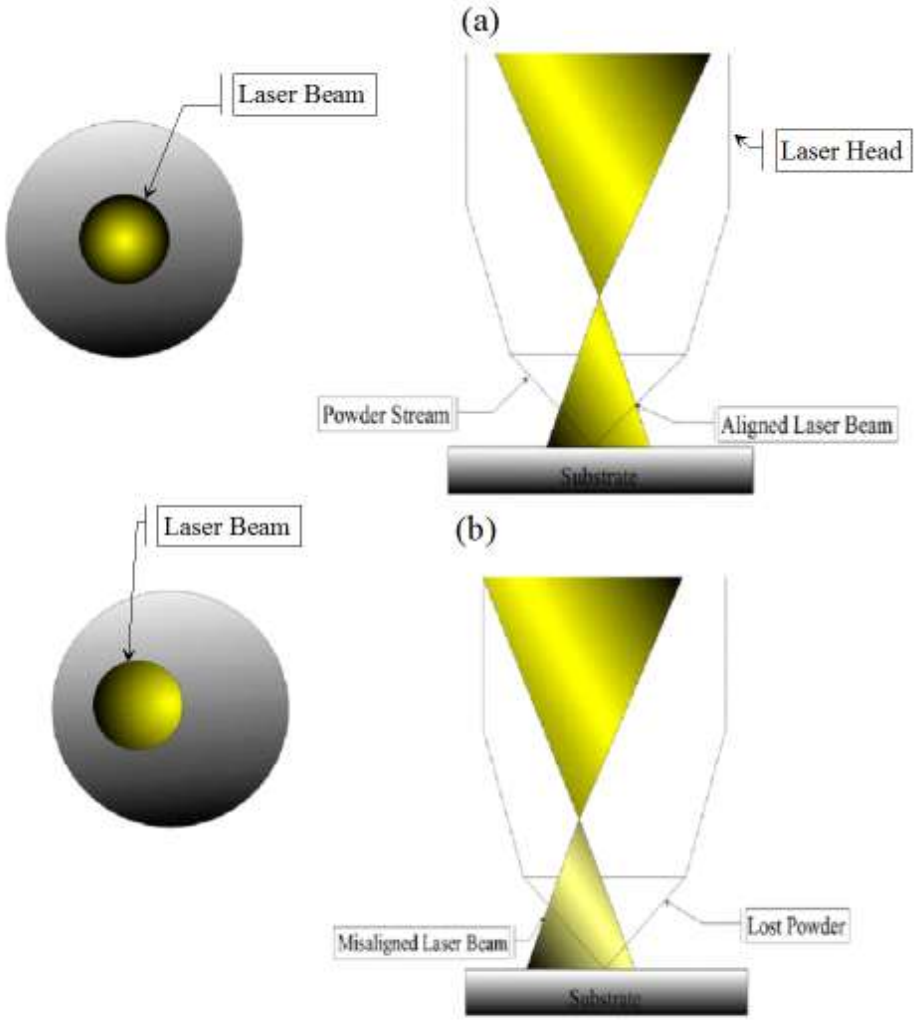

Figure 3.7: Effect of the laser beam alignment on the melting efficiency (a) aligned laser beam (b) misaligned laser beam and lost powder

The powder feeder used was a Sultzer-Metco twin-10 (Figure 3.8). The powder flow rate was set by the powder feeder. Due to the wearing of powder nozzle by the powder itself, the flow rate of powder was not constant and therefore before each cladding the powder flow rate was examined to see if there were any changes in the nozzle. To examine the powder flow rate, the powder feeder would start running for one minute and the powder which came out of it would get collected in a container. Then the powder would be weighed and the flow rate was therefore determined.

Figure 3.8: Sultzer-Metco twin-10 powder feeder

The melt pool was shielded from Oxygen picked up from the atmosphere. Typically Argon and Helium are used as shielding gas. Helium is more expensive but gives a better protection. In this experiment Helium was used both as the carrier gas and as the shielding gas. The flow rate of the shielding gas was 30 Litre/min and the flow rate of the carrier gas was 20 Litre/min.

Another required set up for the experiment was the tilt angle of the laser head. Since the back reflection of the laser beam can melt the nozzle, the head was fixed at 10 degrees with respect to the substrate normal (Figure 3.9). To get consistent clad tracks, the tilt angle was kept constant for all the trials.

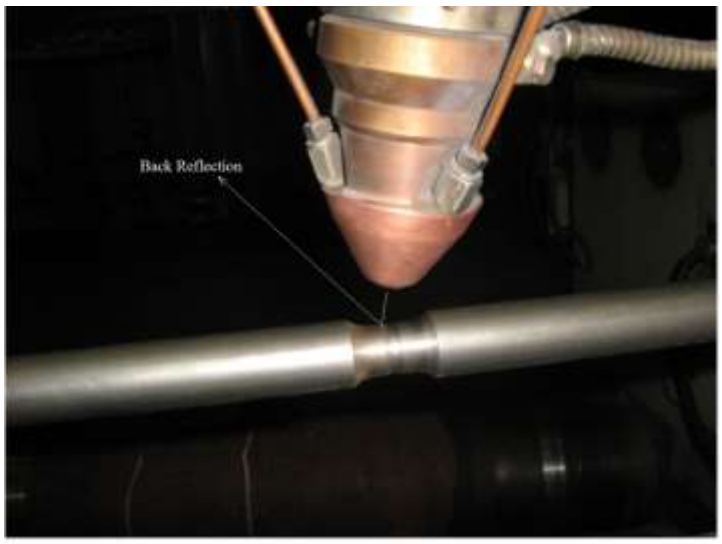

Figure 3.9: Set up of cladding head with respect to the workpiece

3.3 Processing Parameters

Table 3.3 shows the processing parameters used for laser cladding the samples. The samples were set up in a lathe prior to cladding in order to have a rotary motion with respect to the laser head which only had a linear movement.

Table 3.3: Processing parameters for laser cladding

Laser Spot	Laser Power	Scanning Speed	Powder Feed Rate
2 mm	1200 W	750 mm/min	25 g/min

The RPM (revolutions per minute) at which the lathe had to run at was calculated based on the required scanning speed and the diameter of the groove which was the cladding section. The calculations were as below:

Circumference of the groove of the samples:

$2\pi r = 2 \times \pi \times 9 = 56.52$ mm

Therefore:

750 mm/min = (750/56.52) Revolutions/min = 13.26 RPM

Prior to each trial, all the processing parameters including the powder feed rate, laser power and spot size were set to the values given in Table 3.3.

3.4 Preheat

Preheating was done to remove all the moisture on the surface of the samples. The moisture (H_2O) can break into oxygen and hydrogen and the gas can get trapped in the clad layer and produce porosity. All the samples were preheated to 150° C prior to cladding. The preheating was carried out with a torch and the temperature of the sample was continuously monitored by a digital thermometer (Figure 3.10). As soon as the temperature of the part reached 150° C, the cladding started.

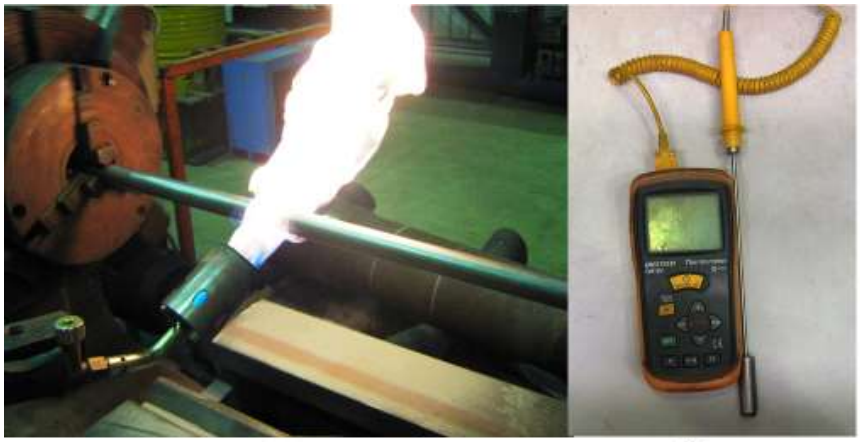

(a) (b)

Figure 3.10: (a) Preheating of a rotating sample (b) Digtal thermometer used for monitoring the temperature

3.5 Cladding Program

The laser cladding programme used for the trials was called “Rotary Step” programme. It was a programme designed to do single tracks (rings) by keeping the laser head steady until the sample rotated once. The waiting period for the laser head was calculated as below:

Time for one rotation: T

$$T = \frac{60\ Seconds}{13.26\ Rounds} = 4.52 \text{ Seconds}$$

The 2 mm laser spot resulted in about 2 mm wide single tracks. 50% step over was chosen to cover the whole groove length (6mm) by 6 single tracks. After each single track (ring) the cladding would stop until the temperature of the part reached the room temperature and then the following track was deposited. Since the samples were not the actual size of the railway axles, they could get overheated easily and the wait after each single track helped avoid this. Figure 3.11 shows a sample being laser clad.

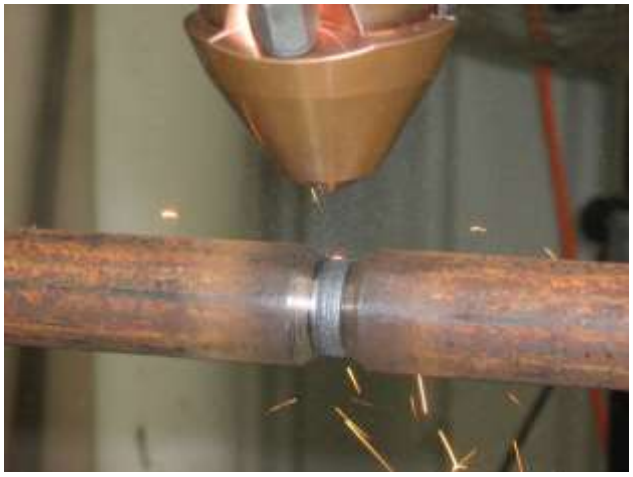

Figure 3.11: A sample being laser clad

3.6 Cladding Materials

To study the effect of cladding material on the fatigue strength of the laser clad railway axles two different cladding materials were used for cladding the samples. First group of samples were clad with 420 stainless steel powder (grade 45-125 μm) supplied by Höganäs Belgium Pty Ltd. Tables 3.4 and 3.5 show the chemical composition and mechanical/Physical properties of 420 stainless steel alloy. Railway axles work in humid environments and in the presence of acids, therefore one of the most important requirements of such components is high corrosion resistance. The high content of Chromium (12.3%) in 420 stainless steel makes this material a good option where high corrosion resistance is required. Morphology of the 420 stainless steel powder particles is given in Figure 3.12.

Table 3.4: Chemical composition of 420 stainless steel (% mass)

C	Fe	Mn	Cr	Si
0.23	Base	1.1	12.3	0.6

Table 3.5: Mechaical and physical properties of 420 stailess steel powder

Density	Flow Rate
4.24 gr/cm^3	15 sec/50 gr

(a)

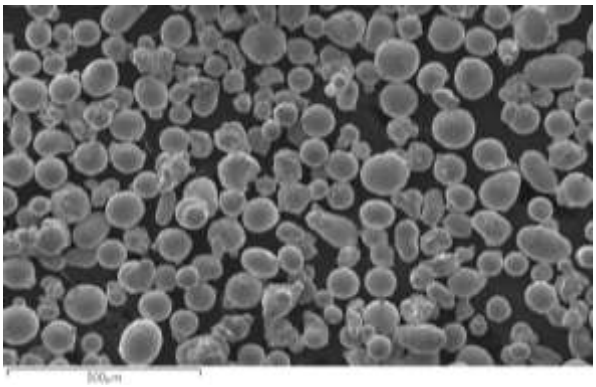

(b)

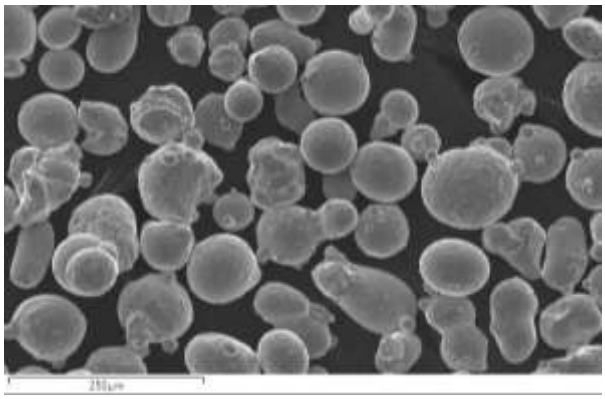

Figure 3.12: SEM images of 420 stainless steel powder at (a) low magnification and (b) high magnification

The next group of samples were clad with 17CrMoV5 gas atomised powder supplied by Stellite Robtec Australasia Pty Ltd. Tables 3.6 and 3.7 show the chemical composition and mechanical properties of the alloy. Rail axles are subjected to high number of load cycles and can suffer from fatigue cracking; therefore using CrMoV which is a relatively ductile material which is less susceptible to brittle cracking can prevent premature failure of the laser clad axles. SEM images of the powder showing spherical type particles with some irregularities are given in Figure 3.13.

Table 3.6: Chemical composition of GS-17CrMoV5 alloy

C	Si	Mn	P	S	Cr	Mo	Ni	V
0.19	0.50	0.70	0.01	0.02	1.35	0.95	0.0	0.22

Table3.7: Mechanical properties of GS-17CrMoV5 alloy

Proof Stress (2%)	Ultimate Tensile Strength	Elongation	Impact ISO-V
441 MPa	588 MPa	15 %	24 Joules

(a)

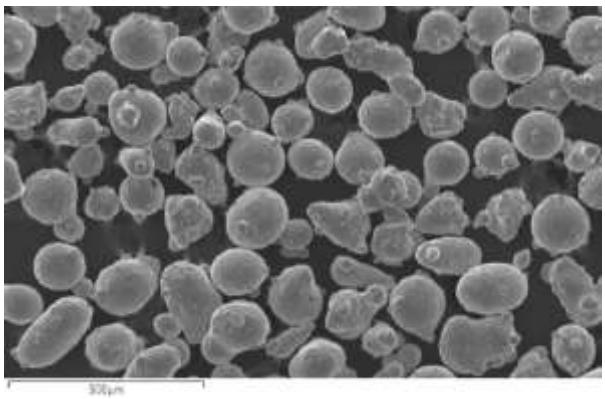

(b)

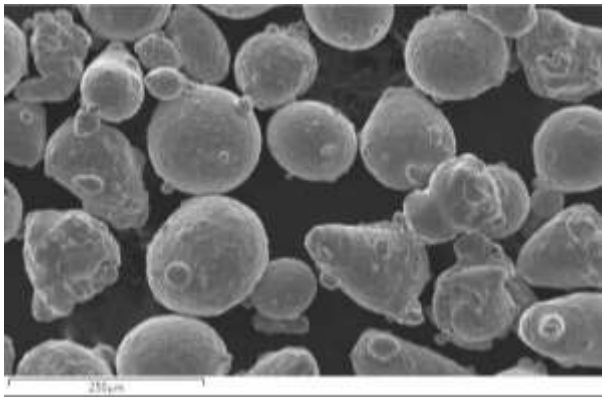

Figure 3.13: SEM images of CrMoV powder at (a) low magnification and (b) high magnification

3.7 Post-Clad Heat Treatment

The residual stresses in the laser clad samples created during laser cladding as a result of high temperature gradients, rapid cooling rates and phase transformation can lead to the pre mature failure of these parts. Post-clad heat treatment releases some of these stresses and therefore is considered to be a preventive method for micro cracking of the clad parts.

In the present research, a wide range of heat treatments were applied to the laser clad samples to investigate the effect of post-clad heat treatment temperature on the fatigue strength of

cladded samples. Table 3.8 summarizes the different heat treatment conditions applied on the samples.

Table 3.8: Experimental design- post clad heat treatment

Sample	Heat Treatment Condition
420 Stainless Steel clad samples	No Post-Clad Heat treatment
420 Stainless Steel clad samples	Heat treated at 200 °C for 1 hour
420 Stainless Steel clad samples	Heat treated at 400 °C for 1 hour
420 Stainless Steel clad samples	Heat treated at 580 °C for 1 hour
GS-17CrMoV5 clad samples	No Post-Clad Heat treatment
GS-17CrMoV5 clad samples	Heat treated at 200 °C for 1 hour
GS-17CrMoV5 clad samples	Heat treated at 400 °C for 1 hour
GS-17CrMoV5 clad samples	Heat treated at 580 °C for 1 hour

3.8 Rotary Bending Fatigue Tests

In order to evaluate the fatigue strength of laser clad axles and compare them with unclad axles, a dedicated rotating bending fatigue test machine was designed and used at Hardchrome Engineering Pty Ltd in Melbourne Australia. The machine uses the very exact principles of such test in that it rotates a round bar at a fixed rotation speed where the RPM is known and the rotation time before fracture is automatically measured by a dedicated counter attached to the motor. The load which needs to be applied to the bar is transferred to the bar using two bearings which are attached to a plate underneath them. The plate is itself attached to a screw which is wound down and locked in place to introduce any desired load and deflection at the centre of the bar where a notch has also been machined out to make it more susceptible to fracture. To ensure the same amount of load and deflection is applied to all bars, the deflection at the centre is measured by a calibrated vernier and the screw and the plate are locked using two nuts at the bottom of the machine. Figures 3.14 and 3.15 show the machine and its main parts.

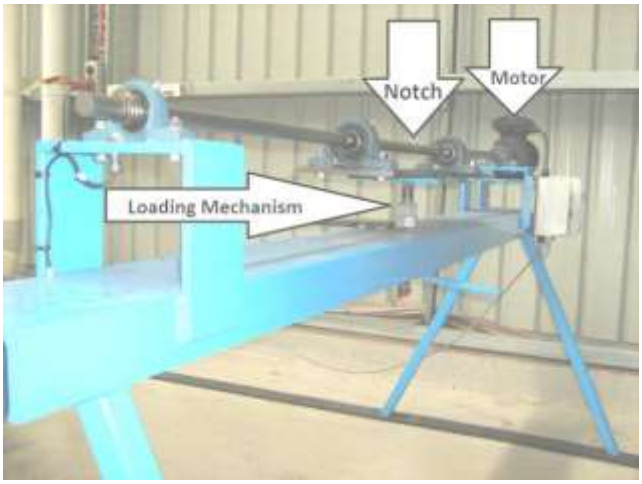

Figure 3.14: Rotary bending fatigue machine designed at Hardchrome Engineering, Melbourne, Australia

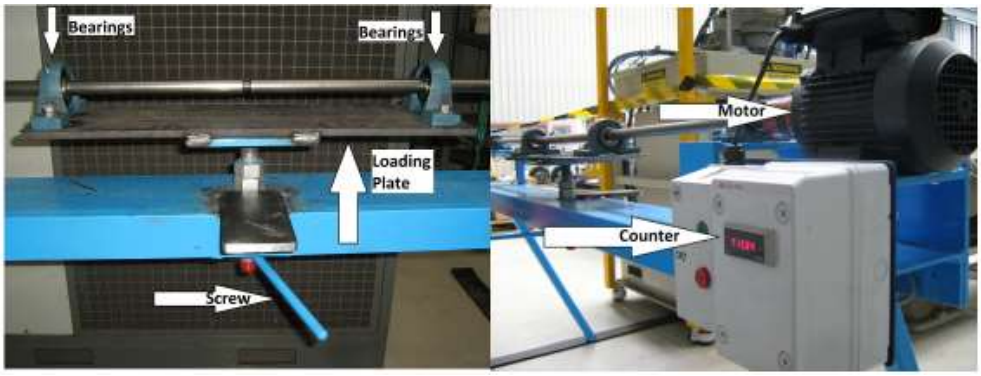

(a) (b)

Figure 3.15: Rotary bending fatigue testing machine (a) Loading plate, screw and bearings (b) Motor and counter

All the tests were done according tointernational standard for rotating metal bar bending fatigue testing (IS0 1143-1975 (E)). The standard specifies that nominally identical test pieces should be used each being rotated and subjected to a bending moment. The test is continued until the test piece fails or until a pre-determined number of stress cycles have been exceeded.

In the case of this research, all samples were tested until fracture. Figure 3.16 shows a fractured sample at the notched zone.

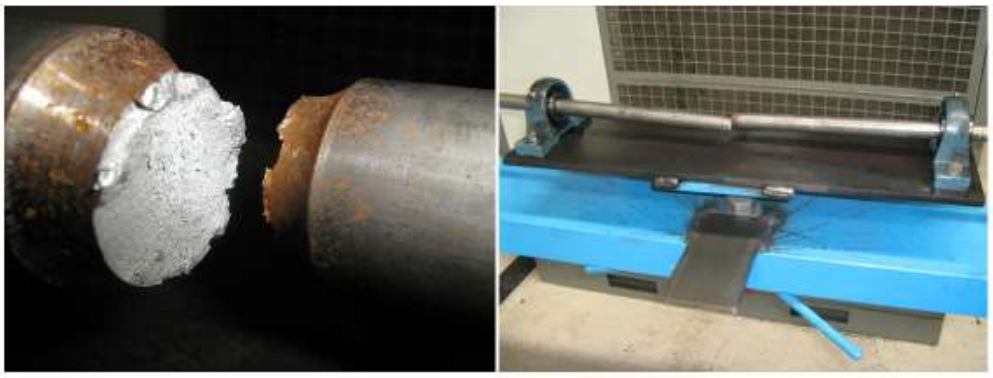

(a) (b)

Figure 3.16: (a) Fractured sample (non-clad) at the notched zone (b) the two bearings holding the sample and the loading system

The deflections of all the samples were kept constant at 18 mm. The applied load was calculated using the beam deflection formula as given below:

The maximum deflection= 18 mm

$\frac{PL^3}{48\ EI}$ = Maximum deflection (Eq 3.1)

Where P is the applied load, L is the distance between the two bearings shown in Figure 3.16(b), E is the elastic modulus of mild steel and I is the moment of inertia of the shaft which has a circular cross section with a diameter of 19 mm in the reduced section of the fatigue samples and is calculated as below:

$I = \pi r^4/4$

$I = \pi \times (19/2)^4/4$

$I = 6393.8\ mm^4$

The distance between the two bearings is 600 mm and the elastic modulus of mild steel is 210,000 MPa. The applied load is calculated by substituting these numbers in equation 3.1:

$\frac{PL^3}{48\ EI}$= 18 mm

$\frac{P\times 600^3\ mm^4}{48\times 210{,}000\ MPa\ \times 6393.8\ mm^4}$= 18 mm

P= 5370.85 N

3.9 Microscopy and Hardness Measurements

The samples were sectioned for failure analysis and to investigate the cause of fracture. To get a good understanding of the quality of the claddings in the samples, 4 sections of each sample were studied (Figure 3.17).

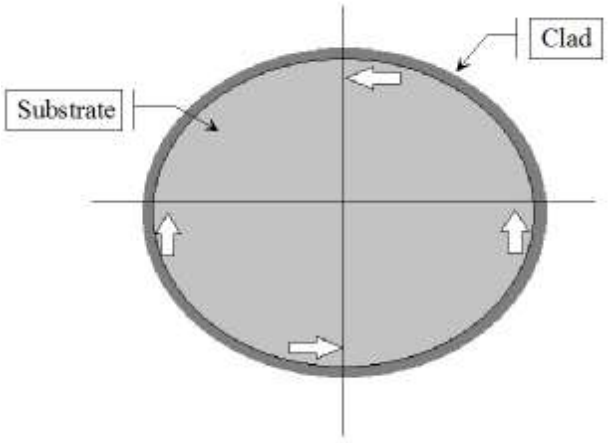

Figure 3.17: The 4 studied sections of each sample

Each sample was prepared for microscopy, in accordance with ASM procedures. A 2% Nital acid solution (2 cc HNO_3 + 98 cc Ethyl alcohol) was used to etch each clad sample. Nital was not a suitable etchant for the cladding material (420 stainless steel or CrMoV). To etch the clad layer for metallurgical investigations, Viella's solution was used which contained 5cc HCl + 2g Picric acid + 100 cc Ethyl alcohol.

Metallurgical examinations were performed using an Olympus GX71 optical microscope and hardness measurement was conducted using a Buehler micro hardness tester (Figure 3.18).

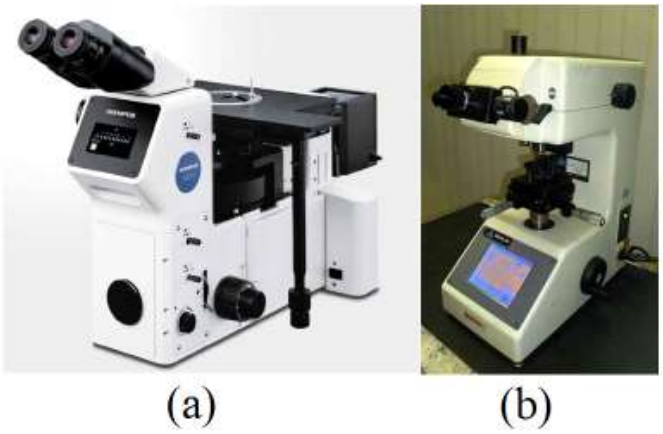

Figure 3.18: Metallurgical investigation (a) Olympus GX71 optical microscope (b) Buehler micro hardness tester

3.10 Post-test Fractography

Fractography of the broken samples was carried out with an XL30 Philips scanning electron microscope (Figure 3.19). Images were taken with high magnifications up to 2000 X to investigate the fracture mode both in the clad and the base material.

Figure 3.19: XL30 Philips scanning electron microscope

Chapter 4

Results and Discussion

4.1 Rotary Bending Fatigue Test Results

The results of the rotary bending fatigue tests are presented as the number of cycles to failure under consistent testing conditions. The load and the RPM of the motor were kept constant for all the samples.

4.1.1 Fatigue Results of Non-Clad Samples

Table 4.1 shows the fatigue results for the non-clad samples. There were two groups of non-clad samples. The first group of samples had a single notch with the outer diameter (OD) of 19 mm. These samples were tested without any cladding to be used as reference samples for future comparison with the fatigue results of laser clad samples. The next group of non-clad samples which had an extra groove in the already reduced section of the hourglass shaped fatigue samples were designed to simulate the worn undersized railway axles.

Figure 4.1 compares the fatigue results of the non-clad samples with different geometries. The average numbers of cycles experienced with each of these two groups of samples are presented in Table 4.2 for comparison. As shown in the table, there is a 48.38% difference between the average number of cycles which were carried out by these two sets of samples. The big difference was caused by the reduced diameter in the undersize machined samples. Under identical testing conditions including the testing load and the rotation speed of the motor, the group of samples with the lower diameter broke earlier than the other group.

Table 4.1: Fatigue results of the non-clad samples with two different diameters

Sample	Geometry of the sample	Number of cycles to failure
1	Single notch with the OD of 19 mm	62,733
2	Single notch with the OD of 19 mm	61,491
5	Single notch with the OD of 19 mm	59,482
19	Single notch with the OD of 19 mm	62,310
20	Single notch with the OD of 19 mm	61,205
21	Single notch with the OD of 19 mm	60,521
36	Single notch with the OD of 19 mm	59,856
16	An extra groove in the notch with the OD of 18 mm	24,562
17	An extra groove in the notch with the OD of 18 mm	34,248
18	An extra groove in the notch with the OD of 18 mm	35,779

Table 4.2: Average number of cycles to failure experienced by non-clad samples with different diamateres

Sample	Average number of cycles to failure
Non-clad samples with an OD of 19 mm in the notched area	**61,085**
Undersize machined non-clad samples with an OD of 18 mm in the notched area	**31,529**
Difference	**-48.38%**

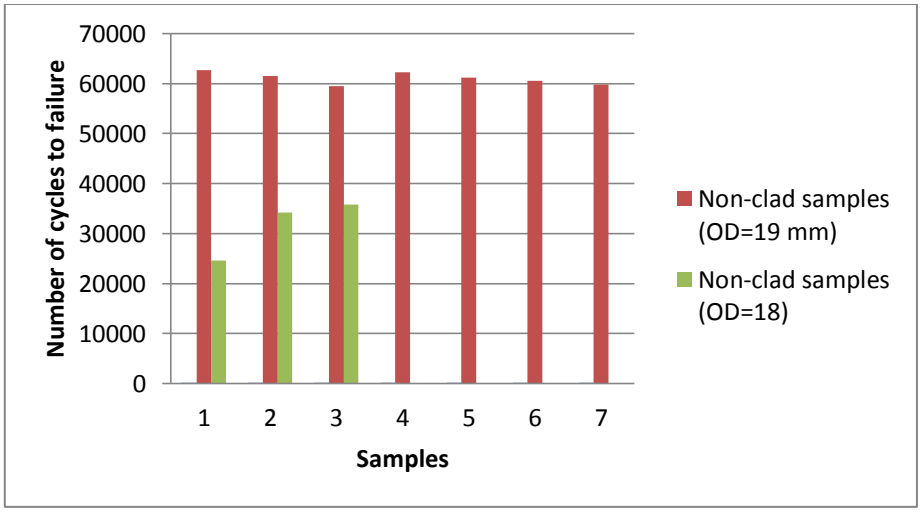

Figure 4.1: Number of cycles to failure experieneced by non-clad samples with different diameters

4.1.2 Fatigue Results of 420 Stainless Steel Clad Samples

4.1.2.1 Fatigue Results of 420 Stainless Steel Clad Samples Heat Treated at 580° C for 1 hour

Table 4.3 shows the rotary bending fatigue test results for laser clad samples clad with 420 stainless steel powder, heat treated at 580° C for 1 hour. All the samples were laser clad with the same cladding parameters and tested under identical testing conditions.

Table 4.3: Number of cycles to failure experienced by 420 stainless steel clad samples heat treated at 580°C for 1 hour

Sample	Heat Treatment Condition	Nf
3	580° C for 1 hour	65,342
4	580° C for 1 hour	59,582
14	580° C for 1 hour	60,331
15	580° C for 1 hour	28,580
22	580° C for 1 hour	50,225
23	580° C for 1 hour	52,060
24	580° C for 1 hour	50,248
25	580° C for 1 hour	49,244
26	580° C for 1 hour	52,138
27	580° C for 1 hour	58,715
30	580° C for 1 hour	61,211
37	580° C for 1 hour	20,879

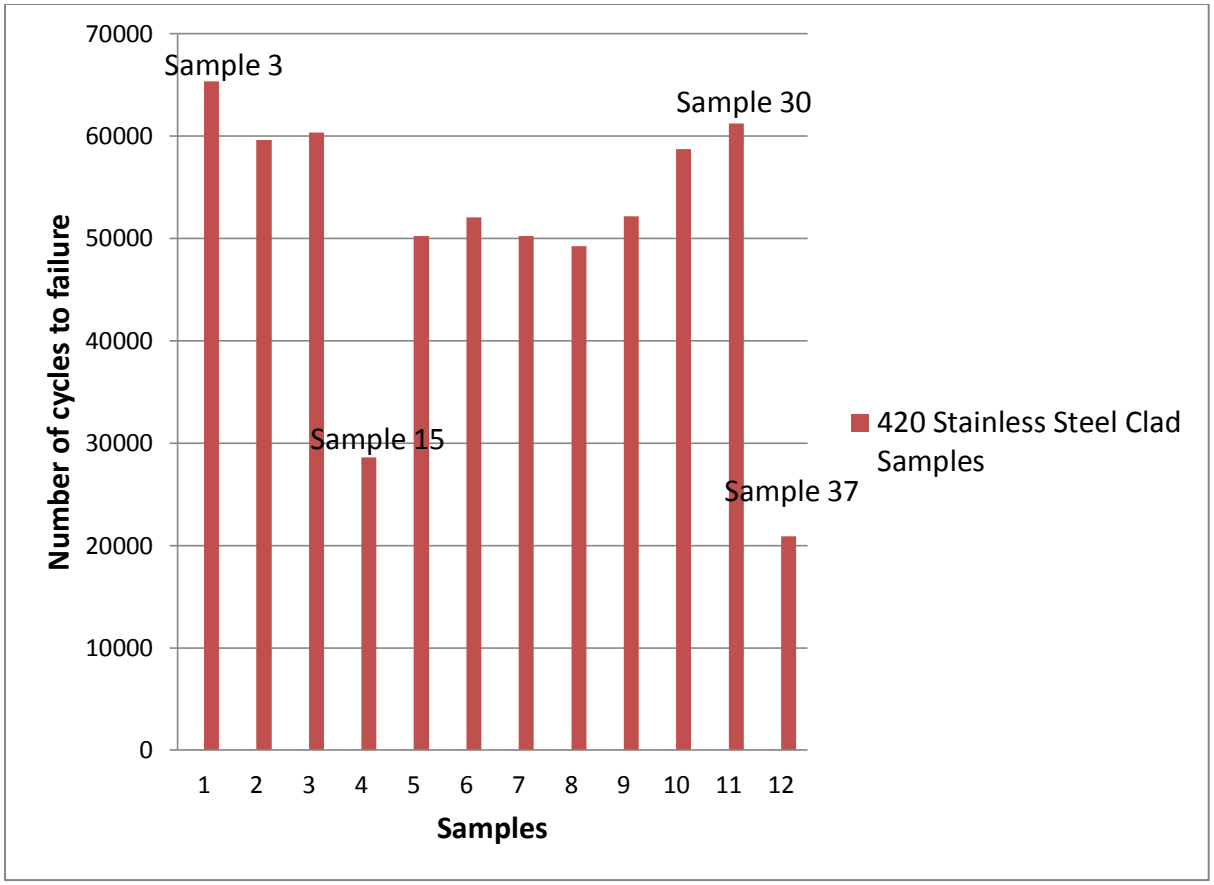

Figure 4.2: Rotary bending fatigue test results for 420 stainless steel clad samples heat treated at 580° C for 1 hour

Figure 4.2 shows the same results on a graph. As can be seen in the graph, samples 3 and 30 lasted the longest number of cycles to failure and samples 15 and 37 lasted the lowest number of cycles.

The first two samples which were sectioned and compared were sample 3 (N_f= 65,342) and sample 15 (N_f= 28,580) with 56.2% difference in their fatigue lives. The cross sectional views of these two samples are shown in Figures 4.3 and 4.4 The macro images show that sample 3 which lasted a relatively high number of cycles to failure had no defects in its clad layer while sample 15 which broke at a number of cycles which was 56.2% less than that of the sample 3 had micro cracks along the clad layer. These micro cracks initiated from the surface of the sample and propagated into the clad layer and substrate and led to the premature failure of the sample. Mechanical defects such as surface roughness and discontinuities could have been the crack initiation sites in the case of this sample. These surface defects act as stress concentrators and become the crack initiation sites when the sample is stressed.

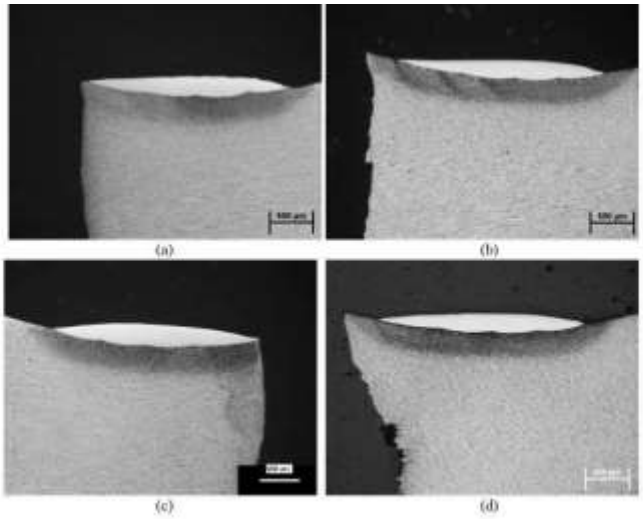

Figure 4.3: The metallurgical images obtained from the different cross sections of sample 3 (420 stainless steel clad, Nf= 65,342) showing no metallurgical defects in the clad

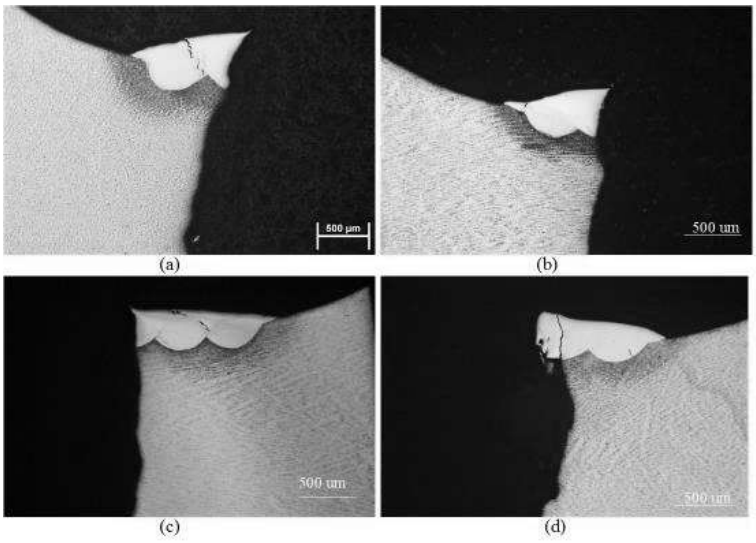

Figure 4.4: The metallurgical images obtained from the different cross sections of sample 15 (420 stainless steel clad, Nf= 28,580) showing micro cracks in the clad layer routing from the surface

Figure 4.5 shows the interface between the clad layer and the substrate in sample 3 which lasted the longest number of cycles among the 420 stainless steel clad samples. As can be seen in the image, the metallurgical bond between the clad and the substrate was very strong for sample 3 and no defects (cracks/porosities) were detected in the clad layer or in the interface between clad and HAZ.

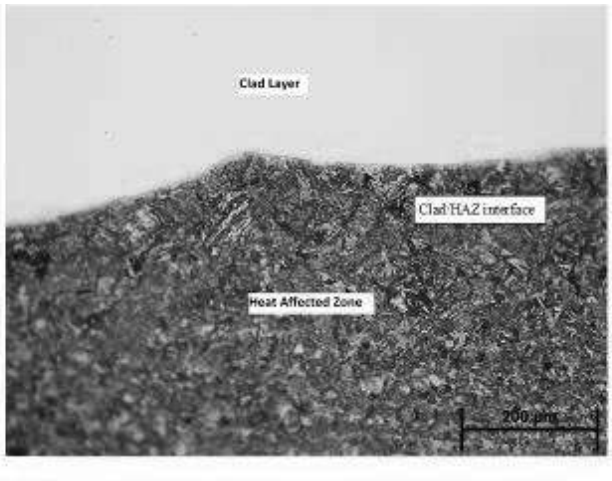

Figure 4.5: Strong metallurgical bond between the 420 stainless steel clad layer and the substrate in sample 3 (420 stainless steel clad , Nf=65,342)

Figure 4.6 shows section “d” of sample 15 (as previously shown in Figure 4.4) with a crack along its clad. Higher magnifications of this section show that the crack which is linked to the fracture surface initiated from the surface and propagated into the substrate and led to the premature failure of the sample. The presence of mechanical defects on the surface of the samples such as surface roughness and discontinuities which act as stress concentrators and crack initiation sites decreased the fatigue strength of the clad sample significantly.

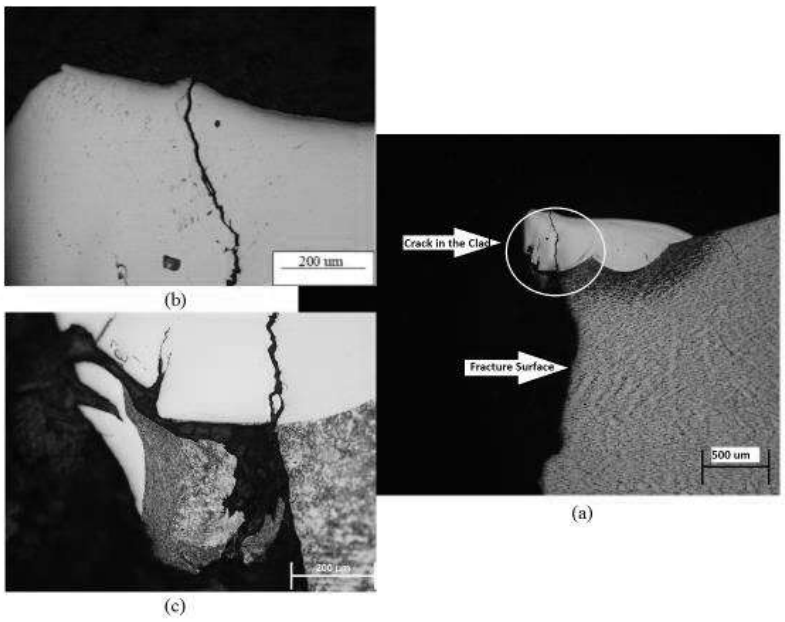

Figure 4.6: Section "d" of sample 15 (420 stainless steel clad ,Nf= 28,580) (a) the clad profile showing the crack along the clad layer linked to the fracture surface (b) the crack initiated from the surface of the clad (c) the crack reached the substrate and led to the premature failure of the sample

The next pair of samples which were investigated to explain the difference between their fatigue results under identical testing conditions were sample 30 (Nf=61,211) and sample 37 (Nf= 20,879) with 65.89% difference in their fatigue lives. The cross sectional views of 4 sections of each of these samples are shown in Figures 4.7 and 4.8.

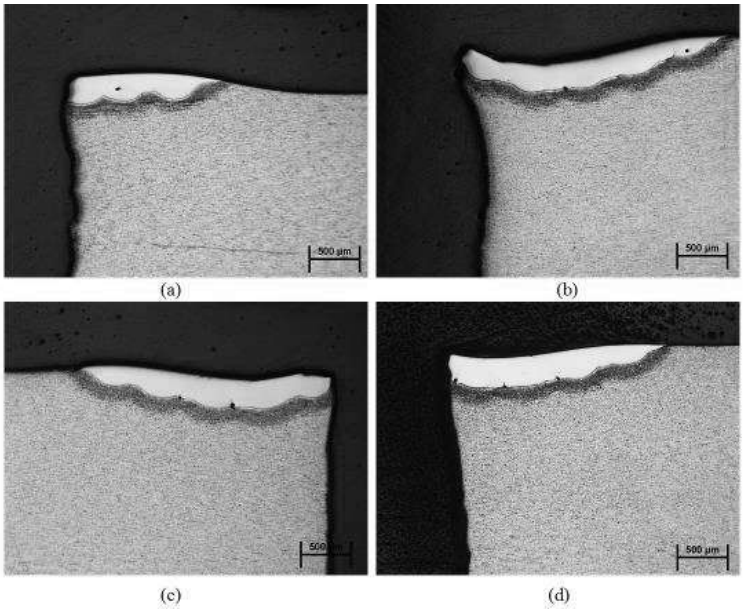

Figure 4.7: The metallurgical images obtaied from 4 different sections of sample 30 (420 stainless steel clad , Nf=61,211)

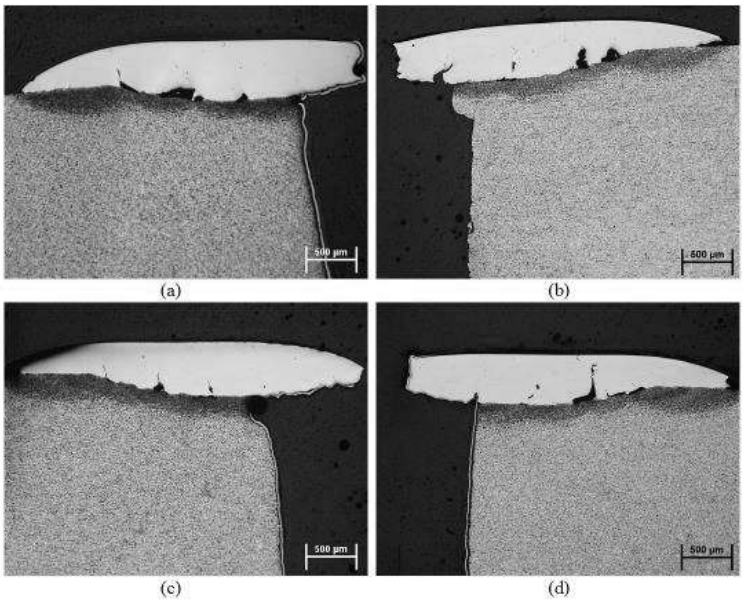

Figure 4.8: The metallurgical images obtained from 4 different sections of sample 37 (420 stainless steel clad , Nf=20,879)

The metallurgical images of both samples show the presence of porosities in the interface of clad layer and substrate. Inter-run porosity is the result of the shape of the clad bead and happens when the clad is too high with respect to its width and it makes an obtuse angle with

the substrate (Figure 4.9). The clad blocks the laser and stops it from reaching and melting the powder between overlapping tracks, causing the formation of inter-run porosity. W.M. Steen (1987) suggests that in order to avoid the formation of porosity in multiple track claddings, the aspect ratio must be above 5 [54].

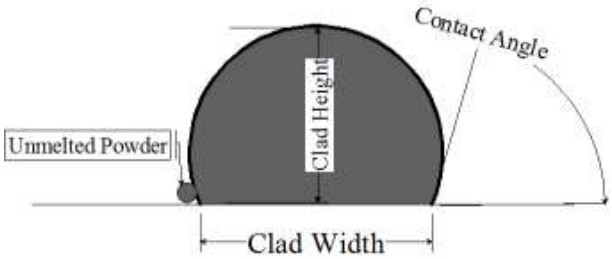

Figure 4.9: Unmelted powder and inter run porosity

Figure 4.10 shows an SEM image taken from one of the porosities in sample 30. The unmelted powder remained trapped between two overlapping tracks, producing a metallurgical defect which weakens the bond between the clad layer and the base material and can act as a stress concentrator and crack initiation site. Figures 4.11 and 4.12 show the porosities in sample 30 and sample 37 and the micro cracks which initiated from them. It can be understood from these images that the presence of porosities decreases the fatigue life of laser clad samples.

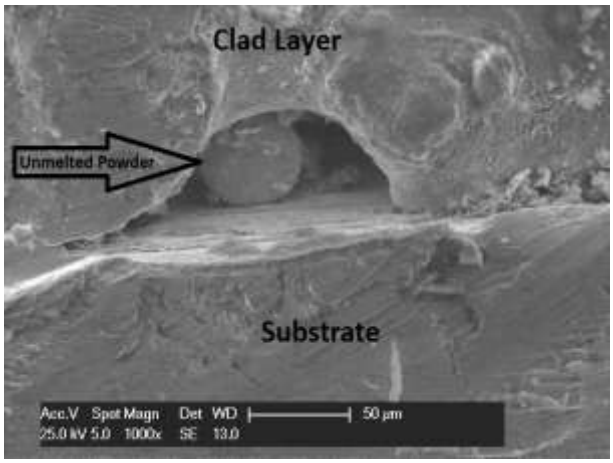

Figure 4.10: SEM image showing one of the pores in sample 30 (420 stainless steel clad)

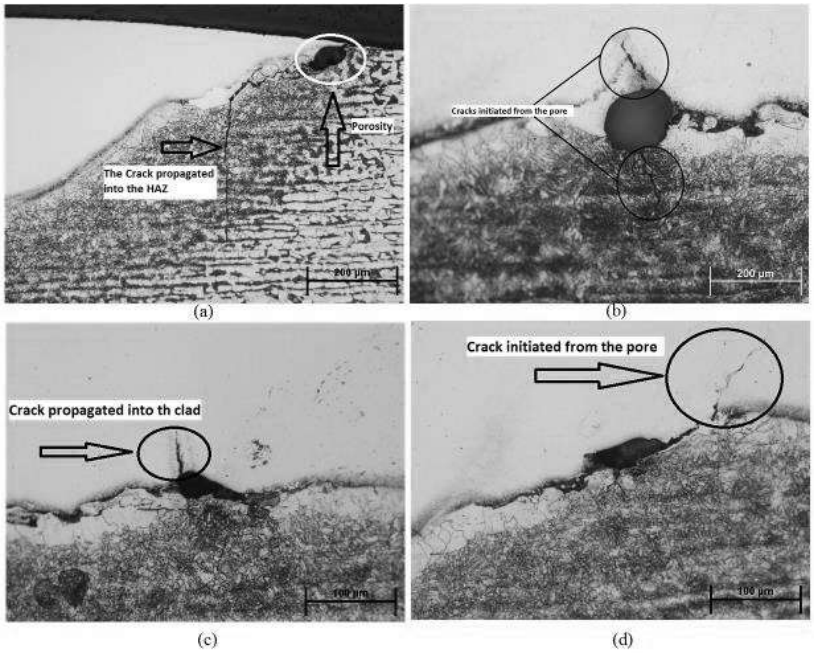

Figure 4.11: Porosities in sample 30(420 stainless steel clad) and the cracks initiated from them

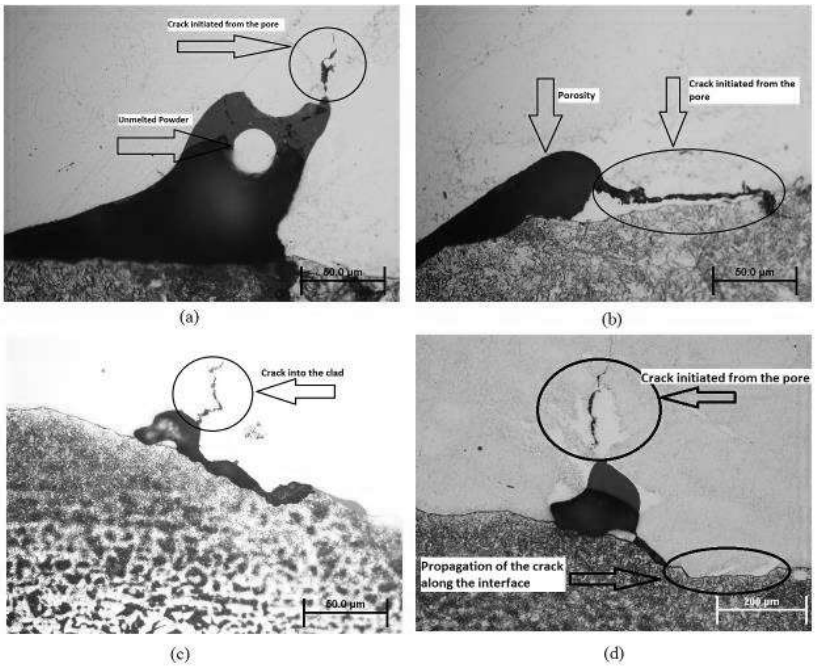

Figure 4.12: Porosities in sample 30 (420 stainless steel clad) and the cracks initiated from them

The cracks which initiate from pores can propagate and reach the critical size and lead to the fracture of the samples. Figure 4.13 shows the porosity which was possibly the initiation site for the crack that caused the failure of sample 37.

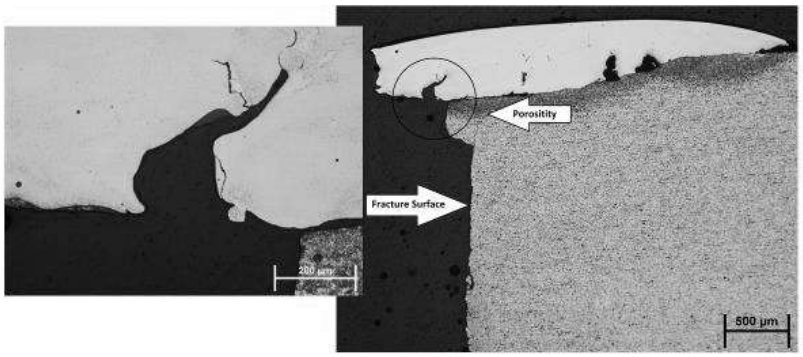

Figure 4.13: Porosity in sample 37 (420 stainless steel clad) linked to the fracture surface

A comparison was made between sample 3 (Nf= 65,342) and sample 30 (Nf= 61,211). The cross sectional images of sample 3 shown in Figure 4.3 indicate that both the clad layer and the interface between the clad and HAZ were defect free. Whereas, the metallurgical images obtained from sample 30 show the presence of pores and the micro cracks which initiated from these pores (Figure 4.11 and Figure 4.12). These metallurgical defects decreased the strength of sample 30 to a value of 61,211 cycles which is 6.32% less than that of sample 3.

Another comparison was made between the fatigue strengths of sample 30 and sample 37. Both of these samples had defects in their clads, therefore the only possible way to compare their clad qualities was by measuring the areas of the defects (porosities) and the areas of the clad layers in all the 4 sections studied for each of these samples in order to calculate the $\frac{total\ defected\ area}{total\ clad\ area}$ ratio for each of these samples. The area measurement was carried out using iGrafx Designer software. The areas of all the pores were measured for all the 4 sections of each sample then they were summed up to get "the total defect area". Figure 4.14 shows the $\frac{total\ defected\ area}{total\ clad\ area}$ % versus number of cycles to failure for these samples. As can be seen in the graph, there is an inverse relationship between the percentage of defected area and the number of cycles to failure experienced by each sample, indicating that metallurgical defects decrease the fatigue life of laser clad samples.

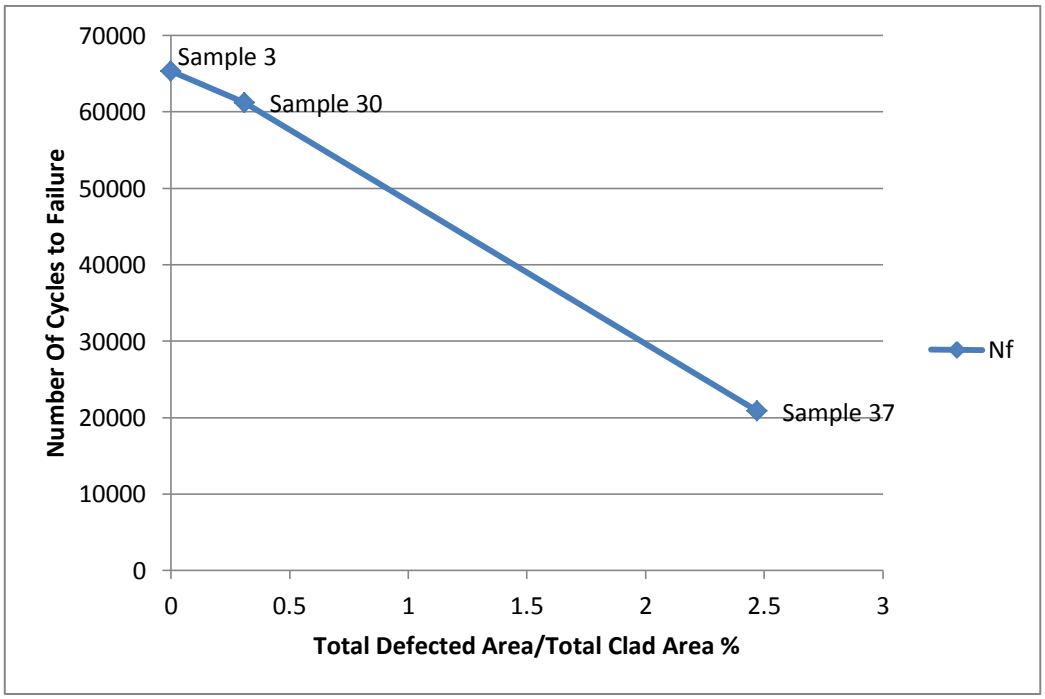

Figure 4.14: Number of cycles to failure versus the percentage of the defected area in the clad layer for samples 3, 30 and 37

4.1.2.2 Fatigue Results of 420 Stainless Steel Clad Samples with Different Post Clad Heat Treatment Conditions

Table 4.4 shows the rotary bending fatigue test results for laser clad samples coated with 420 stainless steel powder, under identical testing conditions but with different post-clad heat

treatments. The numbers in the first column indicate how the samples were labeled for testing. Figure 4.15 compares the average number of cycles to failure for 420 stainless steel clad samples with different post-clad heat treatment conditions. The laser clad samples heat treated at 580° C lasted the longest number of cycles to failure. The second highest average number of cycles was for the samples which were heat treated at 200° C. Laser clad samples with no post-clad heat treatment broke at lower average number of cycles compared to the 580° C heat treated and 200° C heat treated samples, but lasted longer than the 400° C heat treated samples.

Table 4.4: Number of cycles to failure experienced by 420 stainless steel clad samples with different post-clad heat treatment conditions

Sample	Heat Treatment Condition	Nf
3	580° C for 1 hour	65,342
4	580° C for 1 hour	59,582
14	580° C for 1 hour	60,331
15	580° C for 1 hour	28,580
22	580° C for 1 hour	50,225
23	580° C for 1 hour	52,060
24	580° C for 1 hour	50,248
25	580° C for 1 hour	49,244
26	580° C for 1 hour	52,138
27	580° C for 1 hour	58,715
30	580° C for 1 hour	61,211
37	580° C for 1 hour	20,879
57	200° C for 1 hour	49,539
58	200° C for 1 hour	48,124
59	400° C for 1 hour	42,376
60	400° C for 1 hour	41,798
61	No post-clad heat treatment	45,579
62	No post-clad heat treatment	45,326

Table 4.5: Average number of cycles to failure experienced by 420 stainless steel clad samples with different post-clad heat treatment conditions

Post-clad Heat Treatment Condition	Average number of cycles to failure
Heat treated at 580° C for 1 hour for 1 hour	55,908
Heat treated at 400° C for 1 hour	42,087
Heat treated at 200° C for 1 hour	48,831
No post-clad heat treatment	45,452

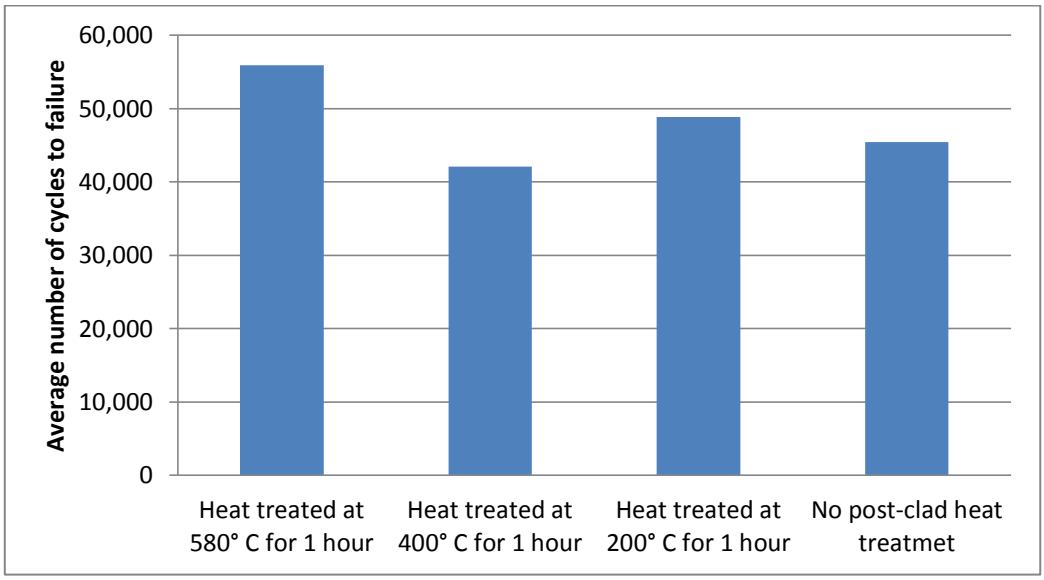

Figure 4.15: Average number of cycles to failure experienced by 420 stainless steel clad samples with different post-clad heat treatment conditions

Micro hardness measurements were done on the 420 stainless steel clad samples with different post-clad heat treatment conditions to investigate the effect of heat treatment on the hardness profiles of the samples. Hardness measurements were carried out from the surface of the clad to the HAZ and the substrate. Figure 4.16 compares the hardness profiles of 420 stainless steel clad samples with different post-clad heat treatment conditions. The results indicate that the samples which were heat treated at 580° C had the lowest hardness in the clad layer (341.8 HV). By decreasing the post-clad heat treatment temperature to 400° C the hardness of the clad layer increased to an average of 413.15 HV. The clad layer of the samples which were heat treated at 200° C after laser cladding had an average of 460.7 HV.

The clad layer of the samples with no post-clad heat treatment had the highest hardness (485.7 HV).

The hardness profiles can explain the fatigue behaviour of 420 stainless steel clad samples. Suitable post-clad heat treatment decreases the brittleness of the clad material and increases its fatigue life by releasing some of the residual stresses that was formed during laser cladding and also by softening the clad layer.

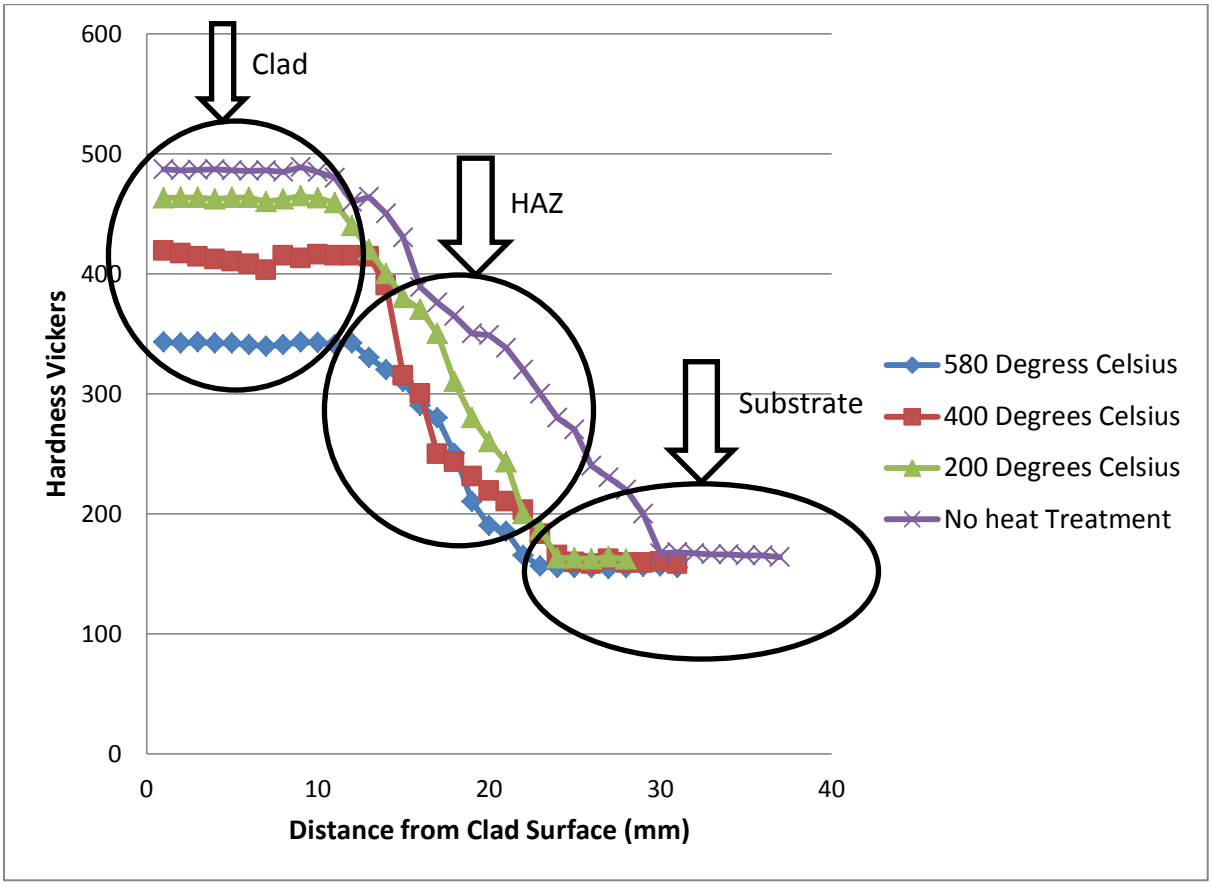

Figure 4.16: Hardness profiles for 420 stainless steel clad samples with different post-clad heat treatments

The samples which were heat treated at 400° C were sectioned for metallurgical investigations to study why they failed before the samples heat treated at 200° C. The cross sectional images obtained from the 4 different sections of sample 60 (Nf=41,798) are shown in Figure 4.17. The sample had porosities in its clad layer and the presence of metallurgical defects led to the failure of the samples at cycles which were even lower than 200° C heat treated or no post-clad heat treated samples. It can be concluded that the presence of metallurgical defects has a stronger negative effect on fatigue properties than the positive effect of post-clad heat treatment.

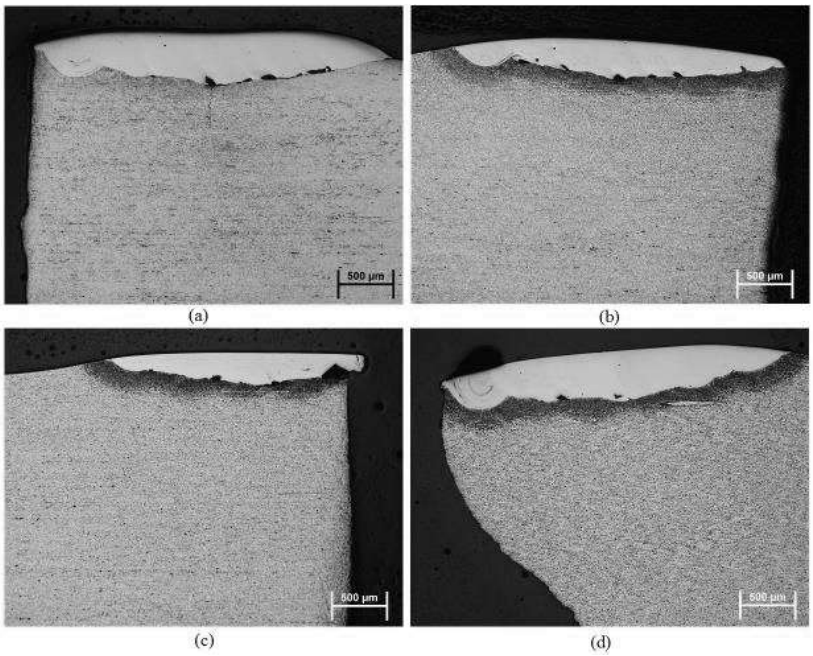

Figure 4.17: The metallurgical images obtained fom the 4 different sections of sample 60 (420 stainless steel clad , heat treated at 400° C) showing porosities in the clad layer and interface

4.1.3 Fatigue Results of CrMoV Clad Samples

4.1.3.1 Fatigue Results of CrMoV Clad Samples Heat Treated at 580° C for 1 hour

Table 4.6 shows the rotary bending fatigue results for CrMoV clad samples which were heat treated at 580° C for 1 hour after laser cladding. All the samples were laser clad with the same cladding parameters and tested under identical testing conditions.

Table 4.6: Number of cycles to failure experienced by CrMoV clad samples heat treated at 580° C for 1 hour

Sample	Heat Treatment Condition	Nf
39	580° C for 1 hour	70,841
38	580° C for 1 hour	24,849
41	580° C for 1 hour	73,214
47	580° C for 1 hour	77,738
43	580° C for 1 hour	69,542
49	580° C for 1 hour	74,715
45	580° C for 1 hour	79,346
46	580° C for 1 hour	68,377
42	580° C for 1 hour	34,774
48	580° C for 1 hour	74,859

Figure 4.18 shows the same results on a graph. As can be seen in the graph, samples 38 and 42 lasted the lowest number of cycles to failure and samples 45 and 47 lasted the longest number of cycles to failure. These samples were sectioned to investigate the cause of this difference.

The first two samples which were sectioned and compared were sample 47 (N_f= 77,738) and sample 38 (N_f= 24,849) with 68.03% difference in their fatigue lives. The cross sectional views of these two samples are shown in Figures 4.19 and 4.20 The percentages of the defected areas in each sample ($\frac{total\ defect\ area}{total\ clad\ area}$ x 100) were calculated by measuring the total defect areas (sum of all the defected areas in all 4 sections) and the clad areas in all the 4 sections. The results indicated that in sample 38 (N_f= 24,849) 2.66% of the clad area was defected while in sample 47 (N_f= 77,738) this figure was only 1.87%.

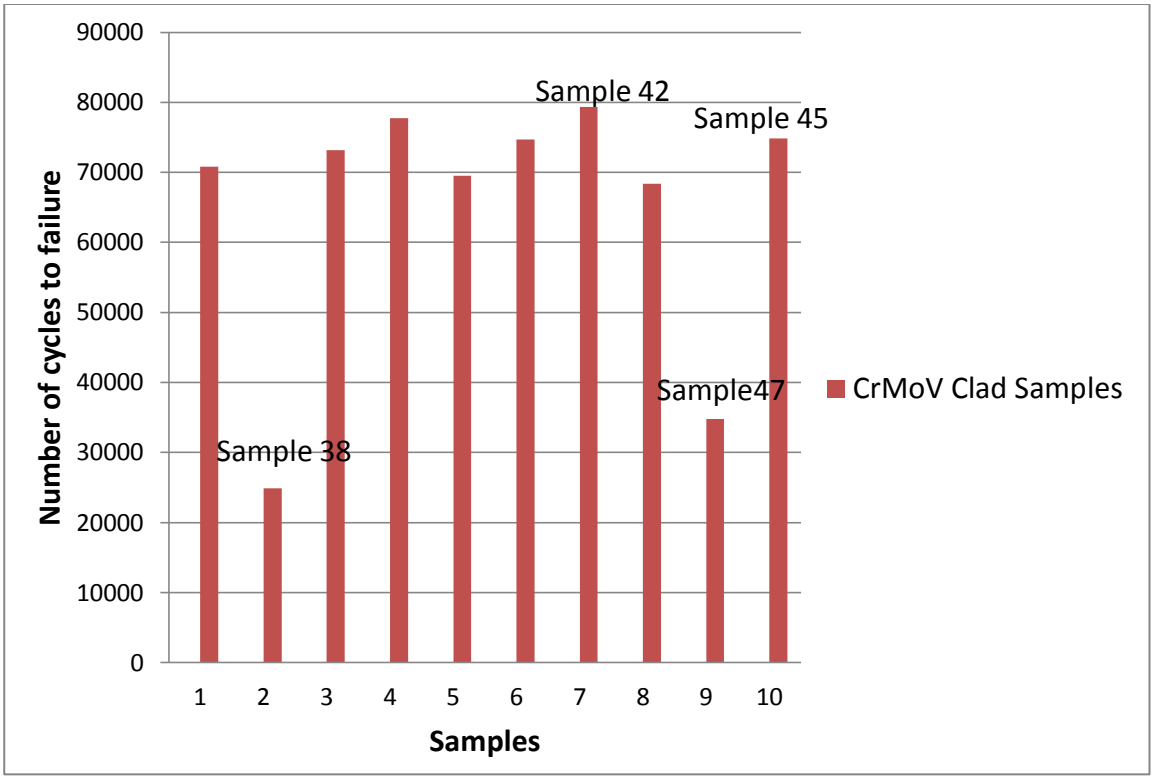

Figure 4.18: Number of cycles to failure for CrMoV clad samples heat treated at 580° C for 1 hour

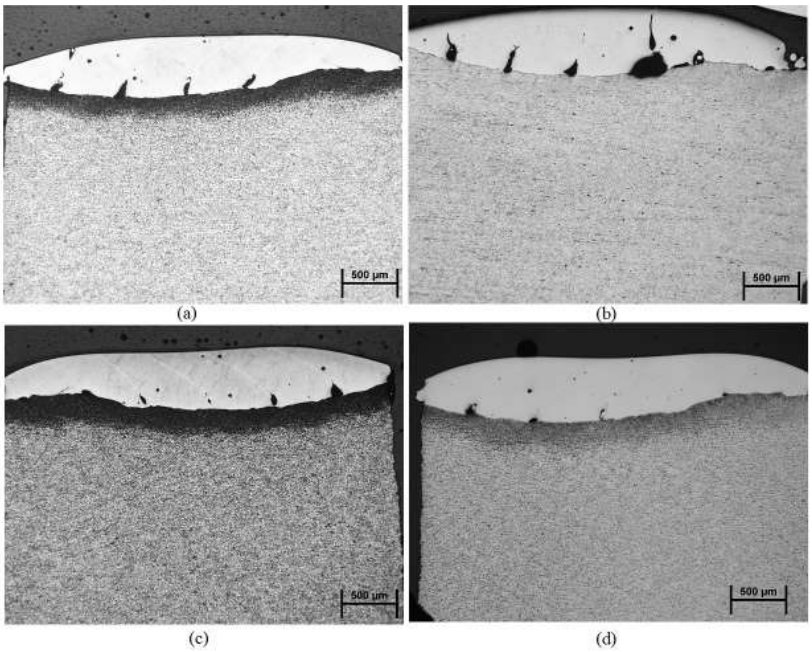

Figure 4.19: Metallurgical images obtained from 4 sections of sample 38 (CrMoV clad, Nf= 24,849)

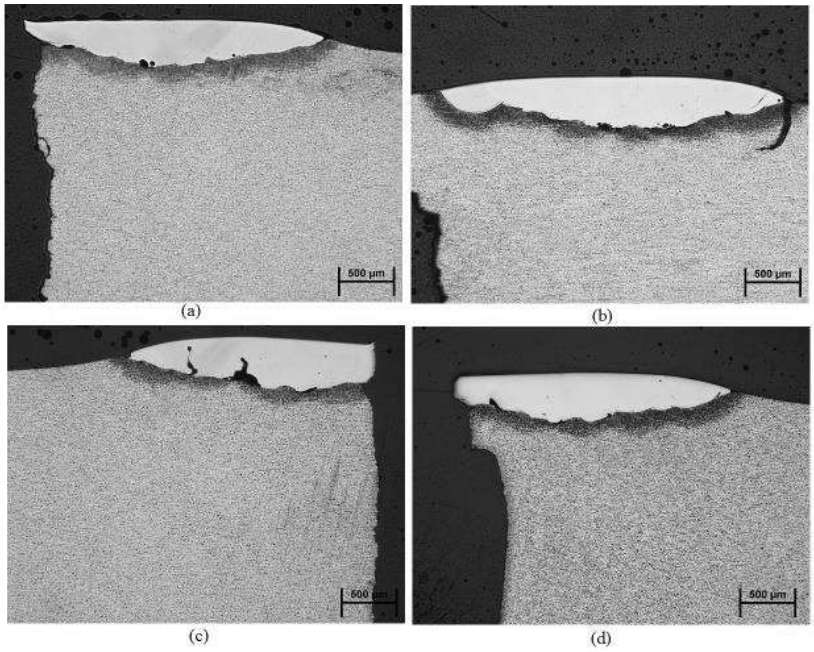

Figure 4.20: Metallurgical images obtained from 4 sections of sample 47 (CrMoV clad, Nf= 77,738)

Another pair of samples which was investigated to explain the difference between their experienced numbers of cycles to failure under identical testing conditions were sample 42 (Nf=34,774) and sample 45 (Nf= 79,346) with 56.17% difference in their fatigue lives. The cross sectional views of 4 sections of each of these samples are shown in Figures 4.21 and 4.22. The results indicated that in sample 42 (N_f= 34,774) 2.26% of the clad area was defected while in sample 45 (N_f= 79,346) this figure was only 0.17%. Figure 4.23 shows the ($\frac{total\ defected\ area}{total\ clad\ area}$ x 100) values versus number of cycles to failure for samples 38, 47, 42 and 45. The graph shows that the number of cycles experienced by each sample to failure has again an inverse relation with its total defected area.

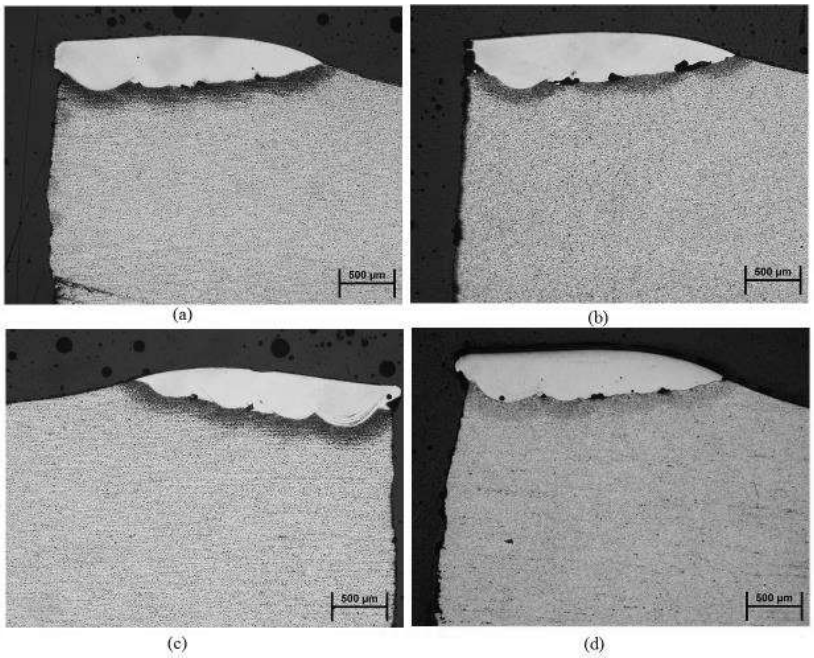

Figure 4.21: Metallurgical images obtained from 4 sections of sample 42 (CrMoV clad, Nf= 34,774)

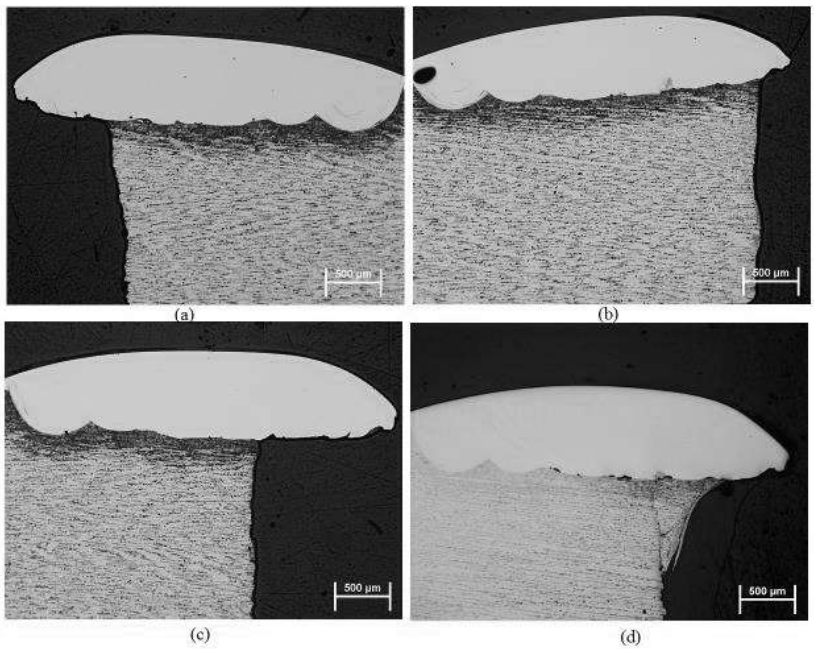

Figure 4.22: Metallurgical images obtained from 4 sections of sample 45 (CrMoV clad, Nf= 79,346)

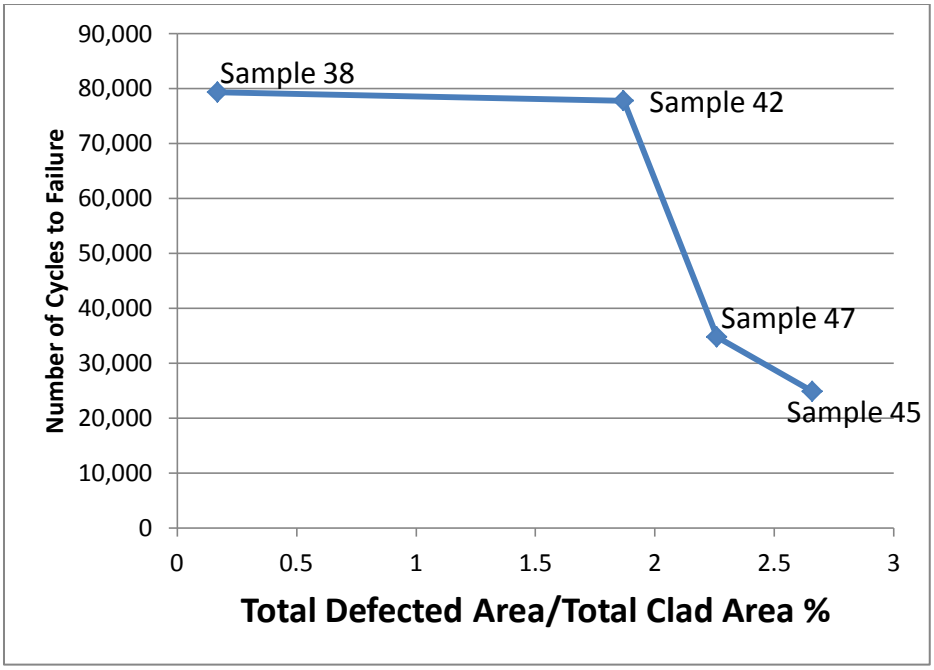

Figure 4.23: Number of cycles to failure versus the percentage of the defected area in the clad layer for samples 38, 42, 45 and 47

4.1.3.2 Fatigue Results of CrMoV Clad Samples with Different Post-Clad Heat Treatment Conditions

Table 4.7 shows the rotary bending fatigue test results for laser clad samples coated with CrMoV powder, under identical testing conditions with different post-clad heat treatments. The numbers in the first column indicate how the samples were labeled for testing. Figure 4.24 compares the average number of cycles experienced with CrMoV clad samples with different post-clad heat treatment conditions. The laser clad samples heat treated at 580° C lasted the longest umber of cycles to failure (an average of 73,579). The second highest average number of cycles was for the samples which were heat treated at 400° C for 1 hour (an average of 45,117). The fatigue strength of laser clad samples decreased to an average of 39,864 when they were heat treated at 200° C after laser cladding. The laser clad samples which were not heat treated lasted the lowest number of cycles before failure (an average of 24,669).

Table 4.7: Number of cycles to failure experienced by CrMoV clad samples with different post-clad heat treatment conditions

Sample	Heat Treatment Condition	Nf
38	580° C for 1 hour	24,849
39	580° C for 1 hour	70,841
41	580° C for 1 hour	73,214
47	580° C for 1 hour	77,738
43	580° C for 1 hour	69,542
49	580° C for 1 hour	74,715
45	580° C for 1 hour	79,346
46	580° C for 1 hour	68,377
42	580° C for 1 hour	34,774
48	580° C for 1 hour	74,859
50	Without Stress Reliving	25,511
51	Without Stress Reliving	22,634
52	Without Stress Reliving	25,862
53	400° C for 1 hour	45,562
54	400° C for 1 hour	44,672
55	200° C for 1 hour	39,810
56	200° C for 1 hour	39,919

Table 4.8: Number of cycles to failure experienced by CrMoV clad samples with different post-clad heat treatment conditions

Post-clad Heat Treatment Condition	Average number of cycles before failure
Heat treated at 580° C for 1 hour	73,579
Heat treated at 400° C for 1 hour	45,117
Heat treated at 200° C for 1 hour	39,864
No post-clad heat treatment	24,669

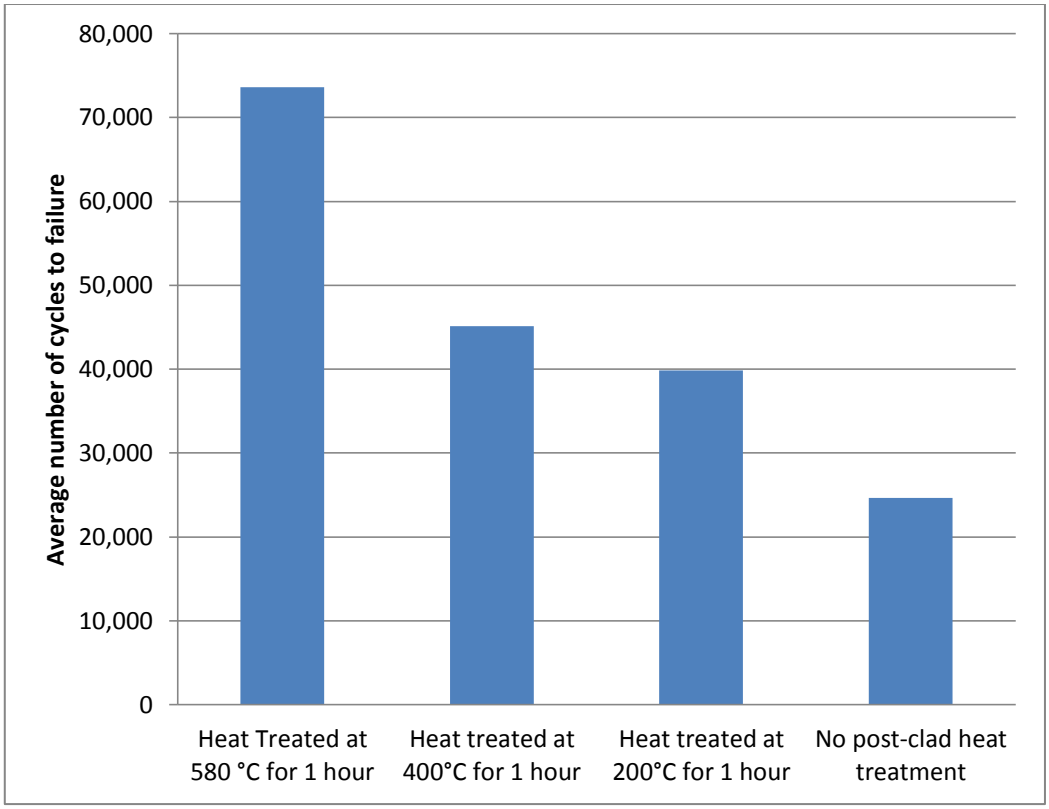

Figure 4.24: Number of cycles to failure experienced by CrMoV clad samples with different post-clad heat treatment conditions

Micro hardness measurements were done on the CrMoV clad samples with different post-clad heat treatment conditions to investigate the effect of heat treatment on the hardness profiles of the samples. Hardness measurements were carried out from the surface of the clad to the HAZ and the substrate. Figure 4.25 compares the hardness profiles of CrMoV clad samples with different post-clad heat treatment conditions. The results indicate that the samples which were heat treated at 580° C had the lowest hardness in the clad layer (311.68 HV). By decreasing the post-clad heat treatment temperature to 400° C the hardness of the clad layer increased to an average of 324.42 HV. The clad layer of the samples which were heat treated at 200° C after laser cladding had an average of 342.65 HV. The clad layer of the samples with no post-clad heat treatment had the highest hardness (366.3 HV).

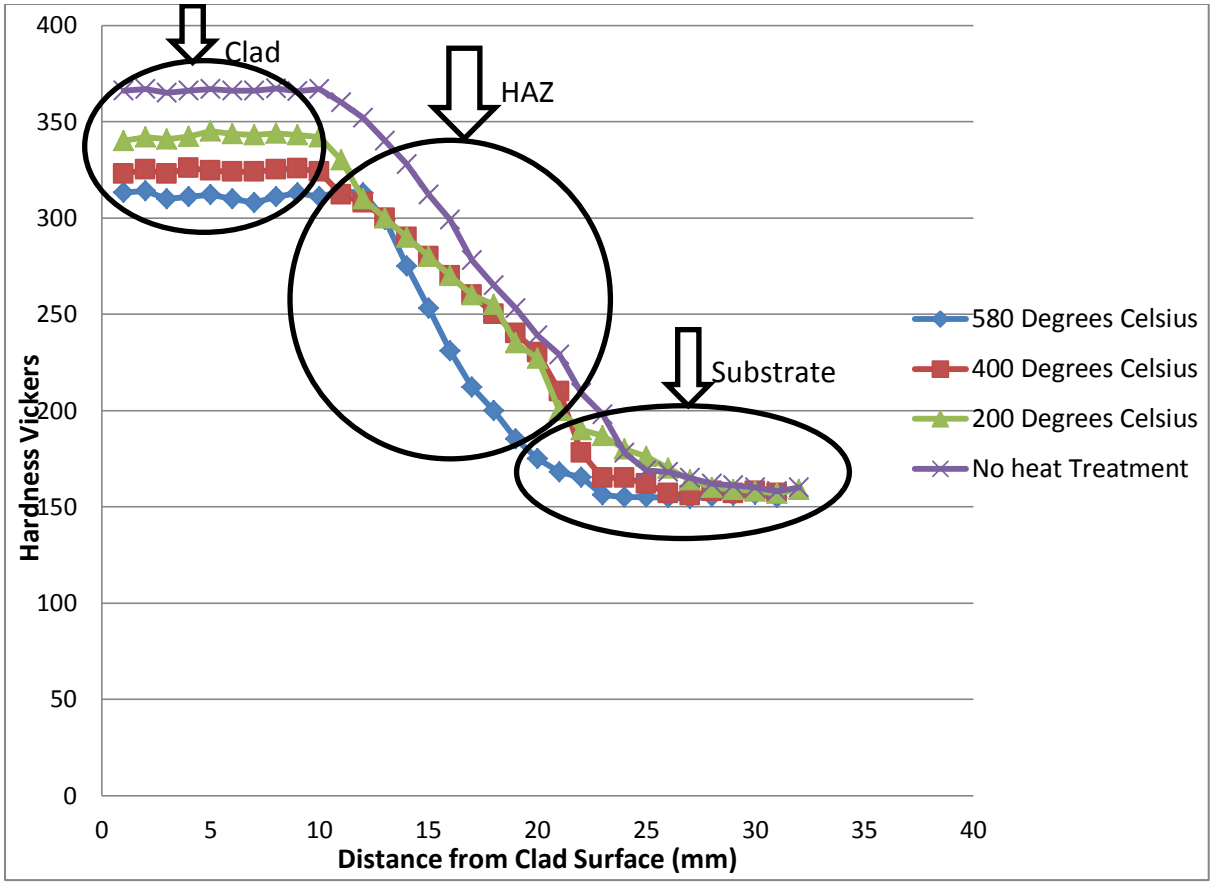

Figure 4.25: Hardness profiles for CrMoV clad samples with differet heat traetment conditions

4.1.4 Comparison between the Fatigue Results of Clad and Non-Clad Samples

The fatigue results of laser clad samples were compared to those of non-clad samples to study the effect of laser cladding on the fatigue properties of railway axle steel. Figure 4.26 compares the fatigue results of 420 stainless steel clad samples, CrMoV clad samples (both heat treated at 580° C) with the fatigue results of non-clad samples with an OD of 19 mm. The results indicate that the average fatigue strength of 420 stainless steel clad samples heat treated at 580° C (55,908 cycles) was less than that of the non-clad samples with a single notch with the diameter of 19 mm (61,085 cycles) which shows that 420 stainless steel is not a suitable choice of material for laser cladding the railway axle steels.

The results also show that CrMoV clad samples heat treated at 580° C for 1 hour had a higher average number of cycles to failure (73,579 cycles) compared to that of the no-clad samples (61,085 cycles). This shows that by laser cladding the worn railway axles using CrMoV powder it is possible to increase the fatigue strength of the axles.

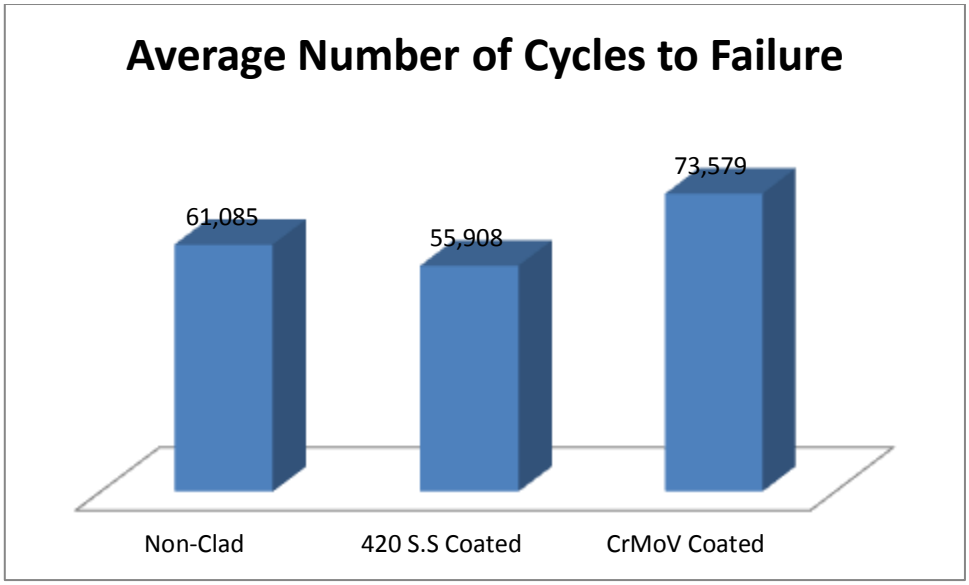

Figure 4.26: Comparison between the fatigue results of clad samples and non-clad samples

4.2 Microstructures

The microstructures of the base material, HAZ and clad layer for both 420 stainless steel clad samples and CrMoV clad samples with all the different post-clad heat treatment conditions are presented.

Figure 4.27 shows the microstructure of the mild steel base material. The mild steel substrate had a ferrite-pearlite microstructure.

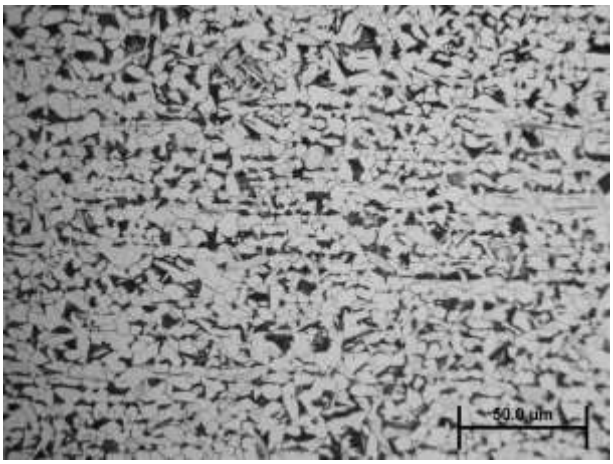

Figure 4.27: Ferrite-pearlite microstructure of mild steel substrate

Figure 4.28 shows the microstructure of the HAZ. During laser cladding, the microstructure of the heat affected zone transfers into a martensitic microstructure as a result of rapid cooling.

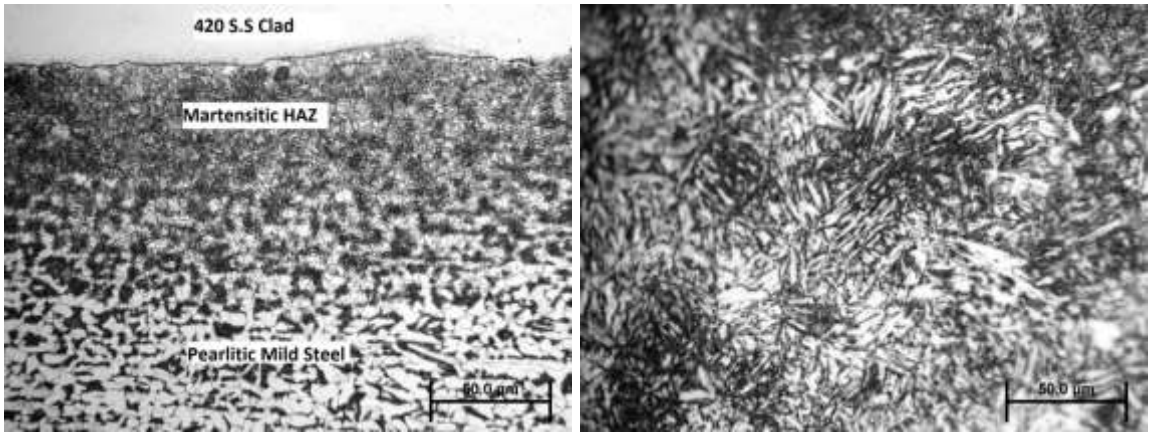

(a) (b)

Figure 4.28: Martensitic microstructure of HAZ at (a) low magnification and (b) high magnification

Figures 4.29 to 4.32 show the martensitic microstructures of the clad layer in 420 stainless steel clad samples with different post clad heat treatment conditions. As shown in the figures, post-clad heat treatments tempered the martensitic microstructure. Precipitation of carbides increases as the tempering temperature increases from 200° C to 580° C.

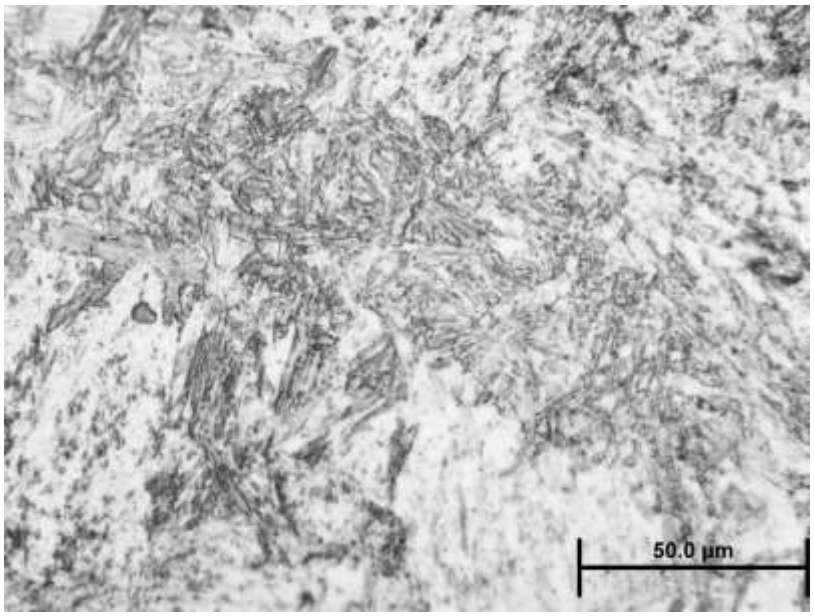

Figure 4.293: Martensitic microstructure of 420 stainless steel clad sample- as clad microstructure

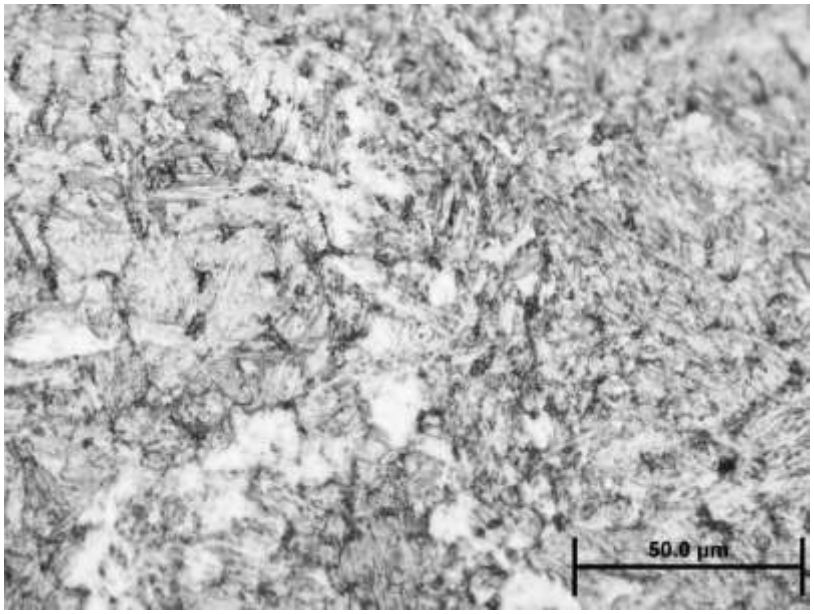

Figure 4.30: Martensitic microstructure of 420 stainless steel clad sample heat treated at 200° C for 1 hour

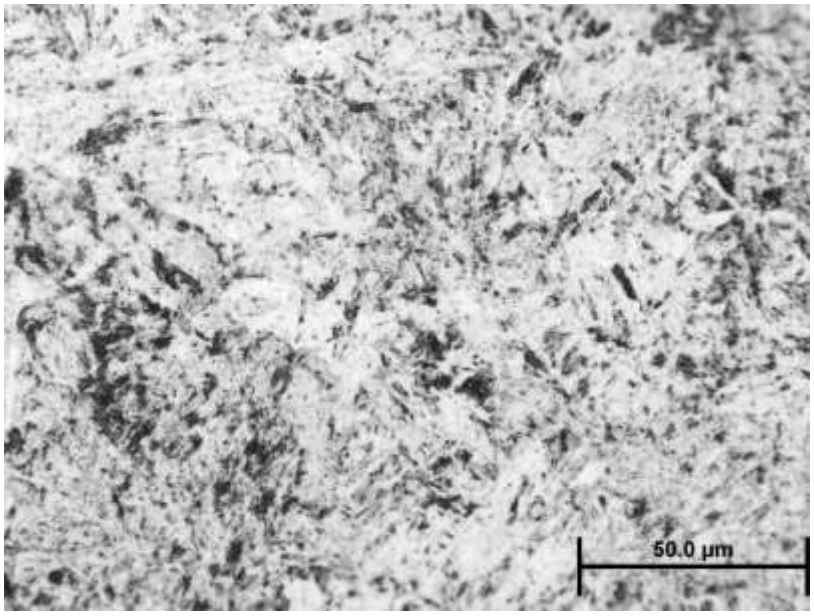

Figure 4.31: Martensitic microstructure of 420 stainless steel clad sample heat treated at 400° C for 1 hour

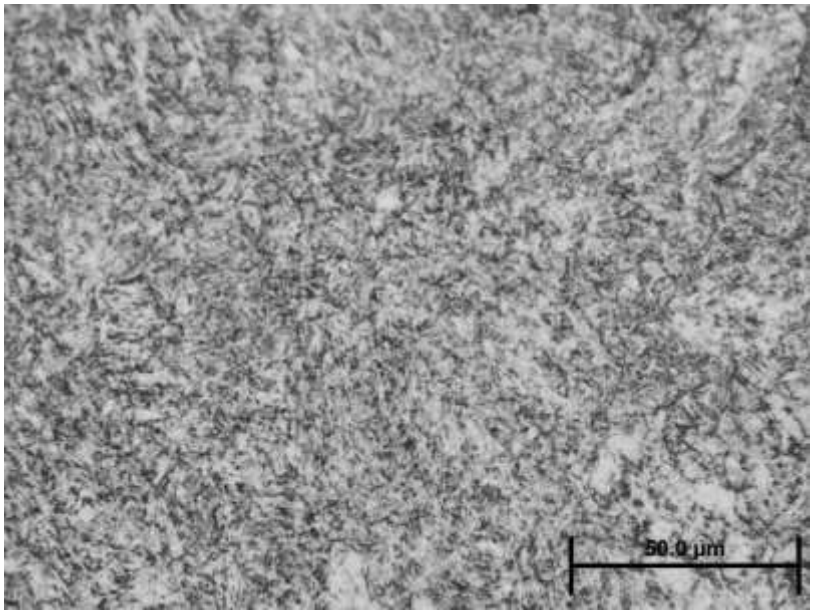

Figure 4.32: Martensitic microstructure of 420 stainless steel clad sample heat treated at 580° C for 1 hour

Figures 4.33 to 4.36 show the microstructures of the clad layer of CrMoV clad samples with different post-clad heat treatment conditions. Similar to 420 stainless steel clad samples, the microstructure of the clad layer was martensitic for all the samples with different post-clad heat treatment conditions. Like 420 stainless steel clad samples, post-clad heat treatment caused tempering of the martensite in CrMoV clad samples and softening of the clad layer.

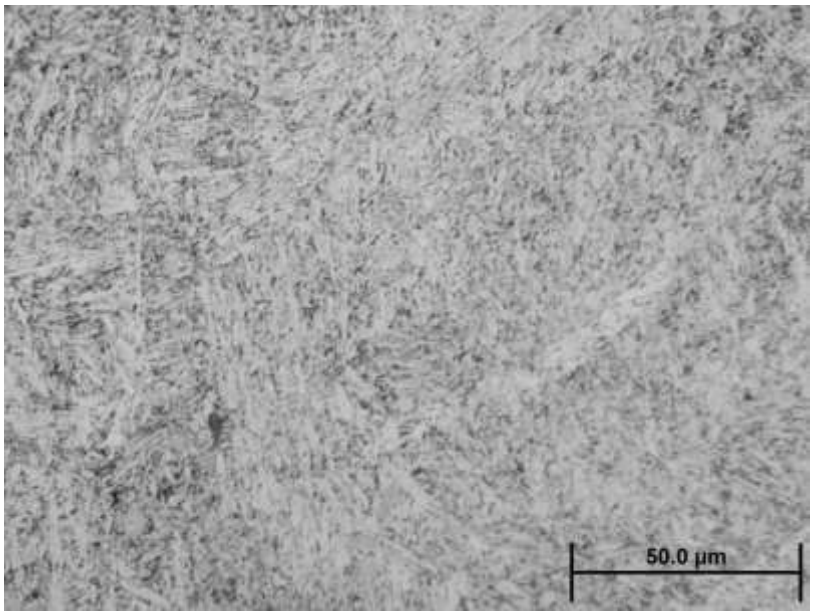

Figure 4.33: Martensitic microstructure of CrMoV clad sample- as clad microstructure

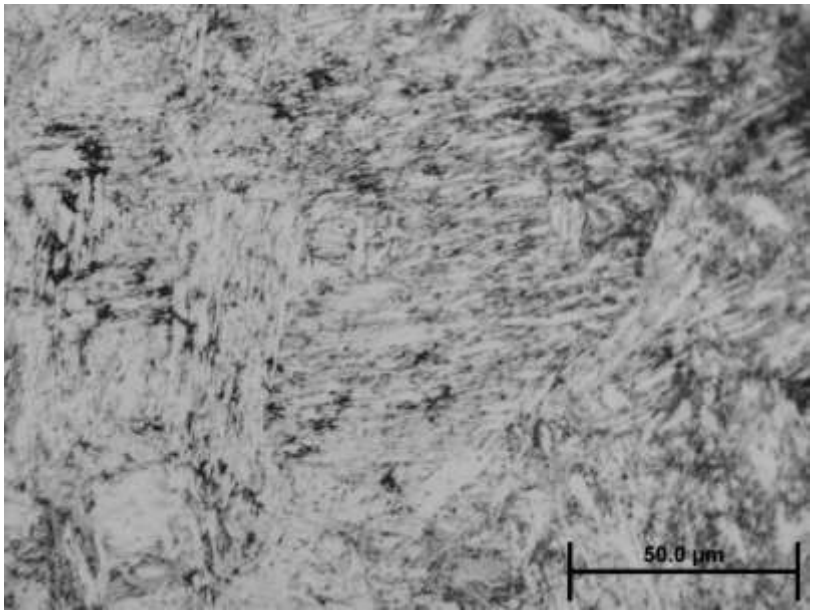

Figure 4.34: Martensitic microstructure of CrMoV clad sample heat treated at 200° C for 1 hour

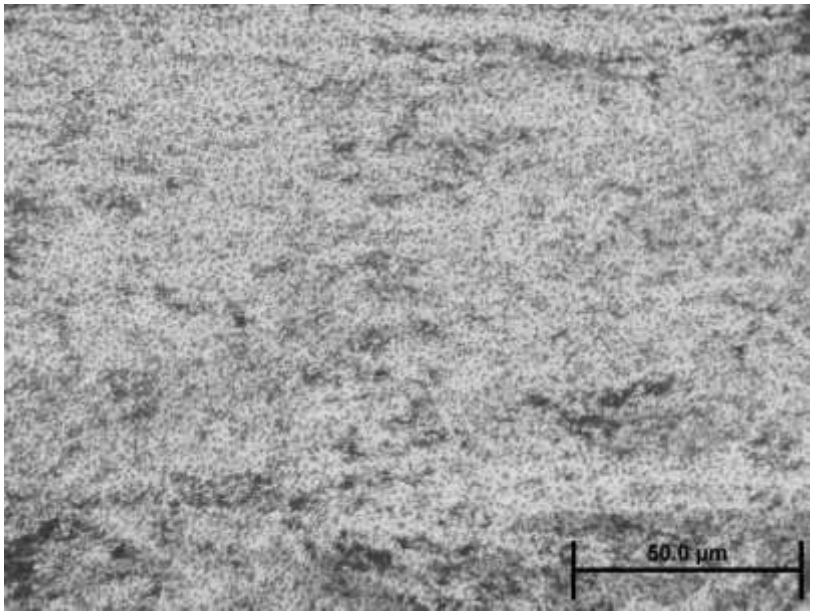

Figure 4.35: Martensitic microstructure of CrMoV clad sample heat treated at 400° C for 1 hour

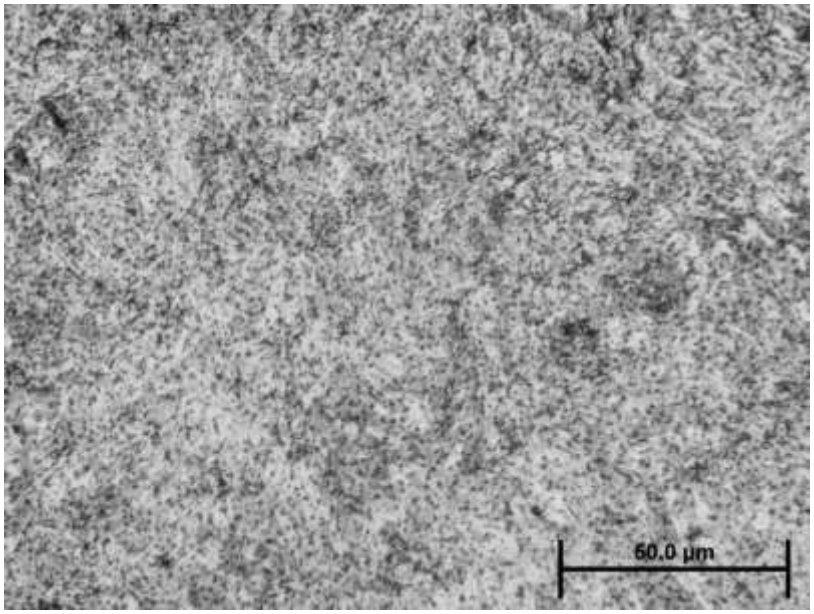

Figure 4.36: Martensitic microstructure of CrMoV clad sample heat treated at 580° C for 1 hour

4.3 Fractography

The fracture surfaces of the broken samples were investigated to study the failure mode and fracture mechanism. A typical fractured surface of a broken fatigue sample usually shows some major features such as origin of crack, slow fracture zone, fast fracture zone, progression marks and ratchet marks (Figure 4.37).

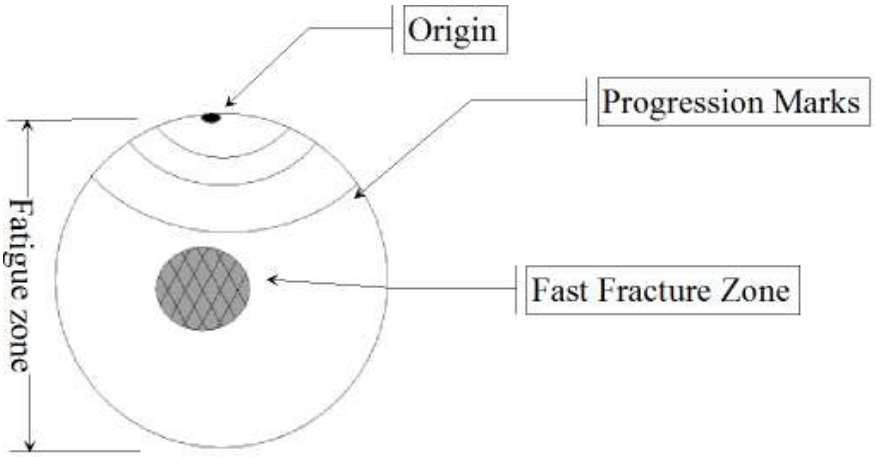

Figure 4.4: The macroscopic features of the fracture surface of a failed fatigue sample

The origin is the crack initiation site. A fracture surface can show one or more origins. A single origin indicates low overstress whereas multiple origins can be the result of high overstress or high number of stress concentrators.

The crack then grows with a typical rate of 10^{-6} mm/stress cycle in the slow fracture zone. An important piece of information that can be achieved by looking at the slow fracture plane is the direction of the maximum stress that led to the fracture of the part since the plane of the slow fracture zone is perpendicular to that of the maximum stress applied on the part [67]. Materials with higher toughness have larger slow fracture zones.

The progression marks indicate changes in the applied load. Any variation in the load experienced by the material leads to a change in the crack growth rate which appears as a progression mark in the fracture surface [67]. The fatigue samples tested under constant loading conditions without any start-stop periods do not show any progression marks. Other features of the fracture surfaces of fatigue samples are Fatigue Striations. Fatigue striations look very much like progression marks and one way to avoid the confusion is the knowing that progression marks can be seen with naked eye whereas fatigue striations can only be seen under high magnifications. Fatigue striations show every cycle experienced by the material (Figure 4.38).

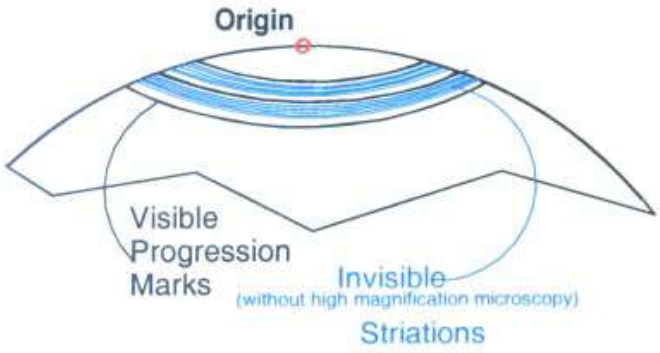

Figure 4.38: Progression marks and fatigue striations [67]

When a crack reaches a point where the remaining material is overstressed, the instantaneous zone or fast fracture zone appears. The nature of the fracture in the fast zone is typically brittle with a small ductile part. The speed of crack propagation in the fast fracture zone is about ½ the speed of sound in the material. Important information that can be obtained from the fast fracture zone is the amount of load experienced by the material at the final stage of fracture. Small overload zone indicates low overstress and large overload zone indicates higher over stresses experienced by the material at the time of final fracture [68]. The crack growth in the brittle overload zone is typically intergranular [67].

Ratchet marks are another important feature of the fracture surfaces of fatigue samples as shown in Figure 4.39. Ratchet marks are the boundaries between the crack growth planes of two adjacent crack origins. Ratchet marks can be a good guide of locating the crack origins. The presence of ratchet marks means that there is more than one origin which leads to the fact that either the overstress or the number of stress concentrators has been high. Combining this information with the size of overload zone can help the clarifying of the fracture condition. For example, for a fracture surface that shows a small over load zone and ratchet marks, it can be concluded that since the small over load zone indicates low over stress then the presence of ratchet marks must be because of the high number of stress concentrators.

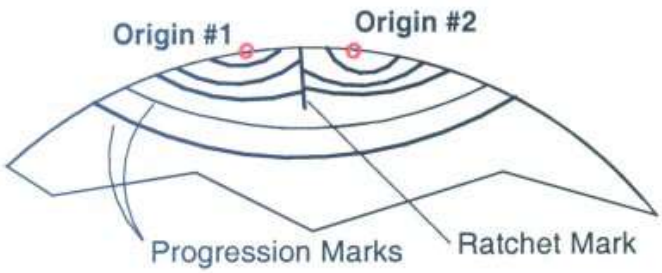

Figure 4.39: Ratchet mark indicating the presence of multiple origins [67]

Also the type of the applied forces on the fatigue sample can be known by looking at the side view of the ratchet marks. Figure 4.40 shows two examples of the ratchet marks side views which are caused by torsional loading (tapered sides) and tension or bending (perpendicular to the fracture surface). In the case of this research the applied load was rotary bending and the side view of the ratchet marks show the pattern shown in Figure 4.40 for bending loads (Figure 4.41).

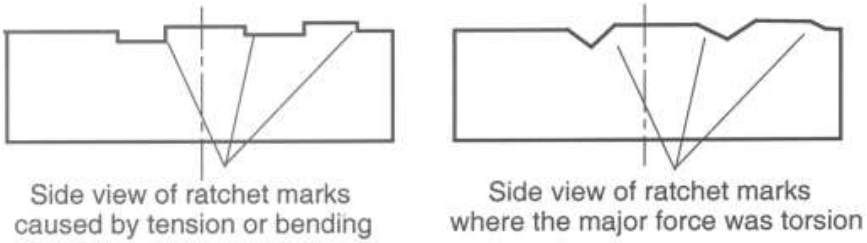

Figure 4.40: Edges of ratchet marks showing the type of allied force [67]

Figure 4.41: Side view of ratchet marks for a non-clad broken fatigue sample indicating bending of the sample

The angles of the ratchet marks can also help identify the primary crack origin. The primary origin is usually between the ratchet marks which are closest to each other on the surface (Figure 4.42).

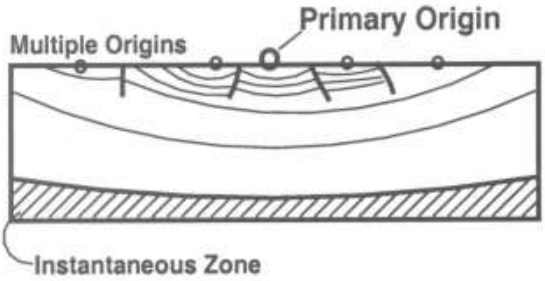

Figure 4.42: Primary crack origin located between two ratchet marks

The last surface feature of the fractured fatigue samples is the river marks (Figure 4.43). River marks show the direction of the crack growth and can be found in the fast growing part of the fatigue zone.

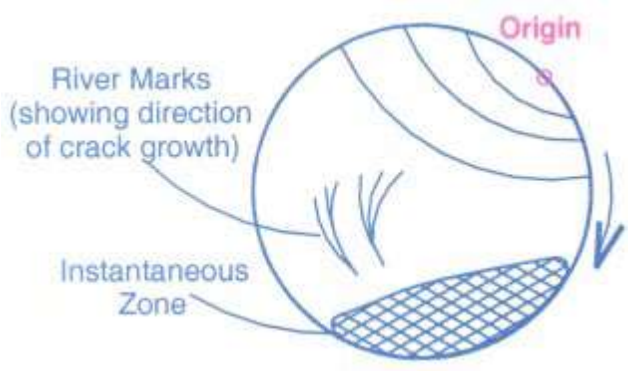

Figure 4.43: River marks showing the direction of crack growth [67]

4.3.1 Fractography of Non-clad Samples

The broken samples were analysed to investigate the site of fractures and fracture mechanisms. In all the non-clad samples the results showed that the fracture happened in the middle of the notch which has the lowest diameter. Figure 4.44 shows a mild steel sample with a single notch (OD of 19 mm) in which the fracture happened in the middle of the notch. Figure 4.45 also shows another non-clad sample with an extra groove in the centre with an OD of 18 mm which resembles the worn railway axles. The site of fracture in this sample is like the previous sample in the middle of the notch.

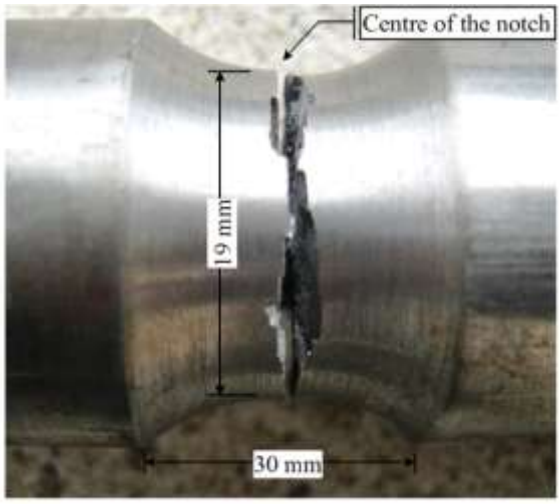

Figure 4.44: Site of fracture in a non-clad mild steel fatigue sample with a single notch with an OD of 19 mm

Figure 4.45: Site of fracture in a non-clad mild steel fatigue sample with an extra groove with an OD of 18 mm

The centre of the notch in the first sample (OD of 19 mm) and the centre of the extra groove in the second sample (OD of 18 mm) have the minimum diameters along the whole length of the sample and that is why they carry the maximum mean stress which makes them more

vulnerable to fracture compared to the rest of the sample. This phenomenon is known as “the notch effect” and fatigue samples are designed based on it.

Figure 4.46 shows the fracture surfaces of a non-clad Mild steel sample with an OD of 19 mm.

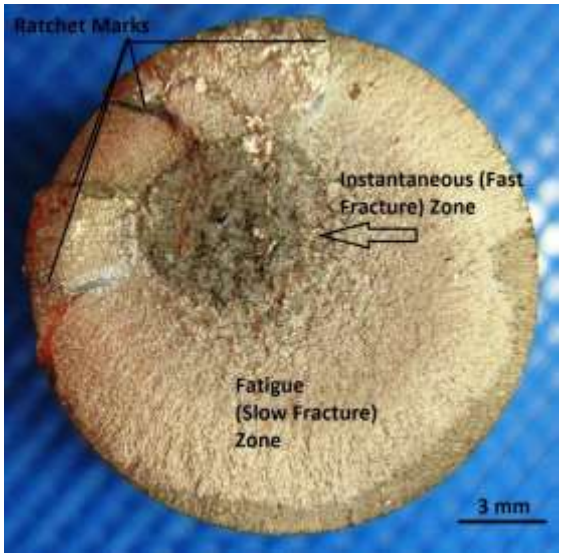

Figure 4.46: Surface features of a non-clad mild steel fatigue sample

The fracture surface shows the typical zones of fatigue and overload. Looking at the fracture surface and the surface features shown in the Figures 4.45 and 4.46 the following points can be concluded:

- The presences of ratchet marks indicate that either the load or the number of stress concentrators was high. Also since ratchet marks are the boundaries between two adjacent crack growth plane corresponding two crack origins, it can be concluded that there were more than one origin in the fracture surface.
- The small over load zone shows that the over stress experienced by the material in the final stage of fracture was low. This combined with the information obtained from the ratchet marks; eliminate the possibility of high over stresses causing the fracture and shows that the fracture was caused by high number of stress concentrators.
- Looking at the angles of the ratchet marks, the primary origin can be located. As shown in Figure 4.47 it is clear that the centre two ratchet marks shown in the image are slightly closer to each other at the surface and it is likely that the primary origin was between them.

- Looking at the side view of the ratchet marks, it can be concluded that the type of load that led to the fracture of the sample was bending since the side view of the ratchet marks is perpendicular to the fracture surface.

Figure 4.47: Locating of the primary origin using the angles of the ratchet marks

SEM images of the fracture surface of non-clad mild steel samples showed a dimpled surface, typical of a ductile fracture (Figure 4.48). In a ductile fracture, the dimples are created by micro void coalescence and their depth can be considered as a measure of ductility of the material.

Unlike the sudden fracture of brittle materials, ductile fracture is a result of a long period of crack or void growth. Ductile failure occurs after some deformation of the material therefore deformation marks are the other main characteristic of the facture surface of ductile materials (Figure 4.49).

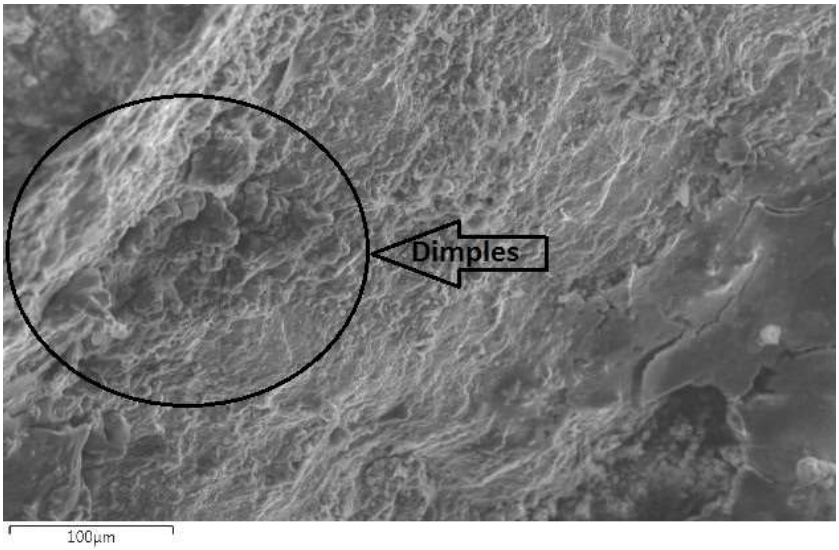

Figure 4.48: Dimpled appearance of fracture surface of non-clad fatigue samples

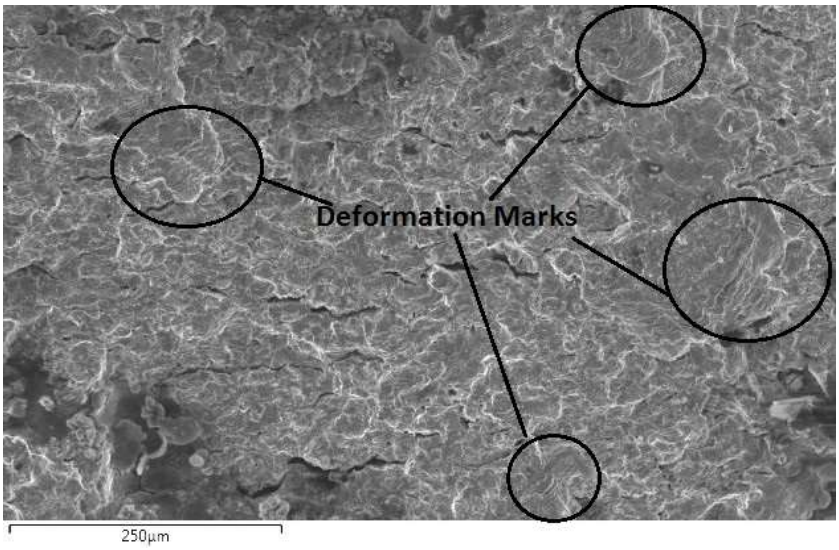

Figure 4.49: Deformation marks showing plastic deformation before fracture indicating a ductile fracture in a non-clad fatigue sample

4.3.2 Fractography of 420 Stainless Steel Clad Samples

SEM images of the clad layer of the 420 stainless steel clad samples showed clear cleavage facets indicating quasi-brittle mode of fracture. Quasi-brittle fractures occur as a result of the presence of preliminary defects such as corrosion pits, inclusions or fatigue cracks. Figure 4.50 and 4.51 show the cleavage facets in the clad layer of a 420 stainless steel clad sample.

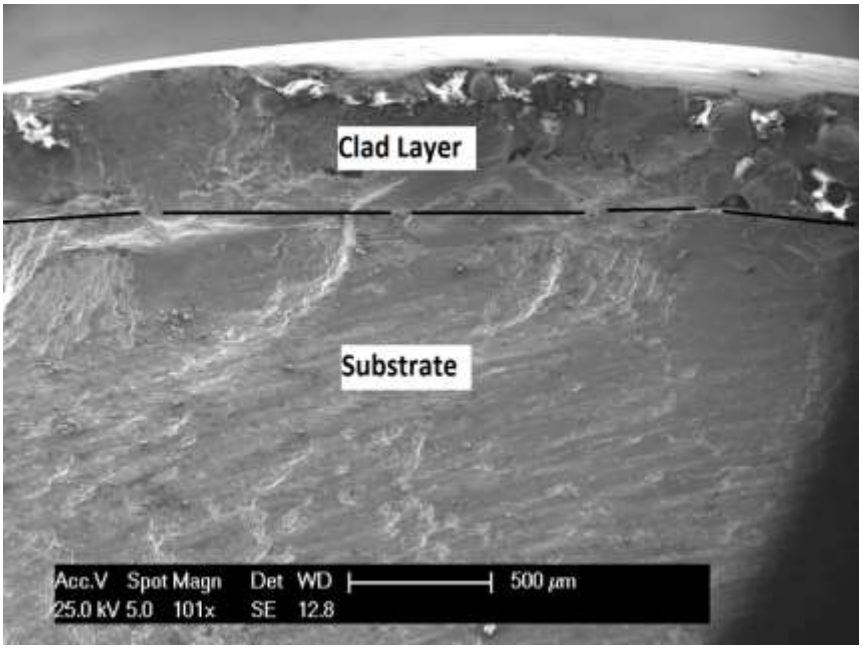

Figure 4.50: Overview of the clad layer and substrate of a 420 stainless steel clad sample

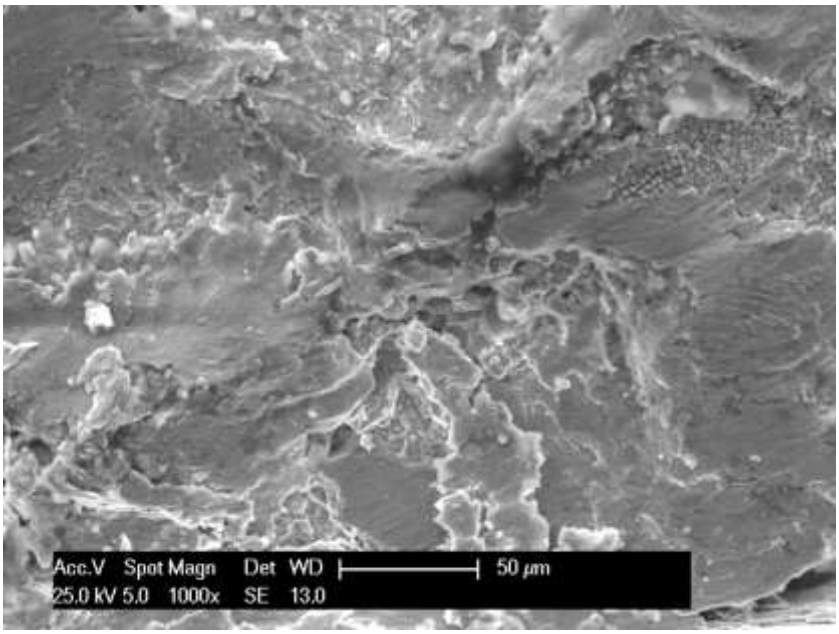

Figure 4.51: Cleavage facet indicating quasi-brittle fracture mode of the clad layer of a 420 stainless steel clad sample

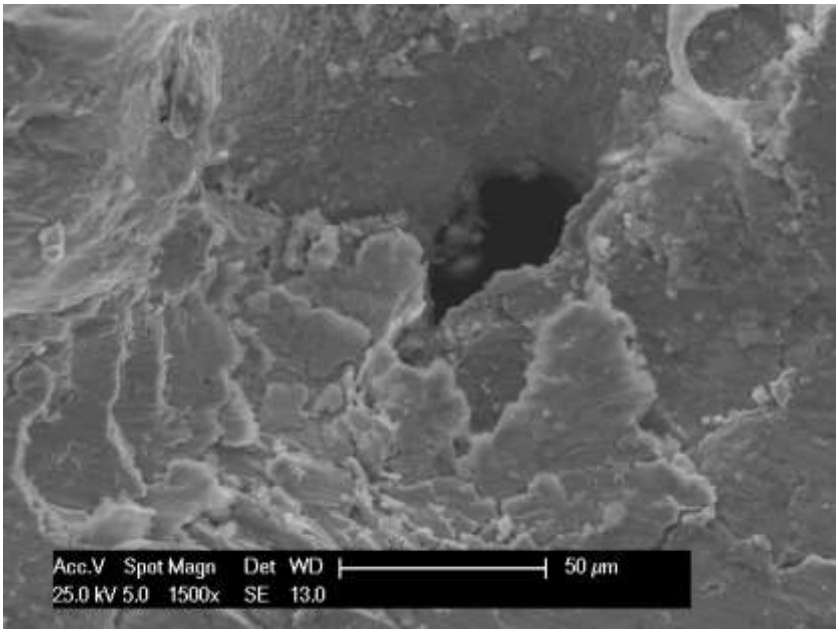

Figure 4.52: Cleavage facet indicating quasi-brittle fracture mode of the clad layer of a 420 stainless steel clad sample

Quasi-brittle mode of fracture contains both dimpled areas indicating ductile fracture and cleavage facet. The failure typically starts with a ductile mechanism and as the remaining material decreases the mean stress experienced by the material reaches a critical value where the brittle fracture occurs. Figure 4.53 shows an SEM image of the 420 stainless steel clad layer showing both dimpled areas and cleavage facets.

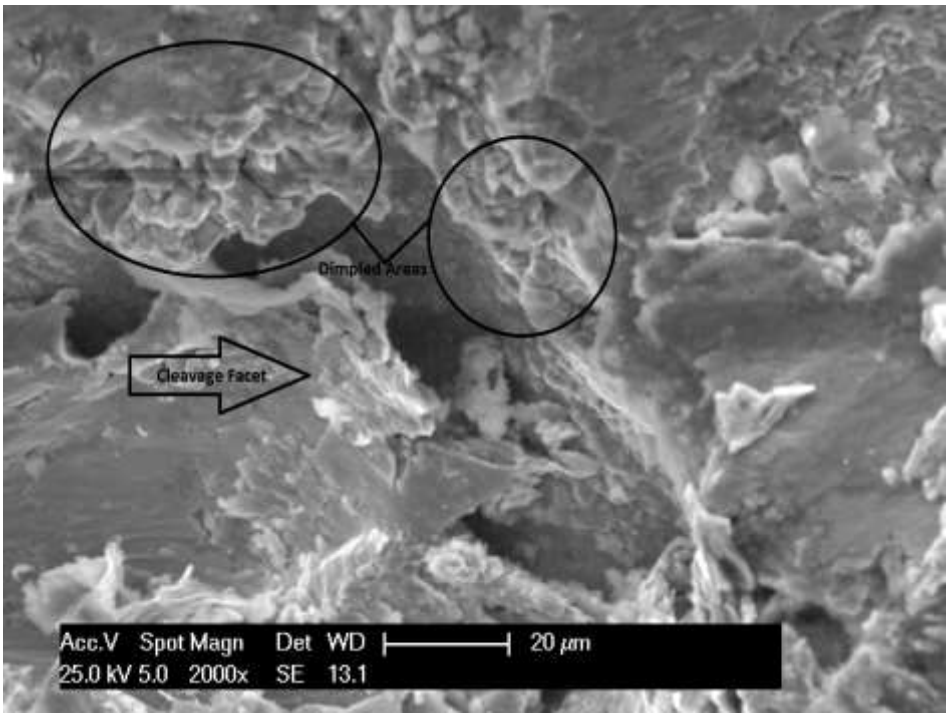

Figure 4.53: Dimpled areas and cleavage facets of a quasi-brittle fracture in the clad layer of a 420 stainless steel clad sample

4.3.3 Fractography of CrMoV Clad Samples

The SEM images obtained from the CrMoV clad layer showed dimpled areas as well as cleavage facets indicating quasi-brittle fracture. Figure 4.54 shows an overview of the clad layer of a CrMoV clad sample. The brighter section of the image corresponds with the dimpled areas which have a relatively rough surface compared to the flat brittle cleavages and therefore absorb more charges during SEM and produce a bright image. The darker section of the image is therefore the brittle section. An image with a higher magnification shows the dimples clearly (Figure 4.55). The cleavage facets of the brittle section are also shown in Figure 4.56.

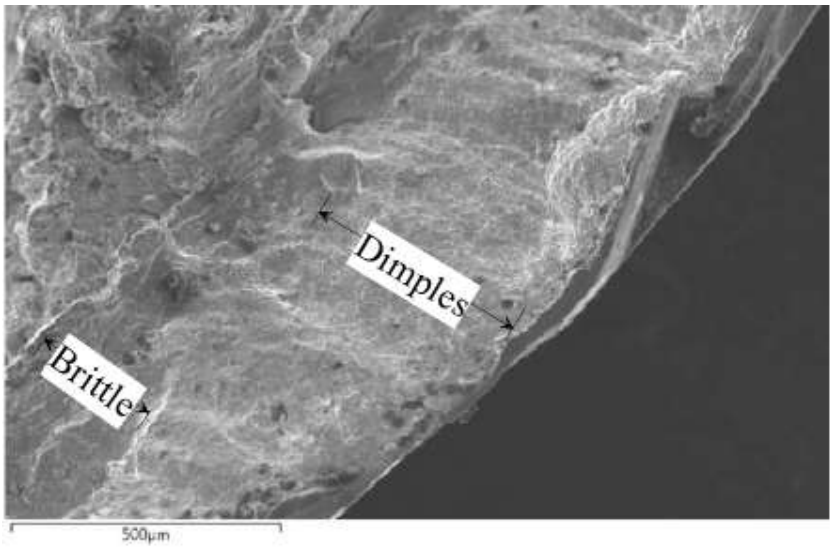

Figure 4.54: Overview of the CrMoV clad layer showing both ductile and brittle fractures

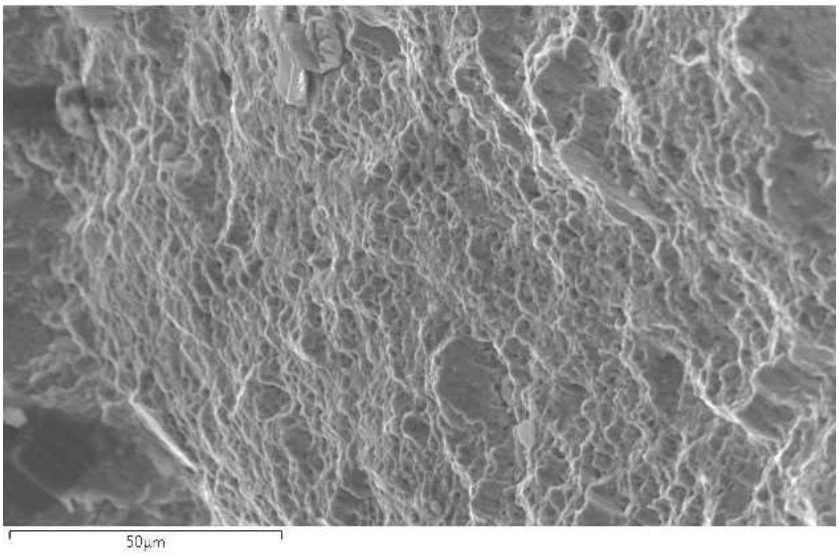

Figure 4.55: Dimples indicating ductile fracture in the CrMoV clad layer

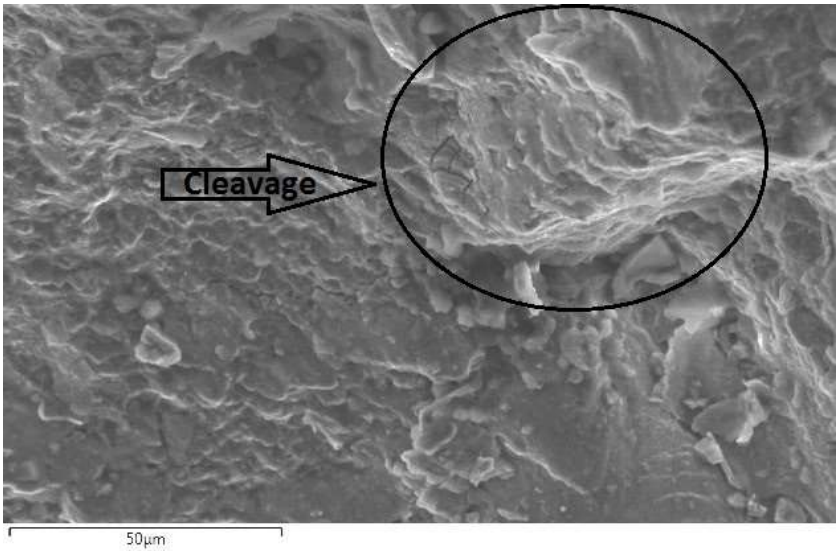

Figure 4.56: Cleavage fracture in the CrMoV clad layer

Chapter 5

Conclusions and Future Developments

5.1 Conclusions

In this thesis the possibility of using laser cladding technology as a repair technology to refurbish worn railway axles was investigated.

Rotary bending fatigue tests were carried out on the non-clad mild steel samples and laser clad samples to study the effect of laser cladding on the fatigue properties of railway axle steel which in the case of this research was mild steel.

Two different materials were used for laser cladding the samples to investigate the effect of cladding material on the fatigue properties of the laser clad samples. 420 stainless steel was used because of its high corrosion resistance and CrMoV was used because of its ductility.

A wide range of post-clad heat treatment conditions were employed to investigate the effect of post-clad heat treatment on the fatigue properties of the laser clad samples.

It was concluded from the results that:

- Laser Cladding can be used to refurbish worn railway axles without affecting their fatigue properties provided that the suitable cladding materials, cladding parameters, preheat and post-clad heat treatment are employed.
- 420 stainless steel is not a right choice of material for laser cladding railway axles due to its brittleness. But CrMoV seems very promising since the CrMoV clad samples had an even higher fatigue life than the non-clad samples in this study.

- Metallurgical defects such as porosities have a major effect on the fatigue properties of laser clad samples. There is an inverse relationship between the total defected areas in each sample with its fatigue life.
- Presence of mechanical defects such as surface roughness decreased the fatigue life of laser clad samples dramatically. These mechanical defects act as stress concentrators and crack initiation sites and therefore fatigue cracks can initiate from them and propagate into the clad layer and substrate and lead to the premature failure of the samples. The surface quality of the laser clad components is very important to avoid fatigue cracking.
- Post-clad heat treatment can improve the fatigue properties of laser clad samples. Post-clad heat treatment releases some of the residual stresses formed in the laser clad samples during laser cladding and cooling and also softens the clad layer.
- Presence of metallurgical defects such as pores has a stronger negative effect than the positive effect of the post-clad heat treatment.

5.2 Future Developments

There are several aspects of significance that should be emphasized and are given below:

- It is recommended that for future study and investigation of laser cladding of railway axles a pre-cladding parameter optimization gets done to obtain the cladding parameters and conditions that avoid the formation of any metallurgical defects. This was not done in this research because one of the main objectives of the present research was to evaluate the effect of metallurgical defects on the fatigue properties of the samples.
- It is suggested to investigate the effect of cladding alloy ductility on fatigue properties of railway axle steels.
- It is essential to understand the role of residual stresses on the fatigue properties of laser clad samples. Measuring the residual stresses after laser cladding and also after post-clad heat treatment is recommended.
- It will be useful to do some modeling work to predict the role of the residual stresses on the fatigue properties of laser deposited railway axels.
- It is suggested to conduct the optimization of the post clad heat treatment for future work.

Chapter 6

References

1. U. Zerbst, M. Schödel, and and H.T. Beier, Parameters affecting the damage tolerance behaviour of railway axles. Engineering Fracture Mechanics, 2011. 5(78): p. 793-809.
2. S. Beretta,et.al Application of fatigue crack growth algorithms to railway axles and comparison of two steel grades. Proceedings of the Institution of Mechanical Engineers, 2004. 218: p. 317-326.
3. M. Madia, S. Beretta, and U. Zerbst, An investigation on the influence of rotary bending and press fitting on stress intensity factors and fatigue crack growth in railway axles. Engineering Fracture Mechanics 2008. 75: p. 1906-1920.
4. Manual of Standards and Recommended Practices Section A, Part III, Association of American Railroads - Operations And Maintenance Department, Mechanical Division. The Association of American Railroads, 1920 - Revised 1984 - L St., N.W. Washington, D.C. 20036.
5. M. Novosad, et al, Fatigue Test of Railway Axles". Procedia Engineering 2, 2010: p. 2259-2268
6. L.P Borrego, Fatigue behaviour of Laser repairing welded joints. Engineering Failure Analysis V14, 2007: p. 1586-1593.
7. Jianqiao Chen and et al, Effect of Laser cladding on Fatigue Strength of an Alloy Steel. Journal of Society of Materials Science, 1995. 44(498): p. 343-34.
8. S. Hillmanson and R.A. Smith, The management of fatigue crack growth in railway axles. Proceedings of the Institution of Mechanical Engineers, Part F: Journal of Rail and Rapid Transit, 2004. 218: p. 327-336.

9. R.A. Smith and S. Hillmanson, A brief historical overview of the fatigue of railway axles. Proceedings of the Institution of Mechanical Engineers, 2004. 218: p. 267-277.
10. http://en.wikipedia.org/wiki/Unsprung_mass
11. M. Bayraktar and N. Tahrali, Design of rail vehicle axles related to failure and life. 5th International Advanced Technologies Symposium (IATS ' 09), 2009.
12. S.L. Dedmon, J.M. Pilch, and C.P. Lonsdale, A comparison of railroad axle stress results using different design sizes, loading criteria and analysis methods. Amerian Society of Mechanical Engineers, Rail Transportation Division (Publication) RTD 21, 2001: p. 197-200.
13. C. Lonsdale and D. Stone, North American axle failure experience. Proceedings of the Institution of Mechanical Engineers, Part F: Journal of Rail and Rapid Transit, 2004. 218: p. 293-298.
14. K. Hirakawa, K. Toyama, and M. Kubota, The analysis and prevention of failure in railway axles. International Journal of Fatigue, 1998. 20: p. 135-144.
15. R. I. Stephens and H.O. Fuchs, Metal Fatigue in engineering. Second ed. 2001.
16. A. Raduta, et al., On the influence of residual stresses on fatigue fracture of railway axles. WSEAS Transactions on Applied and Theoretical Mechanics, 2010. 5: p. 197-207.
17. J.W. Zhang, et al., Analysis on fatigue property of micro shot peened railway axle steel. Materials Science and Engineering A, 2011. 528: p. 1615-1622.
18. T. Berecz, L. Devenyi, and L. Szakacsi, Investigation of the surface strengthening technology of railway-cars' wheel axles for increasing of expectation life of the axles. Materials Science Forum, 2008.
19. B. Yang and Y.X. Zhao, Surface rolling effect on effective short fatigue cracks density for railway LZ50 axle steel. Advanced Materials Research, 2010: p. 75-79.
20. Taizo Makino, Takanori Kato, and Kenji Hirakawa, Review of the fatigue damage tolerance of high-speed railway axles in Japan. Engineering Fracture Mechanics, 2011. 78: p. 810–825.
21. V. Linhart and I. Cerny, An effect of strength of railway axle steels on fatigue resistance under press fit. Engineering Fracture Mechanics, 2011. 78: p. 731-741.
22. J.F. Zheng, et al., Fretting wear behaviours of a railway axle steel. Tribology International, 2010. 43: p. 906-911.

23. S. Beretta, et al., Corrosion-fatigue of A1N railway axle steel exposed to rainwater International Journal of Fatigue, 2010. 32: p. 952-961.
24. M. Novosad, et al., Fatigue tests of railway axles. Procedia Engineering, 2010. 2: p. 2259-2268.
25. I. Le May, A. K. Koul, and R. V. Dainty t, Fracture Mechanisms in a Series of Locomotive Axle Failures. Materials Characterization, 1991. 26: p. 235-251.
26. Viktor Gerdun a, et al., Failures of bearings and axles in railway freight wagons. Engineering Failure Analysis, 2007. 14: p. 884–894.
27. H. F. Moore, A study of fatigue cracks in car axles. Bulletin No. 165 Engineering Experiment Station, 1927.
28. M. Bayraktar, N. Tahrali, and R. Guclu, Reliability and fatigue evaluation of railway axles. Journal of mechanical science and technology 2009. 24(3): p. 671-679.
29. U.zerbst, et al., Safe life and damage tolerance aspects of railway axles- A review. Engineering Fracture Mechanics, 2013. 98: p. 214-271.
30. S. Beretta, A. Ghidini, and F. Lombardo, Fracture mechanics and scale effects in the fatigue of railway axles. Engineering Fracture Mechanics, 2003. 72: p. 195–208.
31. R. A. Smith, Railways and materials: synergetic progress. Iron making and steel making, 2007. 35: p. 505-513.
32. Sulochana and U.K. Joshi, Study on fatigue failure and stress analysis with safe life on railway axle- A review. International journal of Emerging Trends in Engineering and Development, 2013. 2(3): p. 210-215.
33. M. Luke, et al., Fatigue crack growth in railway axles: Assessment concept. Engineering Fracture Mechanics, 2011. 78: p. 714-730.
34. A.S. Watson and K. Timmis, A method of estimating railway axle stress spectra. Engineering Fracture Mechanics, 2011. 78: p. 836–847.
35. H. Alihosseini and K. Dehghani, Modelling and failure analysis of a broken railway axle: effects of surface defects and inclusions. Journal of Failure Analysis and Prevention, 2010. 10: p. 233-239.
36. D.S. Hoddionott, Railway axle failure investigations and fatigue crack growth monitoring of an axle. Proceedings of the Institution of Mechanical Engineers, Part F: Journal of Rail and Rapid Transit, 2004. 218: p. 283-292.

37. M. Vismara, Investigation on the opportunity to introduce prognostic techniques in railway axle's maintenance. Annual conference of the prognostics and health management society, 2011.
38. O. Yasniy , et al., Assessment of lifetime of railway axle. International Journal of Fatigue, 2013. 50: p. 40-46.
39. M. Sangirardi and M. Carboni, Application of eddy currents to the estimation of corrosion-fatigue damage.
40. John Rudlin, et al., Assessment of Corrosion on Rail Axles.
41. Wei Liu , et al., The performances of a thermally sprayed Fe/Ni composite coating to resist fretting fatigue under rotational bending loads. Surface & Coatings Technology, 2013. 217: p. 58–63.
42. Y.X. Zhao, et al., Probabilistic fatigue S-N curves including the super-long life regime of a railway axle steel International Journal of Fatigue, 2009. 31: p. 1550-1558.
43. C. Klinger and D. Bettge, Axle fracture of an ICE3 high speed train. Engineering Failure Analysis, 2013.
44. U. Zerbst , C. Klinger, and D. Klingbeil, Structural assessment of railway axles – A critical review. Engineering Failure Analysis, 2012.
45. D. Crocker, J. Hurrell. Selective brush plating applications for shaft repair, Brooktromics Engineering Corporation.
46. M.H. Jacobs, Surface engineering of materials. Materials and design, 1993. 14(1): p. 33-37.
47. Venkatesan, K., Wear and surface engineering of hot forging dies. PhD thesis, 1997.
48. K.N. Strafford and C. Subramanian, Surface engineering: an enabling technology for manufacturing industry. Journal of Materials processing technology, 1995. 53: p. 393-403.
49. T. Bell, Surface engineering: its current and future impact on tribology. International Conference of Frotiers on tribology, Stratford-upon-Avon, U.K., 1992: p. A297-A306.
50. K.N. Strafford, et al., Surface engineering processes and applications. 1995: Technomic 349.
51. G. Chryssolouris, et al., An Experimental Investigation of Laser Cladding, University of Patras.

52. E. Toyserkani, A. Khajepour, and S. Corbin, Laser Cladding. 2005.
53. M. Zhong and W. Liu, Laser surface cladding: the state of the art and challenges. Mechanical Engineering Science, 2009. 224: p. 1041-1060.
54. W.M. Steen and J. Mazumder, Laser Material Processing. 4th ed. 2010.
55. D. Shiyun, et al., Laser remanufacturing technology and its applications. Lasers in Material Processing and Manufacturing III, 2007. 6825.
56. L. Santo, Laser cladding of metals: a review. Surface Science and Engineering, 2008. 2: p. 327-336.
57. R. Vilar, Laser Cladding. Journal of Laser Applications, 1999. 11: p. 64-79M.
58. L. Costa and R. Vilar, Laser powder deposition. Rapid Prototyping Journal, 2009. 15: p. 264-279.
59. S.D. Sun, M. Brandt, and et. al, Process optimization of laser cladding Aero-grade AISI 4340 steel using Taguchi design and linear regression method. 2012.
60. M. Picasso, et al., A simple but realistic model for laser cladding. Metallurgical and materials transactions, 1994. 25B: p. 281-291.
61. M. Qia, et al., Parametric Studies of Laser Cladding Processes. Materials Processing Technology, 1997(63): p. 590-593.
62. S.D. Sun, et al., Microstructural and mechanical properties of laser cladding repair of AISI 4340 steel, I 28th International congress of the aeronautical sciences
63. M. Brandt, J. Harris, and C. Chipperfield. In-situ laser repair of steam turbine blades. in Proceedings of the Fourth International WLT-Conference on Lasers in Manufacturing. 2007. Munich.
64. ZH. Xiaodong, et al., Control measures for clad cracks of laser cladding remanufacturing.
65. R. Jendrzejewski, et al., Influence of the base preheating on cracking of the laser-cladded coatings. Laser processing of advanced materials and laser microtechnologies, 2003. 5121: p. 356-361.
66. A.H. Wang, C.S. Xie, and W.Y. Wang, Cracking behaviour in the transitional region of laser-clad coatings on Al-Si alloy under multiple impact loading. Materials Characterization, 2003. 49: p. 247-254.
67. N.W. Sachs, Fracture Features, ASM International, 2005, 2: 11-15
68. R.J. Parrington, Fractography of metals and plastics, ASM International.